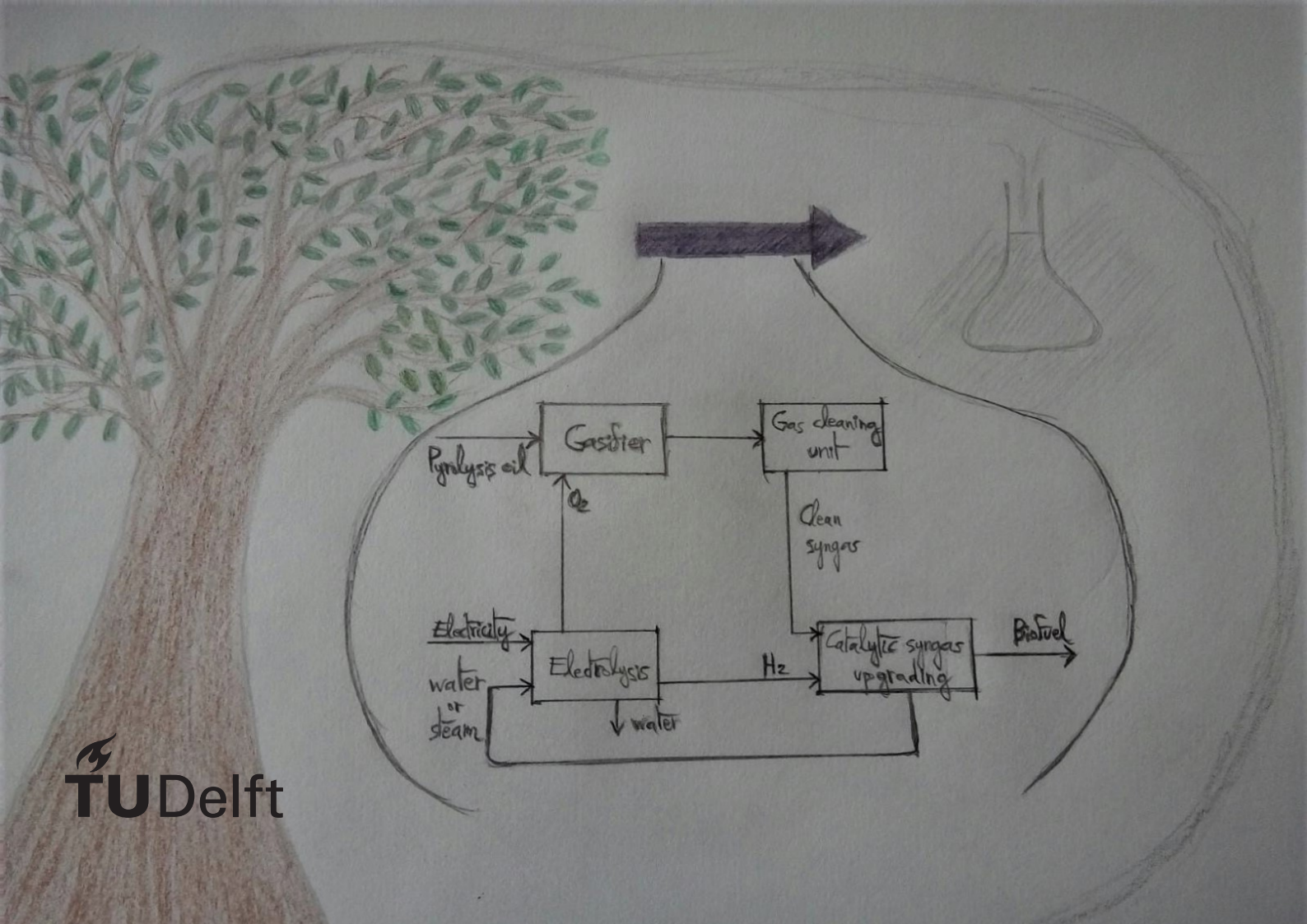


Process Integration of Gasification and Electrolysis for Biofuel Production

A techno-economic assessment

Onsi Hanafi



Process Integration of Gasification and Electrolysis for Biofuel Production

A techno-economic assessment

in partial fulfillment of the requirements of the degree of Master of Science in
Sustainable Energy Technology.
at the Delft University of Technology,

by

Onsi Hanafi

to be defended publicly on Monday August 16, 2021.

Student number: 5142229
Project duration: December 1, 2020 – August 16, 2021
Thesis committee: Prof. dr. W. de Jong TU Delft, supervisor
Dr. W. Guo TU Delft

An electronic version of this thesis is available at <http://repository.tudelft.nl/>.

Preface

This thesis represents the final work of my Master of Sustainable Energy Technology (MSc. SET) at TU Delft. Coming from the other part of the world, studying at TU Delft was a very enjoyable, challenging, self-changing and self-discovering journey.

After having completed my Master, I have the opportunity to reflect on it and learn from my mistakes. If one side of me tells me that I could have done better and studied in a different manner, another side reminds me that I have discovered more my strengths and weaknesses and known more my potentials and my limits. I have now better knowledge not just of the SET topics, but also of what fields I really would like to continue on and invest my time in. In fact, some of the courses I struggled with gave me a sign that they are not the areas I find myself enthusiast and motivated to work on at a later stage of my life. Although I certainly need to challenge myself, to put effort beyond my comfort zone and to allow pressure to make me a better person - as pressure makes diamonds -, I also recognize that there are areas, be it theoretical or practical, which I find myself capable of putting my potentials in an efficient and motivated way, and others that I don't. Bearing knowledge and putting the latter into practice are two sides of the same coin. Indeed, I perceive learning and taking knowledge from my Master studies as a responsibility to apply it in ways that benefit societies, within the scope of my capabilities. On the level of personal development, knowing and understanding ourselves is of highest priority, as it allows us to enhance our strengths and improve on our weaknesses; to use our potentials in the best way. Coming to Delft changed my perspective in many dimensions and opened my eyes on a wide range of topics. I believe that a self-reflection will remain incomplete until those who deserve to be thanked are thanked, although I do not have enough words to express sufficiently my gratitude and respect towards them.

I would like to express my gratitude and praises above all to the Creator, the All-loving and All-caring, the One who makes my heart beats, and gives my brain what it needs; the One who gave me the strength to pursue this work.

Then, I would like to thank with all gratitude my main supervisor, prof. Wiebren de Jong, my daily supervisor, dr. Wenze Guo, as well as prof. Dirk Roekaerts, for their insights, helpful remarks, advice and support. I want to be thankful also to dr. Evert Leijenhurst from BTG company ¹ for providing me with useful information and for giving me advices on technical aspects related to the work of the company.

I want to thank as well my family, especially my dear father, who encouraged me and was constantly checking on me if I am doing well, and who without him, I would not have been able to pursue my studies. As for my lovely and caring sister, she knows that I cannot thank her enough for her support, and comprehensiveness, and for being there when I need it, although she is very busy. My mother, I know that if you were alive, you would have been the most supporting and caring person I can have, and that you would have been very happy seeing me completing my Master. I still thank you for all what you provided me and gave me during your life, from the time of your pregnancy to your last breath. Life is indeed very short, and counts in it every breath...

Last but not least, I would like to thank my friends who are like my family. They all gave me support and helped me in all kinds of ways. They are those who allowed me to discover myself, those who I cried in their arms, those who motivated me and encouraged me, those who taught me life lessons and opened my eyes on new dimensions and new areas, and finally those who

¹this thesis is part of a national project run by BTG.

inspired me on my personal journey and in what I want to do in the next stages of my life.

I do not need to name them, because they surely know themselves and they deserve more than what I have written here. Nevertheless, I would like to gift them these lines:

*We encounter many people in our life.
But those who leave marks in us are true friends.
Those who support us and make us forget our worries.
Friendship cannot be bought and does not have a price.*

Original version of the haiku (I made it first in French with rhymes):

*On rencontre beaucoup de gens dans notre vie.
Mais ceux qui laissent des traces en nous sont des vrais amis.
Ceux qui nous soutiennent et nous font oublier nos soucis.
L'amitié ne s'achète pas et n'a pas de prix.*

*Onsi Hanafi
Delft, August 2021*

Abstract

Onsi Hanafi
Delft, August 2021

The decarbonisation of the transport sector is a major challenge for the transition towards a sustainable economy. Amongst the different measures to lower the impact of road transportation on the environment is the use of biofuels, especially for heavy duty vehicles. For biofuels to be affordable and well integrated, improvements in the production process in terms of energy performance and economic feasibility need to be made.

Consequently, this thesis aims at the techno-economic assessment of the integration of pyrolysis oil gasification with electrolysis and syngas catalytic upgrading. Oxygen, being a co-product of electrolysis, is used as an oxidizer for entrained flow gasification of biomass derived pyrolysis oil. Hydrogen from the electrolyzer is used to enhance the production of biofuel. The process was designed to have a high-temperature solid oxide electrolysis cell (SOEC) and the biofuel was chosen to be compressed natural gas (bio-CNG). The modeling of the process was performed on Aspen Plus software and calculations of parameters for the gasifier and electrolyzer were done using Fortran and Matlab respectively.

As aimed by the integration of electrolysis, the hydrogen produced is added to the syngas to obtain a feed ratio of 3, required for an optimum methane production. The increase in the feed ratio at the level of the gasifier is mainly limited by the oxygen equivalence ratio (OER), considering the extent of combustion reactions and the operating temperature. The amount of steam inputted was found to increase the molar ratio of H_2 to CO without significant change in the feed ratio due to the increase in the concentration of CO_2 . However, steam was still necessary for adjusting the temperature of the gasifier to values that are in accordance with experimental ones in literature. The obtained final product stream of bio-CNG at 250 bar and 15°C has a purity of 98.63 mol% and 99.15 wt%.

Moreover, by applying heat integration to the process, the resulting surplus heat was 10.71 MW, which was assumed to be used to generate steam that is inputted to the SOEC for producing hydrogen as an additional product. The process was found to have an overall efficiency of 73.8% (LHV basis) and 78.2% (HHV basis). Heat integration increased the process efficiency by 15% (LHV basis) and 23% (HHV basis), by removing to a great extent the need for external heat and by having hydrogen as an energy output added to CNG.

As a complement to the energy performance, the economic feasibility of the process was assessed. The total capital investment was found to be 889.5 Euros/ kW_{input} , the net present value was 6.0342 million Euros and the rate of return on investment 30.02%.

Contents

Abstract	v
List of Figures	ix
List of Tables	1
1 Introduction	1
1.1 Problem introduction	1
1.2 Research framework	5
1.3 Research questions	7
1.4 Thesis outline and methodology	8
2 Literature Study	11
2.1 Gasification of pyrolysis oil	11
2.1.1 Fundamentals	11
2.1.2 Types of gasifiers	14
2.2 Gas cleaning	15
2.3 Electrolysis process	16
2.3.1 Proton exchange electrolysis (PEM)	18
2.3.2 Alkaline water electrolysis (AWE) and Anion exchange membrane (AEM)	18
2.3.3 Solid Oxide electrolysis cell (SOEC)	18
2.3.4 Summary	20
2.4 Syngas catalytic upgrading	21
2.4.1 Overview on methanation	22
2.4.2 Methanation reactors	23
2.4.3 Catalysts	24
3 Basis of Design and Model Results	25
3.1 Gasifier	27
3.1.1 Pyrolysis oil feedstock	27
3.1.2 Gasifier modeling	29
3.1.3 Model verification and results	32
3.2 Gas cleaning unit	34
3.3 Electrolyzer	36
3.3.1 SOEC modeling	36
3.3.2 Electrochemical parameters	37
3.3.3 Electrolysis energy demand	39
3.4 Syngas catalytic upgrading	40
3.4.1 Methane reactor modeling	40
3.4.2 Methanation kinetics	41
3.4.3 Model verification and results	44
3.4.4 Final SNG upgrading	46
3.5 Sensitivity analysis	47
3.5.1 Gasifier	47
3.5.2 Methane reactor	51
4 Energy performance analysis	55
4.1 Heat integration	55
4.2 Heat exchanger network	56
4.3 Process energy efficiency	58

5	Economic analysis	61
5.1	Capital cost estimation	61
5.2	Operational cost estimation and revenues	63
5.2.1	Factors affecting the price of CNG.	66
5.2.2	The source of electricity	67
5.3	Profitability analysis	70
6	Conclusion and Recommendations	71
6.1	Answers to the research questions	71
6.2	Recommendations	74
6.2.1	Process variables	74
6.2.2	Further analyses	74
	Bibliography	77
A	Aspen Plus plots	81
B	Heat integration and heat exchanger network calculations	85
C	Economic analysis - Parameters	87

List of Figures

1.1	Direct GHG emissions of the transport sector from 1970 to 2010 in $GtCO_2eq/yr$ [28].	2
1.2	Final energy consumption in the transport sector (NZE2050) [24].	3
1.3	Global supply of low-carbon fuel (2019 and 2040) in Mtoe based on different scenarios [26].	3
1.4	Different product routes considered by BTG.	6
1.5	Simplified block diagram of the integrated system	6
1.6	Flow diagram of the detailed structure of the thesis.	9
2.1	Average heating rate vs. pyrolysis oil diameter. [38]	13
2.2	Char formation vs. pyrolysis oil diameter. [38]	13
2.3	Representation of fluidized bed reactors: BFB (left) and CFB (right). Adapted from [6]	14
2.4	Schematic process diagram of entrained flow gasification plant [15]	15
2.5	Timeline showing methanation development. [54].	22
2.6	Effect of operating conditions on CO methanation and RWGS reaction [35]	23
2.7	TREMP process with three fixed-bed reactors in series with intermediate cooling and gas recycle [54]	24
3.1	Process flow diagram of the integrated process as the final basis of design.	26
3.2	Screenshot of the full simulation of the integrated process in Aspen Plus	26
3.3	Screenshot of the gasification part of the simulation in Aspen Plus	29
3.4	Typical reaction zones in EF gasifier [38]	30
3.5	Screenshot of the gas cleaning part of the simulation in Aspen Plus	34
3.6	Screenshot of the steam electrolysis part of the simulation in Aspen Plus	36
3.7	Schematic of Solid oxide electrolysis cell [51]	37
3.8	Electrolysis energy demand as a function of temperature [51]	39
3.9	Screenshot of the methanation part of the simulation in Aspen Plus	40
3.10	Kinetic specifications for methanation reaction on Aspen Plus	44
3.11	Axial profiles of the product dry gas composition and reactor temperature in a fast fluidized bed [32]	45
3.12	H_2 fraction at different oxygen equivalence ratio (OER) and steam-to-carbon (S-C) ratio values	47
3.13	CO fraction at different oxygen equivalence ratio (OER) and steam-to-carbon (S-C) ratio values	47
3.14	CO_2 fraction at different oxygen equivalence ratio (OER) and steam-to-carbon (S-C) ratio values	48
3.15	H_2/CO ratio at different oxygen equivalence ratio (OER) and steam-to-carbon (S-C) ratio values	49
3.16	Feed ratio at different oxygen equivalence ratio (OER) and steam-to-carbon (S-C) ratio values	49
3.17	Gasifier outlet temperature at different oxygen equivalence ratio (OER) and steam-to-carbon (S-C) ratio values	50
3.18	Gasifier outlet temperature vs. the carbon-to-gas ratio	51
3.19	Gasifier outlet temperature vs. the percentage of heat loss	51
4.1	Process flow diagram with the heat exchanger network	57
5.1	Cost of Product (COP) vs. price of electricity	66

5.2	Cost of Product (COP) vs. cost of pyrolysis oil	66
5.3	Average carbon footprint over the lifetime of passenger cars (segment D) sold in 2020 ($GtCO_{2eq}/km$) - France and Europe [52]	67
5.4	Average carbon footprint over the lifetime of buses sold in 2020 ($GtCO_{2eq}/km$) - France and Europe [52]	68
A.1	Syngas composition (dry basis) vs. the oxygen equivalence ratio (OER) on Aspen Plus	81
A.2	Gasifier outlet temperature vs. the oxygen equivalence ratio (OER) on Aspen Plus	82
A.3	Syngas composition (dry basis) vs. the steam-to-carbon ratio on Aspen Plus	82
A.4	Gasifier outlet temperature vs. the steam-to-carbon ratio on Aspen Plus	83

List of Tables

2.1	Characteristics of electrolysis technologies. Adapted from [10]	20
2.2	Properties of various fuels. Adapted from [40]	21
2.3	Main reactions in methane reactor [33, 54, 59]	22
2.4	Side reactions in methane reactor [33, 54, 59]	23
3.1	Pyrolysis oil composition. Adapted from [11]	27
3.2	Main reactions known to happen in a gasification process	27
3.3	Ultanal Attribute of pyrolysis oil component	28
3.4	Proxanal and Sulfanal Attributes of pyrolysis oil component	28
3.5	Syngas molar composition, at $\lambda=0.4$ and $S-C=0.05$ ($T=1347^{\circ}\text{C}$ and $P=10$ bar)	32
3.6	Gasifier conditions and syngas properties obtained from Aspen Plus model	33
3.7	Main parameters of SOEC in this study and in two other studies	38
3.8	Molar composition (dry basis) of the inlet and outlet streams of the methanation reactor on Aspen Plus with a feed ratio of 0.15	40
3.9	Kinetic parameters for model 12b [30]	43
3.10	Molar composition (dry basis) of the inlet and outlet streams of the methanation reactor on Aspen Plus with the syngas feed ratio of 3	45
3.11	Molar ratio CO_2/CO in the syngas obtained at six different cases of S-C and OER	52
3.12	Molar composition of the inlet and outlet streams of the methanation reactor on Aspen Plus at six cases of OER and S-C values	53
4.1	Summary of the cold and hot streams with their properties for heat integration'	56
4.2	Summary of the cold and hot streams with their properties for heat integration	57
4.3	Energy inputs to the process	59
4.4	Energy outputs of the process	59
5.1	Parameters for the purchased cost at bare conditions Cp_0	62
5.2	Parameters for variable operating costs	64
B.1	Summary of the cold and hot streams with their properties for heat integration	85
B.2	Summary of the intervals and process streams for the pinch analysis	86
B.3	Summary of the cold and hot streams with their properties for heat exchanger network	86
C.1	Material factors for different materials per equipment	87

Nomenclature

Abbreviation

<i>AEM</i>	Anion exchange membrane
<i>ASR</i>	Area specific resistance
<i>AWE</i>	Alkaline water electrolysis
<i>BEV</i>	Battery electric vehicle
<i>CAPEX</i>	Capital expenditure
<i>CNG</i>	Compressed natural gas
<i>ECN</i>	Energy research Centre of the Netherlands
<i>FCEV</i>	Fuel cell electric vehicle
<i>GHG</i>	Greenhouse gas
<i>HDV</i>	Heavy duty vehicles
<i>HHV</i>	High heating value
<i>ICEV</i>	Internal combustion engine vehicle
<i>IPCC</i>	Intergovernmental Panel of Climate Change
<i>LDV</i>	Light duty vehicles
<i>LHHW</i>	Langmuir-Hinshelwood-Hougen-Watson
<i>LHV</i>	Lower heating value
<i>LNG</i>	Liquefied natural gas
<i>MDEA</i>	Methyl diethanolamine
<i>NPV</i>	Net present value
<i>OER</i>	Oxygen equivalence ratio
<i>OPEX</i>	Operational expenditure
<i>PEM</i>	Proton exchange membrane
<i>ROI</i>	Return on investment
<i>RWGS</i>	Reverse water-gas shift
<i>SOEC</i>	Solid oxide electrolysis cell
<i>TCI</i>	Total capital investment
<i>WGS</i>	Water-gas shift

Greek symbols

η	Energy efficiency of the system
--------	---------------------------------

λ Oxygen equivalence ratio

ρ Density

Latin symbols

ΔG Gibbs free energy of formation

I_f Faradic current, A

j Current density, A/cm^2

j_{tn} Thermo-neutral current density, A/cm^2

m Mass flow rate, kg/s

P Pressure at standard condition, bar

P_{std} Pressure at standard condition, 1.013 bar

R Universal gas constant, $J/mol.K$

T Temperature, °C

V_{op} Operating cell voltage, V

V_{rev} Reversible cell voltage, V

V_{tn} Thermo-neutral voltage, V

y_i Molar fraction of component i

1

Introduction

The art and science of asking questions
is the source of all knowledge.

Thomas Berger

This chapter aims to introduce the problem that is tackled by the thesis in section 1.1. Then, the research framework is explained in section 1.2, followed by the research questions and the thesis outline and methodology in sections 1.3 and 1.4.

1.1. Problem introduction

The transition towards a sustainable society and circular economy is technically feasible by decarbonizing all the different sectors of production from one side, and by changing societal consumption behaviour on the other side. A holistic approach to tackle climate change requires the systemic adaptation to the changes imposed by the decrease in the possibility of use of fossil fuels. This leads to lower production capacity that affects industries and services alike. For this, low-carbon (low emissions) processes need to be implemented in energy and heat generation, in agriculture, as well as in the production of transportation fuels, chemicals and materials. The transport sector is very critical as it affects the mobility of people, freight and materials, and it allows for the availability of services. According to the Fifth Assessment Report (AR5) of the Intergovernmental Panel of Climate Change (IPCC), the direct GHG emissions from the transport sector were 7.0 $GtCO_2eq$ in 2010 [28]. The historical development of GHG emissions from transport over the period of 1970 to 2010 (in $GtCO_2eq/yr$) is shown in figure 1.1.

The rate of increase in emissions from transportation have been higher from 1990 to 2010 than from 1970 to 1990. During both periods, the significant increase and contribution in GHG emissions have been and are still associated with road transportation. In 1990, the latter represented 71.0% of the emissions, compared to 72.06% in 2010. This indicates that it is crucial to mitigate the effect of road transportation on climate change.

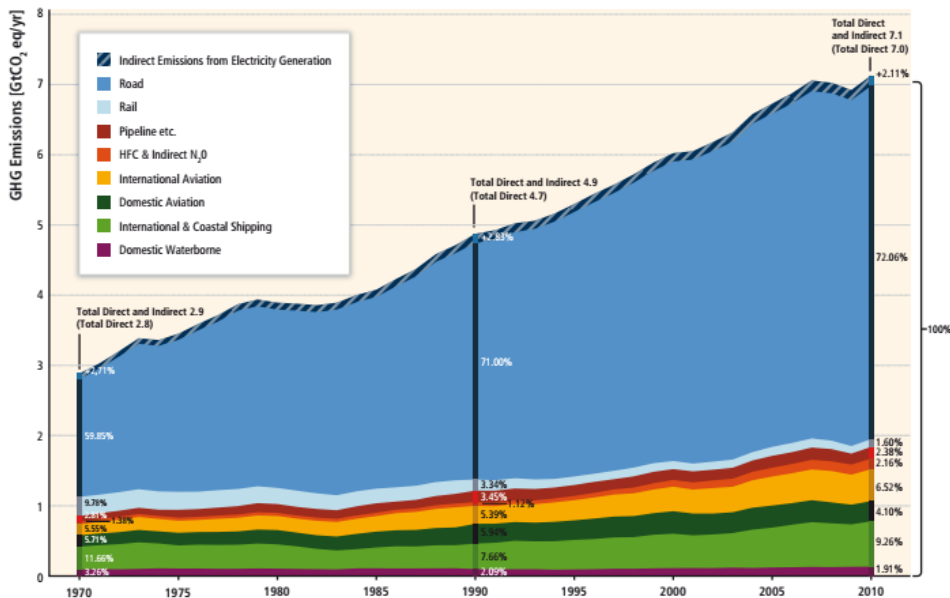


Figure 1.1: Direct GHG emissions of the transport sector from 1970 to 2010 in $GtCO_2eq/yr$ [28].

It is important to note that the use of low-carbon fuels constitutes only one facet of the measures required to reduce transport emissions. This needs to be coupled with improvement in the efficiency of the vehicle, changes in infrastructure and built environment, as well as behavioural changes in the frequency of consumption and the types of the mode of transportation. In fact, there are many factors that affect the total amount of direct GHG emissions. These include the fuel carbon intensity (tCO_2eq/MJ) and the energy intensity (MJ/km). In addition, behavioural changes (such as the distance, the number of journeys, and trip avoidance) affect the amount of passenger km. The infrastructure and system modal choice relates to the modes of transportation used and the urban management required for it.

Figure 1.2 shows the final energy consumption (in $Mtoe^1$) and associated emissions (in $GtCO_2$) of the transport sector from 2010 to 2030, considering the net-zero emissions by 2050 (NZE2050) target [24]. It can be seen that the share fuels from bioenergy (including liquid biofuels and biogases) is expected to grow faster after 2021. Moreover, the International Energy Agency (IEA) estimates hydrogen to be consumed at a considerable amount only after 2024.

¹million tonnes of oil equivalent

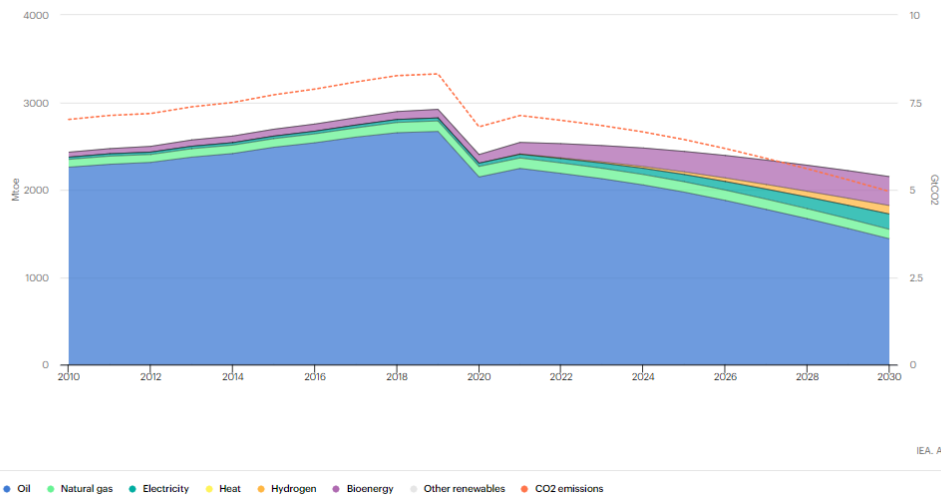


Figure 1.2: Final energy consumption in the transport sector (NZE2050) [24].

In order to achieve the climate change mitigation until reaching net-zero emissions by 2050, while contributing positively to the fulfilment of the energy-related UN's Sustainable Development Goals (SDGs), the IEA has set a 'Sustainable Development Scenario' (SDS). This scenario aims at having a temperature rise below 1.8°C (with 66% probability) [25]. To allow for the decarbonisation of the transport sector in accordance with these targets, the production of low-carbon fuels needs to increase significantly. In fact, following the estimates of the SDS by 2040, 358 Mtoe of liquid biofuels, 221 Mtoe of biogases and 215 Mtoe of low-carbon hydrogen (green hydrogen) are to be supplied, as depicted in figure 1.3. These values are considerably higher than the historical supply of these low-carbon fuels.

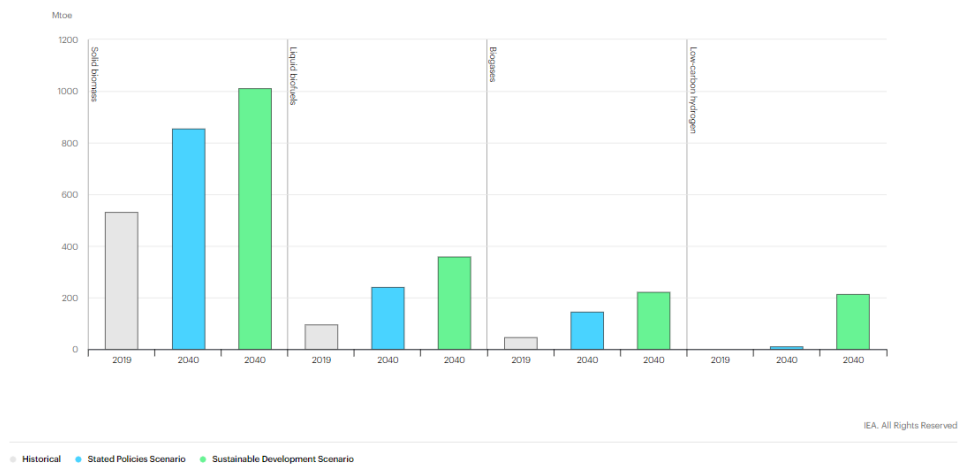


Figure 1.3: Global supply of low-carbon fuel (2019 and 2040) in Mtoe based on different scenarios [26]

Considering the short time frame of these developments, significant effort is to be put in enhancing the technological maturity and economic performance of low-carbon fuels production processes. As decarbonizing the transport sector requires both electrification and the use of sustainable fuels, it is important to note the limitations of both options.

On one hand, the spread of electric vehicles is limited by the size of the battery (battery electric vehicles to a higher extent than fuel cell ones), due to the use of mineral resources and sometimes scarce metals to build the battery. Having large batteries can become a downside in terms of sustainability of materials and environmental (and social) impact. Moreover, large-scale pro-

duction of hydrogen requires more technological maturity and the availability of infrastructure to accommodate the use of fuel cell electric vehicles (FCEV). The electricity used for powering the fuel cell needs also to be fully renewable for the FCEV to have lower environmental impact than internal combustion engine vehicles using conventional fuels, considering the complete lifetime of the vehicle [52]. While it is recommended to have electric mobility mostly for light duty vehicles (LDVs) and public transportation such as buses and trains, the use of biofuels would be more convenient for heavy duty vehicles [52]. On the other hand, biofuel production is limited by land use, availability of the feedstock and potential competition with other critical sectors. The carbon footprint of the biofuel highly depends on the resources used and on the conversion pathway. Compared to hydrogen and electricity, liquid biofuels have a high energy density and are in many cases compatible with the current fuel infrastructure [28]. However, the production of some of these fuels is still under development. Hence, there needs to be a balance between the extent of electrification with a limited size of batteries and the use of low-carbon fuels to have a sustainable transport sector.

From these challenges rises the need to develop processes that efficiently produce biofuels and improve their performance and economic feasibility. In this context, the problem raised is translated into a research framework in the next section.

1.2. Research framework

Many research and studies have been performed on the production of biofuels through diverse routes. These differ in the feedstock used, in the intermediary products and in the conversion technologies. To have a fully sustainable production system, the environmental and social impacts of the feedstocks as well as the emissions caused by the technologies used need to be considered. One potential technological route to biofuel is the production of syngas² from biomass, followed by the catalytic upgrading of the syngas. For most types of biofuels, hydrogen needs to be added to have an efficient conversion process. There are many advantages to this integrated system.

Firstly, the initial feedstock consists of biomass, which helps reduce the environmental impact of the process, under some conditions. If the consumption rate and land management are well managed, biomass can represent a sustainable material to be converted into diverse products. When the exhaust gas of the conversion process is cleaned from toxic compounds, the remaining waste components resulting from the partial combustion of biomass, mainly biochar and ash, can be turned into useful products. The constraining conditions include the mitigation of land use change emissions by limiting the rate of biomass usage. In fact, the rate of consumption should be lower than the rate of planting, otherwise the plantation area will be shrunk over time. This can have many consequences, including a lower capacity for carbon sequestration (in plants and trees) and a displacement of the emissions. Leakage or displacement occur when the reduction in emissions indirectly leads to an increase elsewhere [28]. If the production of a less emitting biofuel causes emissions due to land management, no net reduction is achieved. This is crucial to note when considering the type of biomass used as an initial feedstock. Another condition to consider is the competition with other important sectors of the economy, as in case of using crops that are also harvested for human and animal consumption. Agricultural and forestry residues overcome these challenges but they have a limited capacity.

Therefore, the use of biomass for the low-carbon fuel production constitutes an advantage within the boundaries of these constraints. Further, syngas is a highly versatile intermediate product that can be converted into a wide range of chemicals and fuels. This allows for flexibility in the design of the process when several end-products are compared in order to identify the one that leads to a more efficient system.

Another advantage lies in the production of hydrogen in a sustainable way, through electrolysis. The introduction of renewable and clean electricity for the sustainable production of hydrogen (green hydrogen) allows for the use of surplus electricity that results from the intermittency of solar and wind energies. In addition, if the integration of the different technologies for producing biofuel results in surplus heat, the latter can be harvested to produce hydrogen as a highly valuable product when high-temperature electrolysis is used.

Considering these advantages, more research is being done to study and analyse how the sustainable production of biofuel through the described integrated system can have a higher efficiency and better performance. These studies are crucial as a knowledge support to allow the technologies to develop and gain industrial maturity and economic competitiveness. In the context of the Netherlands, 'Biomass4transport' project is undertaken by Biomass Technology Group (BTG)³ in collaboration with TU Delft. The different options of BTG complete project⁴ are shown in figure 1.4.

²Syngas, also known as synthetic gas, is a mixture of gases, mainly H_2 and CO , that results from the gasification of a carbon feedstock [6].

³BTG is a group of companies that work on the conversion of biomass into energy and fuels. Website: <https://www.btgworld.com/en>

⁴Taken with permission from dr. E. Leijenhorst. Reference: proposal of the 'Biomass4transport' project, contract no TBBE119005.

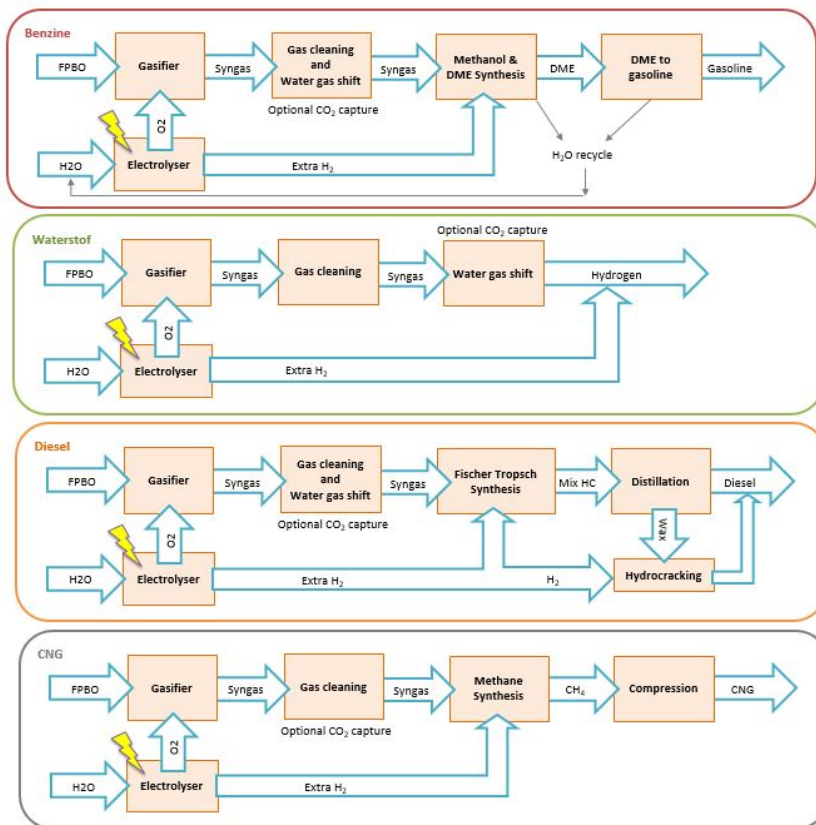


Figure 1.4: Different product routes considered by BTG.

This thesis work is part of this national project, aiming at the techno-economic study of the production of biofuel for transportation uses. The integrated process assessed includes: a gasification section for converting the pyrolysis oil to syngas ; a gas cleaning unit ; an electrolysis section ; and a syngas catalytic upgrading section. The simplified block diagram of the overall process is shown in figure 1.5.

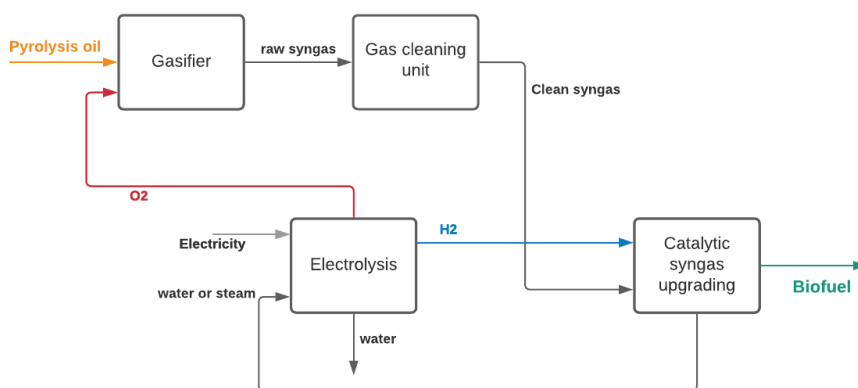


Figure 1.5: Simplified block diagram of the integrated system

1.3. Research questions

Elaborating the research questions is a crucial and a focal point in formulating the thesis definition. To address the challenges of decarbonising the transport sector through the production of biofuels, the main research question of the thesis is:

How can the use of electrolysis derived oxygen as a bio-oil gasifying agent and hydrogen as feedstock for downstream biofuel production result in an efficient integrated process?

To provide an answer to the main research question, five sub-questions (SQ) are extracted. The answer to SQ1 is partially discussed in the literature study and complemented by the sensitivity analyses performed on the simulation of the process. While the second and third sub-questions (SQ2 and SQ3) are answered from literature review, SQ4 and SQ5 are tackled in the analysis of the process model.

SQ1: *What are the important parameters for the gasification process in order to optimize the quality of the syngas?*

In the context of upgrading the syngas for biofuel production, the concentrations of hydrogen, carbon monoxide and carbon dioxide have an impact on the yield of the biofuel. The quality of the syngas is assessed based on the concentrations of these gases.

SQ2: *Which type of electrolysis results in a more efficient integrated process?*

As the main question relates to the use of the electrolysis products such that the integration of electrolysis leads to higher process efficiency, the choice of the electrolyzer is critical to the performance of the overall process.

SQ3: *What is the most suitable product of catalytic syngas upgrading in terms of overall process efficiency?*

The national project of BTG takes into consideration different product routes to assess which biofuel will be the most efficient and economical to produce. For the scope of this thesis, only one product is considered and the choice is justified based on results obtained from literature. Moreover, the research target is to use hydrogen for upgrading the syngas to a end-product of higher energy density (energy per volume). For this reason, hydrogen is not considered as the main product ⁵ in this thesis.

SQ4: *How does the use of the heat generated by the system affect the overall process efficiency?*

In a process that includes units that are endothermic and others that are exothermic, the use of the hot streams to heat the cold streams can compensate (partially or completely) external sources of heat (such as electric heating). This reduction in energy input, and the presence of excess heat if available, will affect the efficiency of the process. Hence, it is important to know the effect of heat integration on the process. This can be achieved by carrying out the energy performance analysis.

SQ5: *Is the integrated process economically feasible?*

After having analysed the technical performance of the process, it is crucial to know whether its implementation in an actual plant is economically feasible, within the limit of the gas price to be competitive in the market.

⁵Additional amount of hydrogen not used for upgrading the syngas can be considered as an extra product, in addition to the biofuel.

1.4. Thesis outline and methodology

A literature review was first performed to give an overview of the main important concepts related to the research questions and to the technologies involved in the process. The review is provided in chapter 2, which is divided according to the sections of the process. Literature review is a crucial initial step to understand the important parameters to consider for the modeling and the analysis. It also forms the theoretical background for developing the basis of design (BOD) of the process, which is presented in the next chapter. In addition, chapter 3 describes the model and lays down the discussion of the results obtained. Sensitivity analyses were made using Aspen Plus 'Model Analysis Tools', as a further assessment of the effect of parameters on the performance of the gasifier and biofuel synthesis reactor.

The modeling of the process was performed using Aspen Plus simulation software. Calculations for controlling the input feeds to the gasifier were computed through Fortran. In addition, the electrochemical parameters of the electrolyser were calculated in Matlab. After presenting the model and the results, chapter 4 discusses the energy performance of the process, including the heat integration study that was performed through Pinch analysis by numerical method and heat exchanger network. The assessment of the energy efficiency of the process is followed by an economic analysis presented in chapter 5. Finally, the main conclusions are derived and the research questions are answered in the last chapter (ch. 6). The thesis ends with areas of further research and recommendations for future work.

The detailed structure of the thesis can be better visualised in a flow diagram which is shown in figure 1.6. The chapters which provide answers to the research questions are specified with their respective number. The answer to the main research question (MRQ) is elaborated in the last chapter.

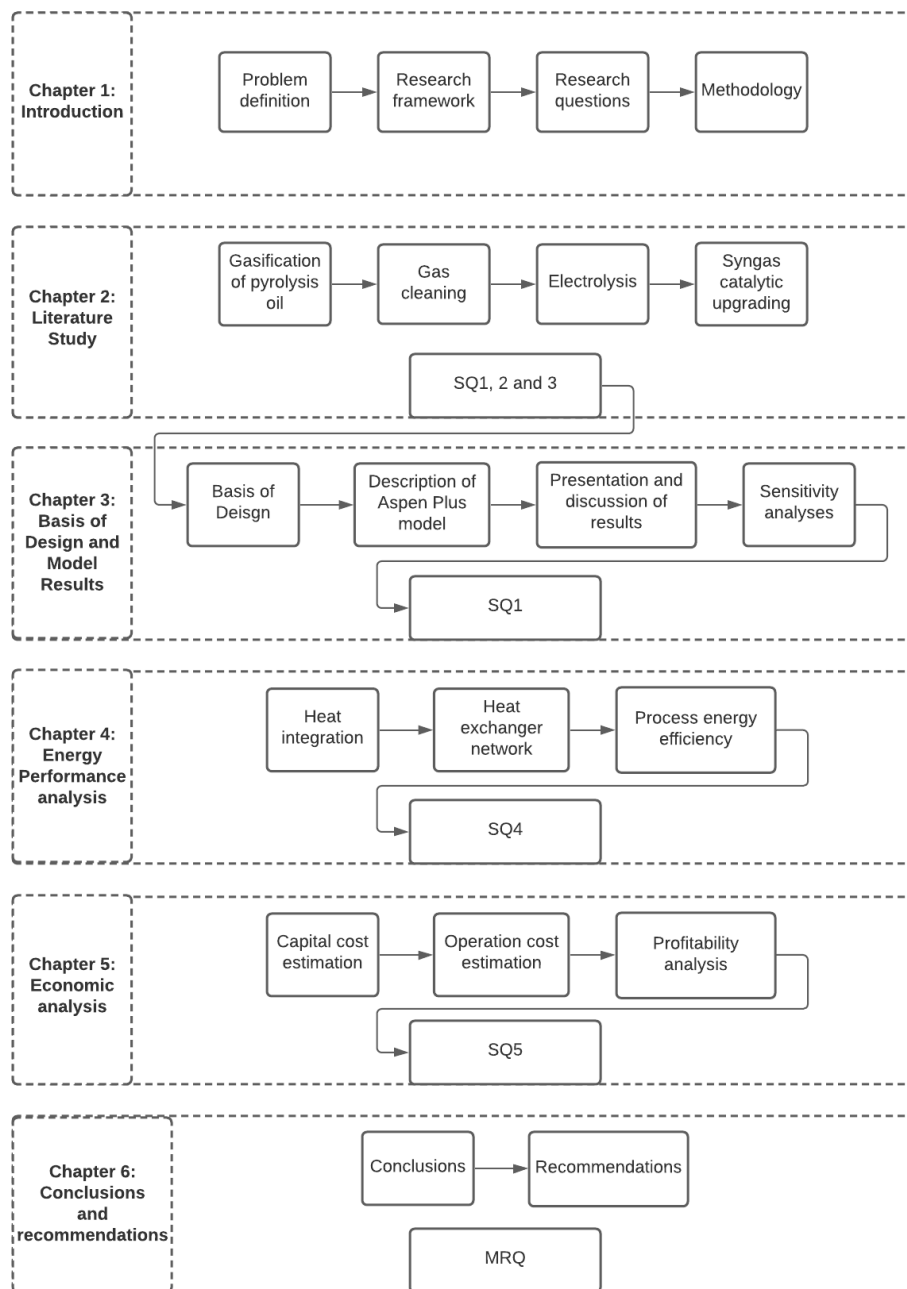


Figure 1.6: Flow diagram of the detailed structure of the thesis.

2

Literature Study

This chapter presents the theoretical background from literature review, focusing on the main sub-processes of the integrated pyrolysis oil to bio-fuel process: gasification, gas cleaning unit, electrolysis, and catalytic upgrading of syngas.

2.1. Gasification of pyrolysis oil

The first part of the process is the gasification of pyrolysis oil, which is considered as an input to the whole system. For this reason, biomass pre-treatment prior to the pyrolysis process will not be tackled in the literature review.

2.1.1. Fundamentals

Pyrolysis is defined as "the thermochemical decomposition of organic material in an oxygen free atmosphere" [38]. The products of pyrolysis are permanent gases, condensable vapours and char. The vapours can be condensed into bio-oil, that is a suitable feedstock for gasification as it does not have inorganic elements that are associated with tar formation and slagging. The addition of char as feedstock increases the energy content of the pyrolysis oil but also introduces the inorganic compounds originally present in the biomass mineral content. The inorganic salts turn into a liquid slag layer that needs to be systematically removed. In this case, when having an entrained flow gasification, a slagging gasifier is required, which is more expensive than a non-slagging reactor. Another drawback to the use of char is the reduction in flexibility in pyrolysis oil from different biomass feedstocks [11].

Adding to this, the use of pyrolysis oil as a feedstock to the gasifier instead of raw biomass represents several advantages. In terms of energy efficiency, the energy density (on volumetric basis) for pyrolysis oil increases by 3 to 10 times compared to solid biomass [11, 21]. Moreover, less work and lower costs are required for pressurizing the oil compared to solid biomass. In addition, ash forming elements are reduced significantly [11].

Gasification is a thermo-chemical conversion process at elevated temperature using a gasifying agent (oxidant) such as pure oxygen, air or steam. The reaction of the carbon in biomass with these agents leads to the production of several gases, including carbon dioxide (CO_2), hydrogen (H_2), carbon monoxide (CO), referred to as syngas. Further reactions happen with the produced gases forming CH_4 and higher hydrocarbons [6, 53]. The product gases get mixed with the oxidizing agent along the length of the reactor, releasing heat due to their combustion. This heat is generally sufficient for enabling the endothermic gasification reactions. There is a limit to the in-situ heat generation as the amount of oxidant flow needs to be below the stoichiometric ratio of full combustion [41].

There are many important parameters to consider in order to have a syngas of good quality. One of the major parameter that influences the temperature of the process as well as the

heating rate is the oxygen equivalence ratio (OER or λ) [15]:

$$\lambda = \frac{O_2 \cdot in}{O_2 \cdot stoic} \quad (2.1)$$

where

- $O_2.in$ is the mass flow of external oxygen supply (kg/h)
- $O_2.stoic$ is the mass flow of the stoichiometric amount of oxygen required for complete combustion of the feedstock (kg/h)

Typical values of the O_2 equivalence ratio are between 0.4 and 0.5 [15]. For optimizing the gasification process, there is a balance that needs to be maintained between having high concentrations of H₂ and CO (at lower λ values) and having enough temperature for the endothermic reactions (at higher λ values). When the oxygen equivalence ratio is increased (by feeding a higher oxygen flow rate), the combustion reactions occur at a higher extent, which will consequently lead to higher temperatures in the reactor [11]. There are two ways in which temperature elevation can be applied: the use of external heat supply (indirect gasification), or in-situ heat generation through partial oxidation, which is referred to as autothermal gasification [6].

Furthermore, in the context of gasification of pyrolysis oil, it is important to consider the oil droplet size as the heating rate is dependent on it. Assuming homogeneous droplet size [29], the heat transfer is affected by the droplet diameter d through the Nusselt-Reynolds correlation [38]:

$$Nu = 2 + F_x \cdot Re^{0.5} \cdot Pr^{0.33} \quad (2.2)$$

where

F_x is a factor depending on the flow pattern and is taken as 0.66 for laminar flow;

Re is Reynolds number:

$$Re = \frac{\rho \cdot v \cdot d}{\mu} \quad (2.3)$$

and Pr is Prandtl number:

$$Pr = \frac{C_p \cdot \mu}{k} \quad (2.4)$$

where

- ρ is the density of the pyrolysis oil (kg/m^3),
- μ is the dynamic viscosity ($Pa \cdot s$),
- v is the flow velocity (m/s),
- k is the thermal conductivity ($W/(m \cdot K)$),
- and C_p is the specific heat ($J/(kg \cdot K)$).

The total evaporation heat of the oil droplets is considered as the increase in temperature from ambient temperature to 100°C, in addition to the evaporation of water (moisture content of pyrolysis oil) and the heat required to increase the temperature of the droplet from 100°C to 500°C [38].

The increase of the average heating rate of the bio-oil as the droplet diameter decreases can be seen in figure 2.1.

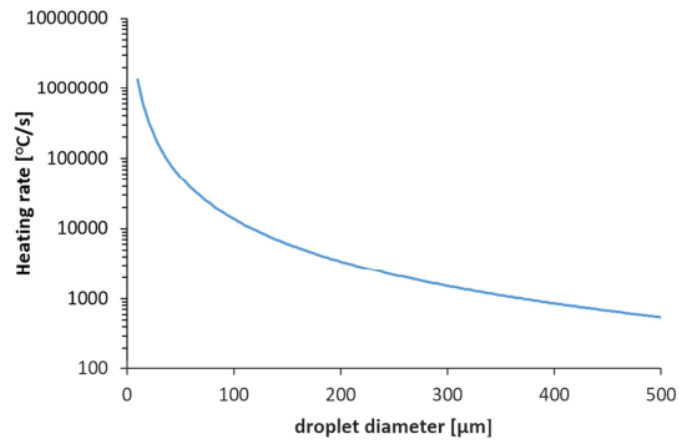


Figure 2.1: Average heating rate vs. pyrolysis oil diameter. [38]

The droplet size affects as well the extent of char formation. At a droplet diameter of $50 \mu\text{m}$, the char formed is 1 wt% and it increases to higher than 2 wt% for diameters above $200 \mu\text{m}$ (figure 2.2) [38].

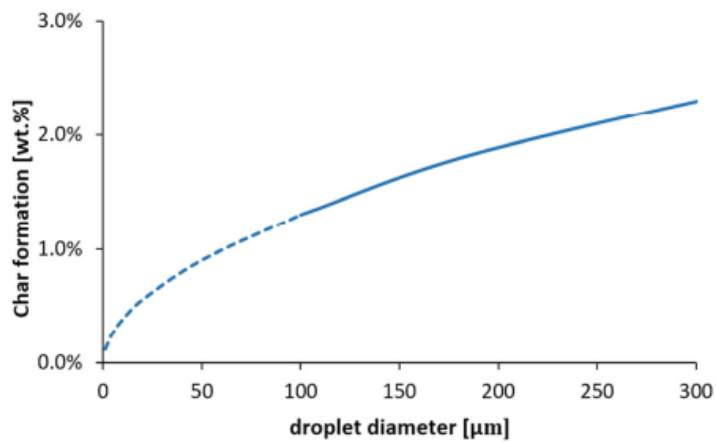


Figure 2.2: Char formation vs. pyrolysis oil diameter. [38]

2.1.2. Types of gasifiers

Several types of gasifiers have been developed since the use of gasification of coal for industrial power generation. When considering which type to implement in a process, the main factors that need to be considered are [6]:

- Scale of the conversion process
- Feedstock flexibility
- Sensitivity to ash (amount and composition)
- Tar formation

As the aim of the process in this thesis is to produce biofuels, large-scale reactors (higher than 10 MW_{th}) have been found to be have higher thermal efficiency and economies of scale [6]. Therefore, entrained flow (EF) and fluidized bed (FB) gasifiers will be discussed, rather than small-scale reactors (fixed/moving bed gasifiers).

Fluidized bed (FB) reactors consist of bed of solid particles (catalyst or inert material) that is fluidized by the turbulent flow of the gasifying agent. The usual operating conditions are 700-900°C, and gauge pressures ranging from 0 to 7 MPa. One of the issues faced is bed sintering due to the formation of low-melting eutectics between the bed material and ash (inorganic components of biomass). The agglomeration of bed particles disturbs the fluidization, which consequently lowers the efficiency of the gasification process. Depending on the fluid dynamics, the reactor can be characterized as a Bubbling Fluidized Bed (BFB) or Circulating Fluidized Bed (CFB), as depicted in figure 2.3.

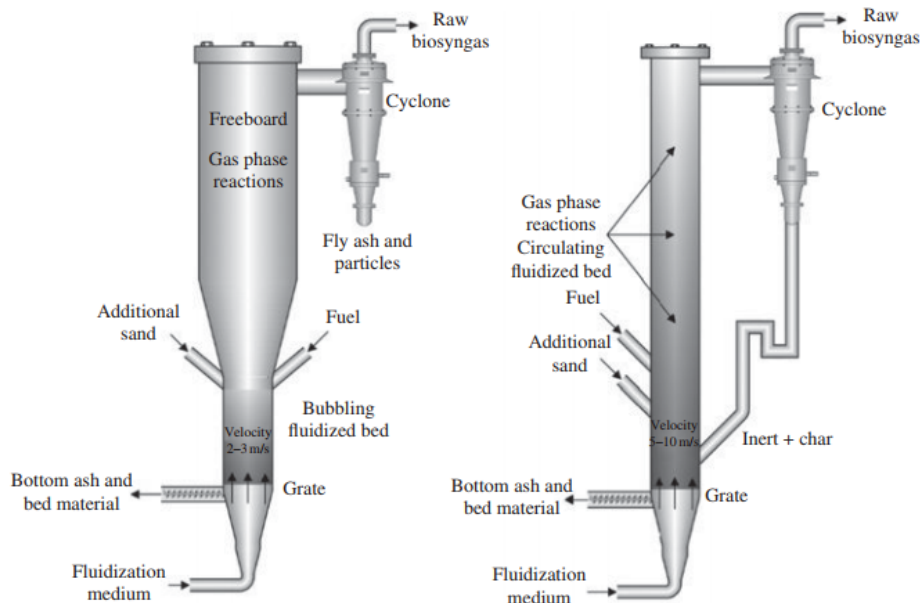


Figure 2.3: Representation of fluidized bed reactors: BFB (left) and CFB (right). Adapted from [6]

Entrained flow reactor is another option for large-scale applications, operating at higher temperatures (800-1600°C) with no catalyst or particle bed. While the EF reactor is more energy demanding for reaching high temperatures, lower tar is obtained in the syngas, which allows for an easier gas cleaning process than in the case of fluidized bed reactor [11, 15]. Tar refers to a variety of organic hydrocarbons larger than benzene, reaching to Polycyclic Aromatic Hydrocarbons (PAHs) [22]. Using oxygen as a gasifying agent helps in achieving temperatures above 1200°C. The addition of steam is however still necessary to control the increase in temperature and to avoid a temperature overflow. Steam can potentially increase the hydrogen

production if it is not counterbalanced by the decrease in conversion rate at lower temperature [15]. The EF operating conditions are advantageous by allowing for a smaller reactors, as well as high conversion rates and less demanding downstream handling. Although the capital cost is around 20% higher than the one required for fluidized bed, the mentioned advantages lead to lower fuel production cost [11, 15]. Figure 2.4 shows a schematic process diagram of the entrained flow gasifier.

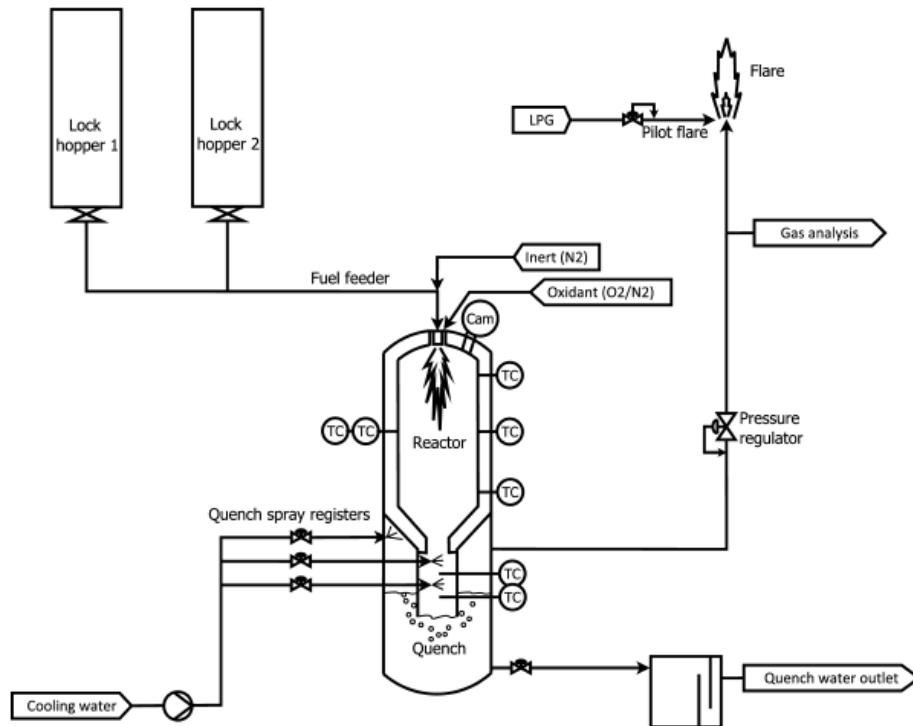


Figure 2.4: Schematic process diagram of entrained flow gasification plant [15]

The challenges typically associated with EF gasifiers are the pre-treatment of biomass for having finely sized fuel and the fouling and slagging of the reactor surfaces [6]. When using pyrolysis oil as a feedstock, both of these disadvantages are avoided at the level of the gasifier. Accordingly, entrained flow has been chosen as the type of gasifier for the process. Further details on the reactor design are mentioned in chapter 3 'Basis of Design and Model Results'.

2.2. Gas cleaning

In order to upgrade the syngas into a biofuel, it is crucial to clean it from contaminants and toxic substances that affect the downstream units. Amongst the impurities present in the syngas, chlorine and sulfuric compounds such as HCl and H_2S are required to be in very low quantities (few ppm depending on the catalyst tolerance) to avoid the degradation of catalysts and unit material, especially at high temperatures. When oxygen and/or steam are used as oxidizing agents, nitrogen compounds such as nitrogen oxides (NO_x) are less problematic and can be assumed to be in negligible amounts. The quantity and type of contaminants depend on the quality and composition of the biomass used as initial feedstock for pyrolysis. In case slagging occurs in the reactor, the slag behaviour is also a variable that needs to be considered for gas cleaning [15]. When pyrolysis oil is gasified at considerably high temperatures ($> 800^\circ C$), the product syngas has low tar content and the amount of solid char is also not significant. The choice of using a cyclone unit for separating the solid particles from the gas can be considered depending on the specificity of the process. Other considerations in gas cleaning include the presence of inert gases such as nitrogen, which are mostly converted in the gasifier to ammonia (NH_3) [41]. Nitrogen inert gas is usually used for safety considerations.

If a high cold gas efficiency (CGE) is required for the gasifier, the concentration of nitrogen can be minimized using a mass flow controller, as higher amount of nitrogen leads to lower CGE [43]. An alternative to nitrogen is CO_2 , which can be recycled back to the gasifier [15].

Prior to the gas cleaning units, it is important to reduce the temperature of the raw syngas from the entrained flow operating range (1200°C- 1600°C) to temperatures that are acceptable for downstream equipment. Amongst different options, this can be achieved by using a water quench, where the produced gases get "through a water spray chamber into a water bath" down the gasifier [41]. The fast cooling makes it dry, which allows for better ash removal from the water bath. Potentially, using a water quench is also helpful in driving the water-gas-shift (WGS) reaction in a subsequent reactor (called shift reactor). The WGS reaction is described as:



Consequently, the concentration of CO gets lower in favour of increased amount of hydrogen and CO_2 .

Furthermore, in order to remove sulfur compounds and carbon dioxide, diverse gas cleanup technologies exist. The processes differ in their removal process (physical/chemical and wet/dry), and in their operating temperature (cold, warm or hot gas cleanup) [7, 42]. A major classification of gas cleaning processes relies on the type of solvent used and the removal mechanism. The choice between chemical and physical solvents depends on the process cleaning and energy requirements, adding to economic and environmental considerations.

Physical solvents are usually favourable when the raw syngas has very high acid gas concentration. As physical solvents have high absorption of hydrocarbons, they are not optimal for the recovery of heavy hydrocarbons. The heat requirements for physical absorption are generally lower than the one for chemical absorption. On one hand, chemical solvent regeneration requires high temperatures. On the other hand, the desorption mechanism for physical solvents is based on pressure difference [7].

Physical absorption technologies that are commercially available include: Rectisol process with methanol washing at low-temperature; Selexol absorption process that uses solvent mixture of dimethyl ethers; and Purisol process with N-methyl-2-pyrrolidone. On the other hand, chemical absorption processes include organic (amine-based) solvents and inorganic solvents [2, 54]. Rectisol, Selexol and amine-based solvents have generally good removal capacity and high selectivity for hydrogen sulfide (H_2S) and bulk CO_2 [41].

2.3. Electrolysis process

The use of the electrolyzer products in an efficient way is one of the main targets of this thesis work. Hence, having an efficient electrolyzer is of high importance. Hydrogen is currently produced majorly from fossil-fuels. The mostly used fossil-based process is hydrocarbon reforming, which can be done through steam reforming, partial oxidation and autothermal reforming [36]. Alternative processes include the treatment of biomass and water splitting. The former includes biological processes (bio-photosynthesis and fermentation) as well as thermochemical processes, such as gasification, combustion and liquefaction. On the other hand, water can be split either by thermolysis, photolysis or electrolysis. The electrolysis efficiency is generally limited by the low hydrogen evolution rate and the high energy consumption [36]. Due to economic and technological constraints, around 0.02% of pure hydrogen (around 200 MW capacity) is currently produced through electrolysis. Electrolyzed hydrogen is still two to three times more expensive than fossil-based hydrogen with carbon capture and storage [10].

In a study done by the International Renewable Energy Agency (IRENA) on the cost reduction of electrolyzed hydrogen, called 'green hydrogen', several factors were identified as having a considerable impact on the cost of electrolyzed hydrogen. These include the electricity costs, the investment costs (CAPEX), the fixed operating costs (OPEX), the number of operating hours of the electrolyzer, as well as its balance of plant (BOP) components [10]. The investment cost will have a larger influence when the electrolyzer runs for a short time. In case renewable elec-

tricity cost and investment cost can be sufficiently reduced, green hydrogen can be competitive to fossil-based one when having a high number of operating hours (> 3000 h/yr) [10].

Electrolysis is defined as the electrochemical split of water into hydrogen (H_2) and oxygen (O_2), requiring electricity and heat input. The overall reaction is:



Important parameters in electrolysis are the current density (j), the reversible cell voltage (V_{rev}), and the area specific resistance (ASR), which are defined respectively as [39]:

$$j = \frac{I}{A} \quad (2.7)$$

$$V_{rev} = \frac{\Delta g}{2 \cdot F} \quad (2.8)$$

$$ASR = \frac{V_{op} - V_{rev}}{j} \quad (2.9)$$

With

- I is the current (A)
- A is the active area of the cell (m^2)
- Δg is the molar Gibbs free energy (kJ/mol)
- F is Faraday's constant ($96,485 C/mol$)
- V_{op} is the operating cell voltage (V)

An important equation that relates the moles of reactant consumed (n_R) to the current density is Faraday's law:

$$n_R = \frac{j \cdot A}{n_e \cdot F} \quad (2.10)$$

With

- n_e the number of electrons involved in electrolysis

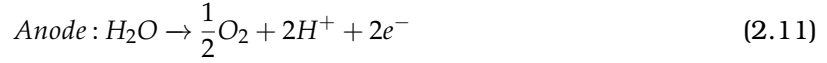
Moreover, there are several possible ways for the electrolysis process to happen, depending on the reaction scheme of water reduction to hydrogen and on the ions involved. Three major types of electrolysis are currently discussed in research papers:

1. Proton exchange membrane electrolysis (PEM)
2. Alkaline water electrolysis (AWE) and Anion exchange membrane (AEM)
3. Solid Oxide electrolysis cell (SOEC)

While alkaline electrolysis and proton exchange membrane are both being used in industries, solid oxide cell is still under research and development.

2.3.1. Proton exchange electrolysis (PEM)

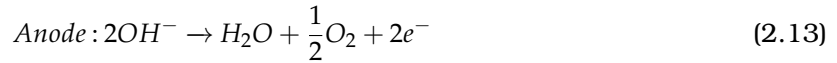
This type of electrolysis is based on the transfer of protons (H^+) through a membrane from the anode to the cathode. The following reactions result in H_2 and O_2 :



The membranes used in PEM allow for high proton conductivity, low gas permeability and can withstand high-pressure. One of the main disadvantages of PEM is the need to use noble metals (such as platinum catalysts or titanium bipolar plates) to enhance the hydrogen evolution reaction (HER) due to the highly acidic environment. This can potentially cause electrolyzer material degradation [12, 36].

2.3.2. Alkaline water electrolysis (AWE) and Anion exchange membrane (AEM)

In AWE, the alkaline electrolyte, composed of KOH and $NaOH$, is reduced to form hydrogen at the cathode and two hydroxyl ions (OH^-) are transferred through the electrolyte and diaphragm. ZrO_2 -based diaphragm and nickel (Ni) coated stainless-steel electrodes are usually used [10]. The hydroxyl ions react with water at the anode to give oxygen. The reactions of the alkaline electrolysis cell are as follows:



The operating conditions of AWE are in the range of 30-80°C. While alkaline electrolyzer is technologically mature, and has low energy requirements, it is limited by the current density ($< 400 \text{ mA/cm}^2$) and results in low energy efficiency. Moreover, due to the permeability of the diaphragm in the solution, the dissolved product gases in the electrolyte get mixed, which limits the ability of the stack to operate at high pressure and the lower power-operating range. If diaphragms of higher thickness are used, there will be more ohmic resistance, leading to lower current densities and lower efficiencies [10]. Nevertheless, improvements are being made in this regard. Other drawbacks of AWE include the formation of carbonates on the electrode, consequently decreasing the performance of the electrolyzer [10, 12, 36].

Accordingly, improvements have been made by combining the advantages of PEM and AWE into Anion exchange membrane (AEM) electrolysis. The hydrogen and oxygen evolution reactions being the same as in alkaline electrolysis, AEM differs in cell arrangement and operating conditions. There is a pressure difference between the cathode and the anode half-cells, which operate respectively at 35 bar and 1 bar. This difference helps in preventing the oxygen from passing over to the high-pressure half-cell, resulting in hydrogen with higher purity (99.9 %) than in AWE [12]. The main issue of AEM electrolyzers are stability and lifetime. Similarly to the next type of electrolysis discussed, AEM technology has not yet reached commercial maturity. Till now, there are few manufacturers of AEM electrolyzer, including Enapter [12].

2.3.3. Solid Oxide electrolysis cell (SOEC)

SOEC works at high pressure and high temperature mostly ranging from 500°C to 900°C. These operating conditions allow for many advantages, including enhanced kinetics, higher efficiency and lower electricity consumption. With better kinetics, high performance can be achieved with low-cost electrodes (such as nickel). In addition, expensive platinum group metals are not required as catalysts [10]. The membrane is composed of ceramic oxide electrolyte layers, typically made of yttria-stabilized zirconia (YSZ). The impermeability of the ceramic membrane allows to have products of high purity. SOEC can be operated as oxide conducting and proton conducting [58]. Contrary to low-temperature electrolysis, heat can be used as energy input for

SOEC, which gives the possibility of better thermal integration, especially with fuel-synthesis process [37].

In SOEC, water is reduced (at the cathode) to result in hydrogen and oxide ions (O^{2-}). Accordingly, the following reactions are involved in solid-oxide electrolytic cells:



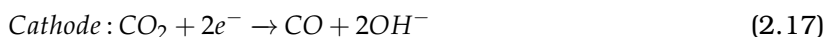
The major challenges of SOEC are high costs, low flexibility (shutdown/ramping), and mechanical failure of ceramic electrolyte layers. The thermo-chemical cycling leads to faster degradation and shorter lifetimes. In addition, there can be sealing problems at high differential pressure and electrode contamination by stack components (silica in sealants, pipes) [10]. The durability of SOEC has been studied at current densities reaching 0.8 A/cm^2 and at operating conditions of 650-850°C. The duration of the tests was mostly below 4,000h, but values of 9,000h and 10,000h were also reached in other tests [37].

In order to counter some of these problems, metal-supported solid oxide cells (MS-SOEC) have been developed. The aim is to use porous stainless steel or other metal to replace part of the Ni-YSZ electrode support. In this way, the support can have a lower thickness, enough for electrochemical function. This can reduce the cell material cost and lead to better cell mechanical strength. Other advantages have been associated with MS-SOECs, such as to tolerate rapid thermal cycling, large temperature difference (higher than 100°C/cm), and redox cycling. The latter is caused by the oxidation of Ni catalyst particles (used on the cathode) as a result of air leakage or high steam content. This will lead to volume expansion of the cathode and mechanical failure of the electrolyte. However, there is still a lack of data to clearly determine the cell performance and durability at harsh operating conditions and situations, such as startup/shut-down cycling, redox cycling, and rapid thermal excursions [58].

Moreover, there are still many challenges, in terms of MS-SOEC cell fabrication and operation, in order to achieve low degradation rate along with high efficiency and high power density. The difficulties for MS-SOECs are mainly in the oxidation of metal supports (causing fast degradation), in electrolyte deposition, as well as in the sintering of electrolyte and metal support [58]. The details of these are beyond the scope of this thesis.

Further, one of the applications of SOEC is the inclusion of CO_2 as an inlet stream to the electrolyzer. either fed alone or along with steam. The latter option is known as co-electrolysis. Depending on the process, the carbon dioxide can be sourced as a external waste or as a side-product within the process, each being a different Carbon Capture and Utilization (CCU) approach. Choosing the source of CO_2 depends on the energy requirement, which affects the overall efficiency and performance of the process. The cost of capturing CO_2 compared to have it as a waste exhaust gas from another industry needs also to be considered. Co-electrolysis is more advantageous than CO_2 electrolysis for two reasons: first, the reverse WGS reaction (RWGS) occurs in the electrolysis, which avoids the need of having a unit for additional CO_2 reduction through RWGS. The second is that there is less carbon deposition in the co-electrolyzer than in CO_2 electrolysis [47].

In a co-electrolysis process, adding to the reduction of water to hydrogen previously described in SOEC, CO_2 is reduced as follows:



Additionally, side reactions that usually occur are the WGS reaction and CO methanation [41].

Moreover, by studying different power-to-fuel systems integrated with solid oxide electrolysis and co-electrolysis, L. Wang et al. (2019) found that co-electrolysis can enhance the efficiency of the systems with fuel synthesis processes that are less exothermic (such as methanol/dimethyl ether) due to better heat integration. However, this effect was observed to be more limited for the production of methane and gasoline [37]. This can be explained by the observation that, for the same amount of fuel produced (same current density), co-electrolysis requires less steam to be fed into the stack, as steam is internally generated through the conversion of CO_2 to CO by RWGS [37].

2.3.4. Summary

After having discussed the operating principles of the main electrolysis systems under research and under operation, the principal characteristics of these technologies mentioned are summarized in table 2.1.

Table 2.1: Characteristics of electrolysis technologies. Adapted from [10]

	PEM	AWE	AEM	SOEC
Nominal current density (A/cm^2)	1-2	0.2-0.8	0.2-2	0.3-1
Operating temperature	50-80°C	70-90°C	40-60°C	700-850°C
Stack lifetime (hours)	50,000 - 80,000	60,000	> 5,000	< 20,000
Cold start to normal load (minutes)	< 20	< 50	< 50	> 600
Voltage efficiency	50-68%	50-68%	52-67%	75-85%

Considering the energy performance of process integration of biofuel synthesis, along with gasification and electrolysis, **solid oxide electrolysis cell** has been chosen as the electrolyzer type as it leads to higher energy efficiency and better heat integration in the system. This has been confirmed by a large number of studies aiming at biofuel production as well as large-scale electricity storage [4, 9, 14, 18, 34, 39, 41, 51, 55].

2.4. Syngas catalytic upgrading

The third major section of the integrated process is syngas catalytic upgrading aiming at the production of biofuel.

S. Ali et al. (2020) have reported that the external source of hydrogen added to the gasification process results in higher system efficiencies in case of bio-fuels synthesis [51]. The advantages lie in many aspects. The low hydrogen content in the syngas produced from gasification is one aspect. The clean syngas mixed with the hydrogen obtained from electrolysis can potentially be converted into one of the following biofuels: methanol (or further into Dimethyl Ether), Fischer-Tropsch diesel, gasoline or substitute natural gas (SNG).

In a study done on the synthesis of fuels integrated with SOEC electrolysis, F. Monaco et al. (2018) found that the production of substitute/synthetic natural gas (SNG) from gasified biomass (as a carbon source) gave the higher conversion efficiency (74%), compared to the conversion efficiency of DME and FT diesel (73% and 66% respectively) [14]. In another study done by L. Wang et al. (2019), different power-to-fuel pathways were studied using both solid-oxide electrolysis and co-electrolysis. The types of fuel considered were hydrogen, methanol (and dimethyl ether), methane and gasoline. The assessment of the system efficiency was done from the stack to system levels, including the electrolysis stack performance and durability, and heat integration at the system-level. The conversion efficiency found for each fuel based on the higher heating value is: around 95% for hydrogen, 83% for methane. 70-80% for methanol and dimethyl ether, and lastly 65% for gasoline [37]. Hence, both studies have found that the integration of solid oxide electrolysis with methane production led to higher efficiency than with gasoline, biodiesel and dimethyl ether. In addition, a gasification process has a higher cold gas efficiency (CGE) when an increased concentration of CH_4 is present in the syngas [15]. Although tiny amounts of methane is produced from entrained flow gasification, there would be no need for its removal in case of synthetic natural gas (SNG) production.

The biofuels are also compared in terms of CO_2 emission factor and the capacity to give energy on a weight basis evaluated using the Lower Heating Value (LHV). The Joint Research Centre of the European Commission (JEC) has done a "well-to-wheels analysis of future automotive fuels and powertrains" considering the context of Europe [40]. As explained in their report, the CO_2 emission factor accounts for the emissions produced from the complete combustion of the carbon present in the fuel. Hence, both LHV and CO_2 emission factor are independent of the production process and are only related to the chemical and physical properties of the fuel [40]. The properties of the fuels relevant to the integrated process studied are shown in table 2.2:

Table 2.2: Properties of various fuels. Adapted from [40]

Fuel type	LHV (MJ/kg)	LHV (MJ/L)	CO_2 emission factor (kg/kg)
Gasoline 2016 (E0)	43.2	31.4	3.17
Diesel	43.1	35.9	3.16
FT Diesel	44.0	34.3	3.12
Methanol	19.9	15.8	1.37
DME	28.4	19.0	1.91
LNG*	49.1	20.8	2.77

* The Liquefied Natural Gas (LNG) mentioned in the table is the EU mix 2016/2030. Although natural gas (LNG or CNG) has the highest energy content per weight (LHV MJ/kg), it does not have a higher energy density (MJ/L) than gasoline and diesel due to its lower liquid density. However, it is still more advantageous than gasoline and diesel in terms of CO_2 emission factor.

From the JEC well-to-tank study of various synthetic fuels, it is difficult to favour one fuel over another based on the results of the total energy expended and GHG emissions, Thus, the design option of the biofuel is based on the previously mentioned criteria, giving more weight to the overall process efficiency in the production of the biofuel and to the CO_2 emission factor. Accordingly, substitute natural gas (SNG) is chosen over the other fuels. More specifically, to

allow for the gas to be easily integrated in the current transportation fuel infrastructure, the final product of the integrated process is decided to be **compressed natural gas**.

It is important to note that methane produced from syngas (from biomass) is referred to as substitute natural gas (SNG or bio-SNG), in contrast with the conventional natural gas obtained from or as a fossil fuel. Similarly, the compressed natural gas obtained by converting the syngas resulting from bio-oil gasification is called bio-CNG, in order to avoid confusion with the fossil-based CNG.

Further, the methanation process for converting cleaned syngas to methane will be further explained in this section.

2.4.1. Overview on methanation

Methane production from syngas is a well researched and well established process. It has been first pioneered by Sabatier and Senderens in 1902, followed by other developments along the past century, as shown in figure 2.5.

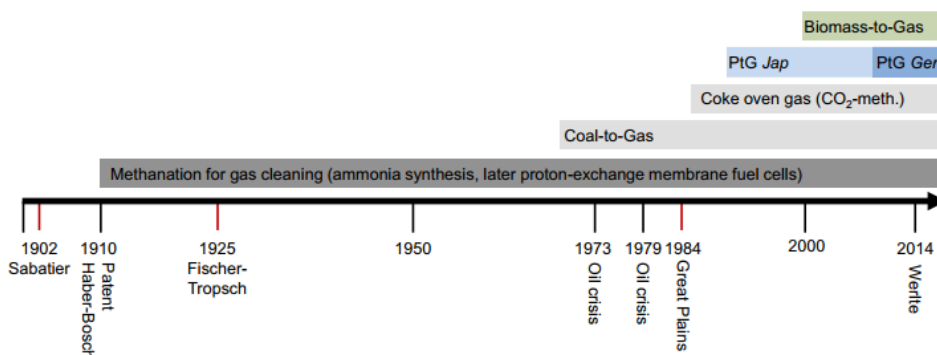


Figure 2.5: Timeline showing methanation development. [54]

The production of SNG (via CO methanation) using biomass as a feedstock has reached commercialization. GOBIGAS plant in Sweden is currently operating at a capacity of 20 MW (gas output) [54]. In addition, there are new emerging projects in Europe working on the same concept, such as the planned E.ON Bio2G project in Sweden, as well as projects run by the Biomass Technology Group (BTG) and the Energy Research Centre (ECN) in the Netherlands. Other plants are based on CO₂ methanation, such as E-Gas/PtG BETA plant in Germany [54].

After this brief overview of natural gas production history, the methanation process and currently developed reactor configurations are discussed. Methanation process involves the hydrogenation of CO and CO₂, accompanied with the reverse water-gas-shift (RWGS) reaction. The main and side reactions in the methane reactor are shown in tables 2.3 and 2.4 respectively:

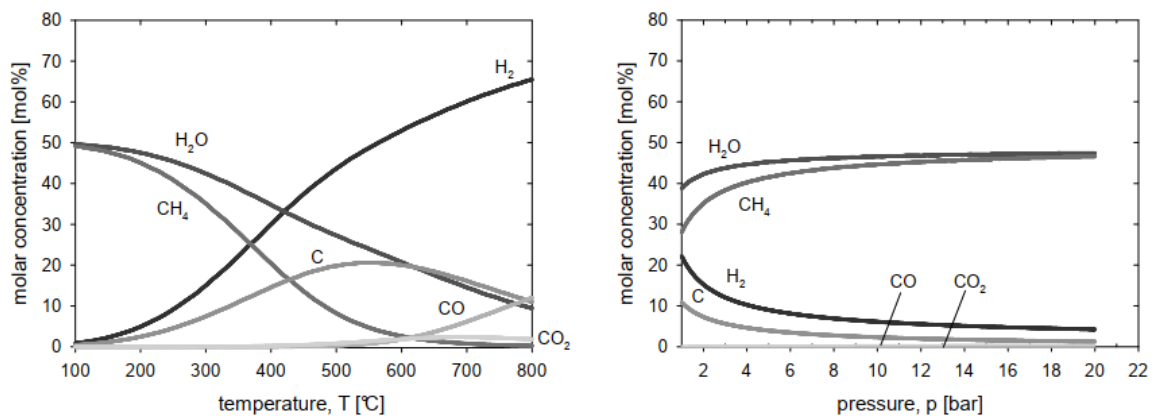
Table 2.3: Main reactions in methane reactor [33, 54, 59]

Reaction	Heat of reaction (Δh)
$CO + 3H_2 \rightarrow CH_4 + H_2O$	-206 kJ/mol
$CO_2 + 4H_2 \rightarrow CH_4 + 2H_2O$	-164 kJ/mol
$CO_2 + H_2 \rightarrow CO + H_2O$	41 kJ/mol

Table 2.4: Side reactions in methane reactor [33, 54, 59]

Reaction	Heat of reaction (Δh)
$\text{CO}_2 + \text{CH}_4 \rightarrow 2\text{H}_2 + 2\text{CO}$	247 kJ/mol
$2\text{CO} \rightarrow \text{C} + \text{CO}_2$	-172 kJ/mol
$\text{CH}_4 \rightarrow \text{C} + 2\text{H}_2$	75 kJ/mol
$\text{CO} + \text{H}_2 \rightarrow \text{C} + \text{H}_2\text{O}$	-131 kJ/mol

The production of methane can be optimized by having the suitable operating conditions and by avoiding catalyst deactivation. As the methanation reactions are highly exothermic, methane production is thermodynamically favoured at low to moderate temperatures (200°C to 500°C) and high pressures (> 5 bar) [35, 54]. At high temperatures (above 550-700°C), the formation of methane is limited and the catalysts are not stable. The effect of temperature and pressure on both CO methanation and RWGS reaction can be seen in figure 2.6. CO and CO₂ consumption, and CH₄ formation are mostly affected by pressure at values below 15 bar [35]. Further, an important process decision is whether CO₂ needs to be removed upstream or downstream the methane reactor. Whereas the reactor heating is limited by syngas dilution with CO₂, higher energy demand is required in case of an upstream gas compression of diluted syngas [54].

**Figure 2.6:** Effect of operating conditions on CO methanation and RWGS reaction [35]

2.4.2. Methanation reactors

There are three major types of reactors that are used for methanation: 1) fixed-bed ; 2) fluidized-bed ; and 3) three-phase reactors. As temperature control is a critical factor in methanation process, the temperature profile in the reactor is the main point of distinction between the methanation processes. The most common temperature profiles obtained are adiabatic, isothermal, and polytropic. The parameters that characterize the temperature profile are the heating rate and cooling rate [54]. Choosing the desirable temperature profile requires the assessment of advantages and limitations of each one. Depending on the preferred specifications, trade-off will be made between reaction rate and efficiency, cost, and complexity of setup.

Adiabatic and polytropic fixed-bed are the most common type of methanation reactors, followed by fluidized-bed reactors. They have been commercialized many decades ago by several company. One of the earliest methanation processes that uses fixed-bed reactors is Lurgi process. Another developed process that uses a series of adiabatic fixed-bed reactors with inter-cooling is the *Haldor – TopseTrem*TM process, commercialized by the Danish company of Haldor Topsoe [54]. A common configuration of the Trempp process with inter-cooling and gas recycling is shown in figure 2.7. Other types of reactor such as three-phase slurry reactors and micro-channel reactors are under research.

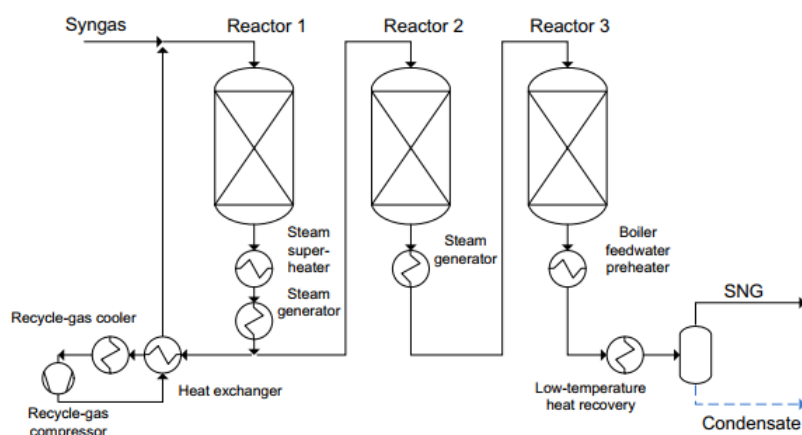


Fig. 7. Exemplary fixed-bed methanation with intermediate cooling and gas recycle (TREMP adapted from Haldrup Topsoe [35]).

Figure 2.7: TREMP process with three fixed-bed reactors in series with intermediate cooling and gas recycle [54]

In a fluidized bed reactor, the process is more difficult to managed and control. This type of reactor was implemented in many companies in Germany for methane production, using heat exchangers in the bed reactor. As for three-phase methanation, temperature control in the reactor is achieved using a liquid with high heat capacity. Some challenges of this reactor configuration include the evaporation and decomposition of the heat transfer fluid, adding to the gas-liquid mass transfer resistance [54].

2.4.3. Catalysts

In addition to the reactor configuration and the operating conditions, the choice of catalyst is a crucial point of consideration for methanation reaction.

Catalysts that were found to be active and efficient for syngas methanation are based on transition-metals such as nickel (Ni), cobalt (Co), iron (Fe) and on noble metals such as rhodium (Rh), ruthenium (Ru) and platinum (Pt) [54, 59].

Nickel-based catalysts are a suitable choice as they result in high activity and selectivity, good sulfur tolerance and they are less expensive than noble metals [1, 54, 59]. Moreover, nickel is available in considerable amounts with world resources of around 300 million tons in 2019, according to the U.S. geological survey [27]. Although iron is also relatively abundant (resources of 81 million tons [3]) and cheap, it has the lowest selectivity towards methane, along with ruthenium, amongst the most commonly used catalysts.

Research has been performed to improve the activity of Ni-based catalysts, especially for when operating at low temperatures. Ni/Al_2O_3 catalyst is one of the most commonly used catalyst. However, one of the main challenges faced is carbon deposition, which reduces its stability. This can be avoided when operating at pressures higher than 15 bar [13]. Further research is ongoing to increase the performance of Ni/Al_2O_3 .

In most cases, a support is required to obtain the high activity and selectivity of catalysts. Commonly used supports include hydrotalcites, zeolites, and metal oxide supports (SiO_2 , CeO_2 , TiO_2 ...) [54, 59]. Other types of supports have recently been developed, such as foams and biochar [54]. One of the main positive effects of supports is the increase in surface area, allowing a better dispersion of the metal particles. The activity of the catalyst is also enhanced through metal-support interactions, electron transfer between the metal and support and the formation of defect sites on the support [59].

In addition to supports, promoters are used to enhance the performance and stability of catalysts. Examples of promoters used with Ni catalyst are MgO , La_2O_3 [1, 54].

3

Basis of Design and Model Results

In this chapter, the basis of design of the integrated process, the model development and results are discussed. The gasification section is first tackled in section 3.1, followed by the gas cleaning section, the electrolyzer, and the methanation section in sections 3.2 to 3.4. The last section presents the sensitivity analyses performed on Aspen Plus for studying the effect of parameters on the performance of both the gasifier and methane reactor, and on the composition of syngas and methanation outlet stream respectively.

After having performed the literature review, the required design choices were made for completing the basis of design. The pyrolysis oil to biofuel process is designed to include solid oxide electrolysis cell (SOEC) as the type of electrolyzer, and to produce compressed natural gas (CNG) as the final product. The process flow diagram of the complete process is shown in figure 3.1.

3.1. Gasifier

The first unit that is modeled is the gasifier. The feedstock to the gasifier is wood-derived pyrolysis oil, which properties and elemental composition were taken from the experimental data of E. Leijenhurst et al. (2015) [11]. The bio-oil was obtained from the pyrolysis pilot plant of Biomass Technology Group (BTG) laboratory in the Netherlands. For the accuracy of the data, the pyrolysis oil properties were derived as the average values of the obtained oil stored in seven containers [11].

3.1.1. Pyrolysis oil feedstock

The composition of pine wood based pyrolysis oil is presented in table 3.1.

Table 3.1: Pyrolysis oil composition. Adapted from [11]

Proximate analysis	(wt%)
Moisture (a.r.)	21.1
Ash (dry)	0.09
Solids (a.r.)	0.01
Elements (dry)	(wt%)
C	57.4
H	6.6
N	<0.1
O (diff.)	35.9
S	0.0046

Pyrolysis oil contains organic compounds such as depolymerization products, including carboxylic acids, alcohols, aldehydes, ketones, esters, furans, and aromatics. These are mainly the products of depolymerization of cellulose, as the reactions with hemicelluloses and lignin are even more complex to estimate [6, 20]. For this reason, the gasification of pyrolysis oil is a very complex process involving a large number of species and reactions [46]. Nevertheless, some of the common reactions known to happen during gasification are [53]:

Table 3.2: Main reactions known to happen in a gasification process

Reactions	Heat of reaction ΔH (kJ/mol)	Reaction number
$C(s) + O_2 \rightarrow CO_2$	-394	R-1
$C(s) + 0.5 O_2 \rightarrow CO$	-111	R-2
$CO + 0.5 O_2 \rightarrow CO_2$	-283	R-3
$C(s) + H_2O \rightarrow CO + H_2$	+131	R-4
$H_2 + 0.5 O_2 \rightarrow H_2O$	-242	R-5
$C(s) + 2H_2 \rightarrow CH_4$	-75	R-6
$C(s) + CO_2 \rightarrow 2CO$	+173	R-7
$CO + H_2O \rightarrow CO_2 + H_2$	-41	R-8
$CH_4 + H_2O \rightarrow CO + 3H_2$	+206	R-9

In exception to sulfur, the inorganic and metal elements in the pine wood based pyrolysis oil are in negligible amounts, ranging from < 1 ppm to 9.5 ppm. All of Sb, Cr, Mn, Cu, Ni, Li, Sn Cd, Co and As are at less than 1 ppm concentration combined together. E. Leijenhurst et al. (2015) noted that 48% of sulfur is transferred from the pine wood to the pyrolysis oil, compared to 1% for potassium [11]. Due to the high temperature reached in the process and the minute concentration of inorganic compounds, it is safe to assume that no tar is formed in the gasifier. In addition, no nitrogen stream is used for the gasifier, which means that the only contaminant assumed to be present in the syngas is hydrogen sulfide (H_2S). Moreover, considering that the feedstock used is wood based pyrolysis oil with 0.01 wt% of solids and with an ash content of 0.09 wt%, ash and solid char are neglected in the outlet stream of the gasifier in the Aspen model. As the thesis project is focused on the integration of three major processes, gasification being one of them, it is reasonable to neglect the ash in the simulation

in order to simplify the model.

As previously explained in the literature review chapter (section 2.1), a smaller droplet size of the pyrolysis oil results in less char formation and higher heating rate. The particle size distribution needs to be specified on Aspen Plus as part of the required input data defining a non-conventional solid component. It was chosen to be below 60 μm , with 84 wt% being between 20 μm and 40 μm . However, the values inputted do not affect the results from the gasifier in the simulation as an equilibrium reactor based on minimization of Gibbs free energy is used to model the gasifier.

In accordance with Aspen plus guide "Getting Started Modeling Processes with Solids", the stream class in Aspen Setup needs to be specified as MCINCPSD in order to consider the carbon graphite (C) as a solid when being placed in the CIPSD class. This class includes all of MIXED, CIPSD and NCPSD substreams. While MIXED class accounts for all the vapour and liquid phases components, CIPSD is for representing solid components, and NCPSD for non-conventional components [57]. The property method used for the gasification section of the model is Peng-Robinson equation of state with Boston-Mathias modifications (PR-BM).

For simulating the gasification of pyrolysis oil on Aspen Plus, Zhang et al. (2020) represented the bio-oil as a non-conventional component (NC solid) [61, 62]. Accordingly, the proxanal, ultanal, and sulfanal component attributes are specified on Aspen based on its proximate and ultimate analysis. The property models used for calculating the enthalpy and density of the pyrolysis oil are 'HCOALGEN' and 'DCOALIGT' respectively. The flow rate of pyrolysis oil was set as 5 ton/h. Based on the experimental data of the composition of the wood-derived bio-oil (table 3.1) and without accounting for ash, the following component attributes are inputted on Aspen Plus:

Table 3.3: Ultanal Attribute of pyrolysis oil component

Ultanal	Ash	C	H	N	Cl	S	O
	0	57.49 ¹	6.6	0.05	0	0.0046	35.8554 ¹

¹ In order to preserve the atomic balance in the simulation, the 0.09 wt% of ash is accounted for as carbon and the amount of oxygen is the remaining quantity to have a total sum of 100 wt%.

Table 3.4: Proxanal and Sulfanal Attributes of pyrolysis oil component

Proxanal	Moisture	Fixed Carbon (FC)	Volatile Matter (VM)	Ash
	21.1	0.01	99.9	0
Sulfanal	Pyritic	Sulfate	Organic	
	0.0046	0	0	

3.1.2. Gasifier modeling

An overview of the gasification section model on Aspen Plus can be seen in figure 3.3.

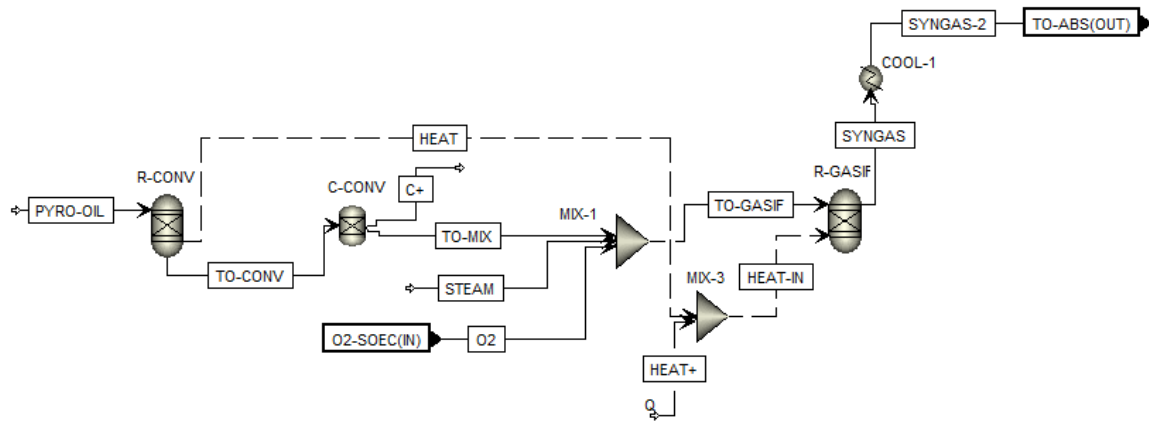


Figure 3.3: Screenshot of the gasification part of the simulation in Aspen Plus

The first unit after defining the feedstock stream is a yield reactor (RYield), needed to convert the non-conventional pyrolysis oil into its ultimate constituents, namely C, H, N, O, S. This step is only for modeling purposes for having the constituent atoms of the pyrolysis oil available for Aspen Plus in order to be able to compute and simulate reactions. As this phase usually happens at 500°C on average [62], the operating conditions of RYield reactor are 500°C and at a pressure similar to the one of the gasifier.

Using pyrolysis oil as a feedstock, there are three reaction zones that can be identified in the entrained flow (EF) gasifier (fig. 3.4):

- The droplet evaporation zone
- The partial oxidation zone
- The thermal reforming zone

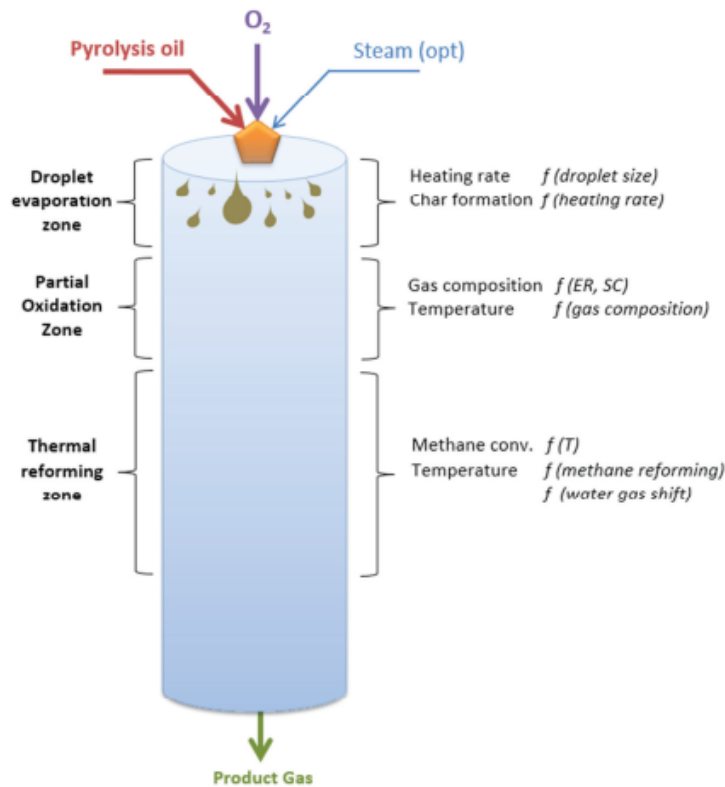


Figure 3.4: Typical reaction zones in EF gasifier [38]

The three reaction zones were accounted for in one reactor in the simulation, similar to real-life application. Further, in order to simplify the model, the following assumptions were made for the gasifier:

- All gases are considered ideal gases and are uniformly distributed.
- Reactions occur at a chemical equilibrium state and pressure loss is ignored.
- The gasification process is steady-state and quasi-adiabatic.

Considering these assumptions, the gasifier was modeled on Aspen Plus as an equilibrium Gibbs reactor (RGibbs), which solves multi-phase chemical equilibrium by minimizing Gibbs free energy [47, 62]. Simulating the gasification of pyrolysis oil using kinetics based on experimental data is an extensive work that goes beyond the aim of this thesis. The kinetics studies available in literature cannot be used for this process as the feedstock to the gasifier is different. Therefore, it was decided to model the gasifier using an equilibrium reactor, which allows to specify the desired products and to study the effect of input parameters on the outlet temperature and syngas composition, which are the most relevant in the context of process integration.

Several calculation options for RGibbs have been considered, along with other specifications, to identify which one gives results closer to experimental values, in terms of reactor

conditions and syngas composition. In order to compare the model with experimental findings, the work of Leijenhurst et al. (2015) [11] was used as a reference. Their work was performed using the pressurized entrained flow gasifier (PEFG) of the Energy Technology Centre located in Pitea, Sweden [15].

Accordingly, the following has been used to model the gasification process:

- The calculation option was chosen to be: 'Restrict chemical equilibrium - specify temperature approach or reactions'.
- The equilibrium was restricted by an entire system temperature approach of 0 °C.
- The components specified as 'possible products' in the equilibrium reactor are: C (pure solid), H_2 , CO , CO_2 , H_2O , CH_4 , O_2 , N_2 , S, and H_2S .

One of the most challenging steps in simulating the gasifier on Aspen Plus was to obtain values for the reactor outlet temperature and heat duty that are close to experimental findings. For this, a heat stream going out of the R-Yield reactor (*R-CONV* in the simulation) is inputted to the gasifier (*R-GASIF*), along with another heat stream to model the heat loss in the reactor. The use of the heat streams is to model the internal heat generation of gasification as a quasi-adiabatic process with a heat loss of 5% of the bio-oil thermal input (17.2 MJ/kg LHV) [11]. As a side note, the heat generated comes mainly from the combustion reactions¹ as some of the gasification reactions are endothermic [49]. The amount of heat loss for a large-scale gasifier was taken slightly higher than the one in literature [39, 55].

In the absence of an outlet heat stream, the amount of heat inputted will affect the outlet temperature of the reactor. In this case, the operating temperature of the gasifier is not a user specified input but an output.

There are many factors that influence the outlet temperature of the gasifier, including the oxygen equivalence ratio or OER (section 2.1) and the amount of steam fed. The amount of oxygen alter the extent of combustion reactions, and consequently the amount of carbon converted, also referred to as the Carbon-to-Gas (CtG) ratio or carbon-to-gas conversion [11]. This ratio was obtained experimentally by Leijenhurst et al. (2015) and found to be equal to 0.96 [11], which means that 4% of the inlet carbon is unconverted. Using the RGibbs reactor, all the carbon gets converted in the gasifier. Hence, 4% of the inlet carbon was manually split from the pyrolysis oil feed stream using a separator unit. The oxygen used for gasification is entirely produced from the electrolyzer downstream the process. The quantity of oxygen ($O_2.in$) required to achieve the desired oxygen equivalence ratio (OER or λ) is controlled using a design spec block and is calculated as:

$$O_2 \cdot in = \lambda \cdot stoic \cdot m_{pyro} \quad (3.1)$$

where m_{pyro} is the mass flow of pyrolysis oil (kg/h).

stoic parameter represents the stoichiometric amount of oxygen for the complete combustion of 1 kg/h of pyrolysis oil. This value depends on its elemental composition, and is thus specific to bio-oil derived from pine wood. In order to account for the unconverted carbon, *stoic* is computed on Fortran as:

$$stoic = \left(\frac{2 \cdot x}{Mw_C} + \frac{(x - 0.933)}{Mw_O} + 33.07 \right) \cdot Mw_O \quad (3.2)$$

where

- Mw_C is the molecular weight of carbon (C), 0.012 kg/mol
- Mw_O is the molecular weight of carbon (O), 0.016 kg/mol
- x is the amount of carbon present in the pyrolysis oil, that can be converted to syngas.

¹In contrast with a burner, only a fraction of the oxygen required for complete combustion is inputted to the gasifier. The oxygen fraction is known as the oxygen equivalence ratio [11].

Considering this, x is calculated as the original amount of carbon present in the pyrolysis oil (57.49%) subtracted by the percentage of unconverted carbon. When the value of CtG is changed, there are two fixed numbers in the computation of *stoic*:

- The first one represents the amount of oxygen required for complete combustion in regards to hydrogen (H) and nitrogen (N). In the case of wood-derived pyrolysis oil, the oxygen required for H and N is calculated using the weight fraction of each (table 3.1) and their respective molecular weight:

$$0.5 \cdot \frac{0.066}{0.001} + 2 \cdot \frac{0.001}{0.014} = 33.07 \quad (3.3)$$

- The second fixed number is the wt% of nitrogen and hydrogen combined, used to get the fraction of oxygen in pyrolysis oil as the remaining wt% at changing values of the carbon fraction. This value subtracted by 1 gives (-0.933), (taken from table 3.1).

The calculations of x and *stoic* are done using Fortran statements in a design spec block. It is important to note that the unconverted carbon is only accounted for in the calculation of the OER as the amount of inlet oxygen is directly related to the extent of combustion reactions. On the other hand, the amount of steam inputted is based on the carbon initially present in the pyrolysis oil considering a specific molar ratio.

In actual application, a higher amount of unconverted carbon leads to lower outlet temperatures. This is due to the fact that, at a fixed λ value, a lower amount of oxygen is stoichiometrically required when a larger portion of carbon is unconverted. Thus, $O_{2.in}$ would decrease at higher amount of unconverted carbon (as depicted in equation 3.1), which consequently leads to lower output temperature of the gasifier. Moreover, the extent of combustion reactions in the gasifier decreases at lower CtG values. Accordingly, this is equivalent to saying that higher carbon-to-gas ratio leads to an increase in temperature.

Along with the pyrolysis oil and the oxygen feed, steam is inputted to the gasifier, at an amount that is determined in a calculator block. The molar ratio of input steam to the amount of carbon initially present in the pyrolysis oil (for short steam-to-carbon (S-C) ratio) was specified using a Fortran statement. Moreover, the pressure of the gasifier was chosen to be 10 bar, which is within the range of the experimental reference [11]. Elevated pressures are advantageous as it leads to better economic performance of the integrated process by having lower cost in case of in-situ compression compared to post-gasifier compression of the output syngas.

3.1.3. Model verification and results

The gasifier model was first verified with experimental values from literature. Then, some of the parameters were tuned to improve the process in terms of operating conditions and syngas composition. For the model verification, a λ value of 0.4 and a steam-to-carbon (S-C) ratio of 0.05 were used. Accordingly, the outlet temperature of the gasifier was found to be 1347°C, which is 1.97% higher than the maximum temperature of the gasifier obtained experimentally at an oxygen equivalence ratio of 0.4 [11].

The composition of the obtained syngas is presented in table 3.5 and compared to experimental work of Leijenhurst et al. (2015) for pine wood based pyrolysis oil gasification. In order to compare the values obtained by simulation to the ones in literature, nitrogen is inputted to the gasifier at 15% volume fraction of the inlet feedstock.

Table 3.5: Syngas molar composition, at $\lambda=0.4$ and S-C=0.05 (T=1347°C and P=10 bar)

Gas composition (dry, N_2 free)	Aspen values	Experimental values [11]	Relative error (%)
CO	47.3%	45.6%	3.78
H_2	31.5%	30.1%	4.66
CO ₂	21.2%	22.5%	5.89
H_2/CO	0.665	0.66	0.86

As it can be seen in table 3.5, the syngas composition obtained by simulation is very close to experimental findings, with a relative error ranging from 3.78% for CO to 5.89% for CO₂.

The final syngas composition (presented in table 3.6) used for the integrated process was obtained with similar process conditions except for the steam-to-carbon ratio that was increased to 0.85. A higher amount of inlet steam was considered to obtain an outlet gasifier temperature within the range confirmed experimentally [11, 15]. Consequently, the H₂ to CO ratio was increased to 1.14 (71.4% higher) and the molar concentration of CO₂ increased from 21.2 mol% to 29.5 mol%. As the syngas is used for biofuel production, it has to be upgraded to maximize the production of methane. For this, the syngas composition needs to be at a specific stoichiometric feed ratio of the reactants, that is optimum for the biofuel synthesis reaction. In case of CO methanation, the reactants involved are H₂, CO and CO₂. Hence, the feed ratio is defined as [9]:

$$\text{Feed ratio} = \frac{H_2 - CO_2}{CO_2 + CO} = 3 \quad (3.4)$$

where H₂, CO, CO₂ are the molar flow rates in kmol/h of the gas components in the syngas.

According to literature [9], the methanation feed ratio is required to be minimum 3 at the inlet of the methanation reactor. The effect of syngas composition on the production of methane will be further investigated in section 3.5.

Table 3.6: Gasifier conditions and syngas properties obtained from Aspen Plus model

Gasifier conditions	
Temperature	1169.5°C
Pressure	10 bar
λ	0.4
S-C	0.85
Syngas composition (dry basis)	
CO	33.3%
H ₂	38.0%
CO ₂	28.7%
H ₂ /CO	1.14

By using an inlet heat stream to the equilibrium reactor RGibbs, and by controlling the amount of steam and oxygen inputted and the CtG ratio, it was possible to model the gasifier with an outlet temperature within the range obtained experimentally in literature. Moreover, the input heat to the reactor was equal to -8.42 MW, while the net heat duty of the reactor is 0, which means that the gasifier is simulated to operate in quasi-adiabatic conditions, considering 5% heat loss. The real application conditions of an entrained flow gasifier are close to adiabatic, with a heat loss that depends on the scale of the reactor.

3.2. Gas cleaning unit

The gas cleaning unit consists of the removal of hydrogen sulfide H_2S from the syngas. The raw syngas exits the gasifier unit at 1169.5°C and 10 bar with a H_2S concentration of 10.7 ppm. In order to avoid the poisoning of the catalyst for methanation, its concentration needs to be lowered to less than 1 ppm. The model of this section is shown in figure 3.5.

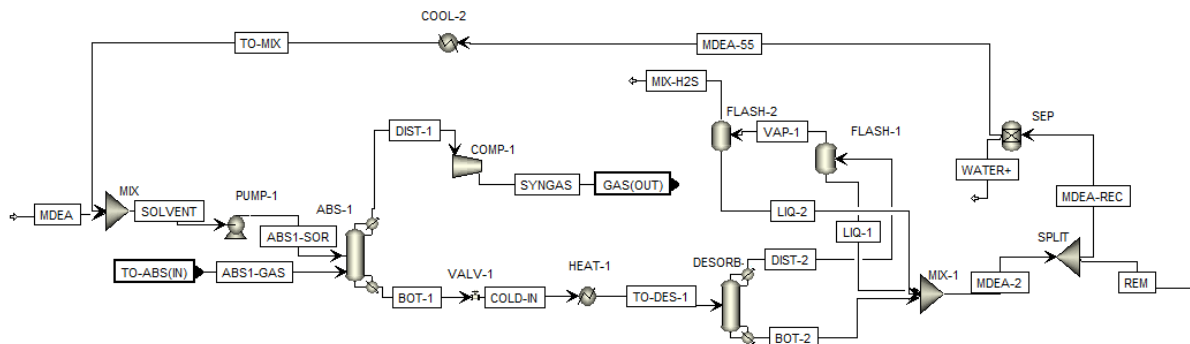


Figure 3.5: Screenshot of the gas cleaning part of the simulation in Aspen Plus

Before being inputted to the absorber column, the gas needs to be cooled to 60°C. The cooling is achieved by heat integration using other cold streams in the process. H_2S removal is done by chemical absorption, using methyl diethanolamine (MDEA) solvent. The advantages of MDEA are: high H_2S removal efficiency (98-99%), moderate operating conditions, and low capital cost [42]. The solvent is a mixture of 45 wt% of water and 55 wt% of MDEA at 40°C and it is pumped to 10 bar. The solvent stream was initially set to enter the column with a solvent-to-gas mass ratio of 0.16, before being recycled back after completing the first runs of the simulation. The H_2S absorber and desorber (stripper) units operate at low pressures, while CO_2 absorption process requires high pressures (> 40 bar) [56]. Hence, the main energy requirement for H_2S removal lies in the heating of the solvent in order to enhance the desorption process. It has been confirmed experimentally by Kopyscinski et al. (2010) that the presence of CO_2 as a reactant in the methane reactor allows for better CO conversion and it enhances methane and water formation at operating temperatures higher than 280°C [30]. In the meantime, high concentrations of CO_2 in the syngas will lower the methanation feed ratio. Therefore, there is a trade off between the energy required for CO_2 removal by MDEA absorption and the amount of power needed to have more hydrogen produced from electrolysis to achieve the target feed ratio when having high CO_2 concentrations. Based on simulation results from Aspen Plus, it was decided that CO_2 will not be removed and will be kept at its molar concentration (dry basis) of 28.67% (raw syngas) due to significant increase in methane production in the presence of CO_2 . The discussion of these results will be elaborated in section 3.4 tackling syngas catalytic upgrading.

Regarding the simulation of the absorption unit, the physical property package used was 'Electrolyte-NRTL' along with the specifications of Electrolyte Wizard, in order to model the electrolyte reactions with MDEA, water and hydrogen sulfide. In this way, Aspen Plus can account for all of $MDEA^+$, H_3O^+ , OH^- , HS^- , and S^{2-} ions and for Henry components. The column was modeled as a 'rigorous 2- or 3-phase fractionation for single columns' (Radfrac unit). It was specified as having 15 stages with no condenser or reboiler. Although the absorber can be run at lower pressure, the syngas is kept at the operating pressure of the gasifier (10 bar). The condenser pressure of the absorber is 9.5 bar and the stage pressure drop was set at 0.03 bar. This leads to lower power requirement for compressing the syngas for the methanation process. In order to ensure that the absorption column converges properly in Aspen Plus, the efficiencies specifications were changed. The efficiency type was set to 'Murphree efficiencies' and the component efficiency of H_2S at the first and last stages was set to 0.98, according to literature [42, 56]. H_2S was absorbed at an efficiency of 99%, leading to a

concentration close to 0 ppm in the distillate stream.

The bottoms of the absorber (contaminated solvent) was depressurized to 2.2 bar before being heated to 105°C to enter the stripper, where the solvent was partially cleaned from H_2S gas. The stripper column was modeled as 'RadFrac' unit with 19 stages, with a partial-vapor condenser and a kettle reboiler. The molar reflux and boilup ratios were initially set as 0.01 and 0.2 respectively. Both ratios were then increased to 0.4. The condenser pressure was set to 1.2 bar and the column pressure drop to 0.2 bar. The distillate passes then into two flash drums to separate the gases from the remaining water in the distillate of the stripper. These gases mainly consist of hydrogen sulfide along with other components of the syngas (H_2 , CO and CO_2) that were absorbed by MDEA in the bottoms of the absorber column. While the first flash drum was set to operate at 95°C and a pressure drop of 0.01 bar, the second one operated at 40°C and a pressure drop of 0.8 bar. The water from the liquid product of the flash drums was recycled with the solvent. When the raw syngas was cooled to 60°C, the water got liquefied and hence ended up mostly in the bottoms stream of the absorber. Even though the MDEA solvent has an excess amount of water, there is an advantage in recycling the water from the stripper. The recovered solvent leaves the stripper at roughly 110°C and it has to be cooled back to 40°C to be recycled to the absorber column. As the recycled water is at lower temperatures (95°C and 40°C), the MDEA-water mixture gets cooled to around 76°C. Using a separator unit, part of the water is removed from the MDEA solvent recycle stream to keep a MDEA mass fraction close to 55 wt%. The recycled solvent is then cooled to 40°C before entering the absorber column. A small fraction of the recycle stream needed to be split for the recycle loop to converge in Aspen Plus.

Moreover, the mixture of recovered gases ended up with a composition of: 63.1 mol% of CO , 16.8 mol% of CO_2 , 0.87 mol% of H_2 , 0.28 mol% of H_2S and 19.0 mol% of H_2O . The cleaned syngas in the distillate of the absorber column is at 47.5°C and 9.5 bar. For the syngas to be compressed to 20 bar, the ratio of the outlet pressure to the inlet pressure is less than 4. Hence, only one compressor is required. The heating up of the gas due to compression work is also advantageous as the inlet stream to the methane reactor needs to be heated to temperatures higher than 200°C. The compressor was set as isentropic with an efficiency of 90% and a mechanical efficiency of 98%, in accordance with literature [55].

3.3. Electrolyzer

In this section, the modeling of the solid oxide electrolysis cell (SOEC) is explained. The electrolyzer is an important part of the process as its main products, hydrogen and oxygen, are integrated in the system in order to enhance its efficiency. The simulation of the SOEC is presented in figure 3.6.

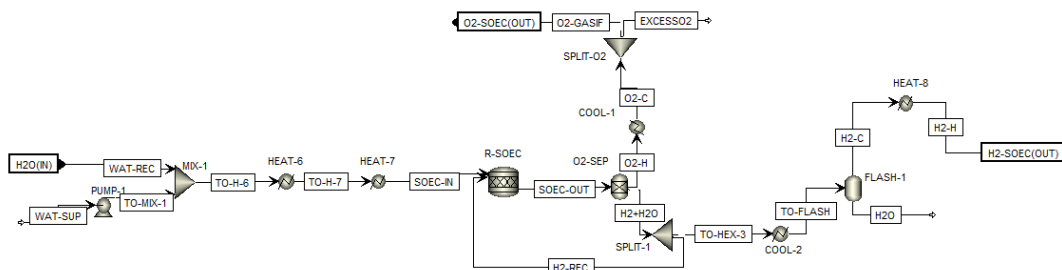


Figure 3.6: Screenshot of the steam electrolysis part of the simulation in Aspen Plus

3.3.1. SOEC modeling

Aspen Plus library does not include a unit operation model for solid oxide electrolysis. SOEC model is therefore built using a stoichiometric reactor, along with design specifications [9, 41]. While the electrolyzer is modeled using the non-random two-liquid (NRTL) property method, the rest of the electrolysis block in Aspen (called 'SOEC') is modeled using Redlich-Kwong-Soave equation of state with Boston-Mathias modifications (RKS-BM). The inlet stream to the electrolyzer is composed of the water recovered from the methanation section, and an additional quantity of water (called surplus water) that is needed to produce sufficient amount of hydrogen for syngas upgrading. The amount of water required is controlled using a design spec block on Aspen. The feed ratio is set at 3 and is defined in the block as in equation 3.4 except that two hydrogen components are used: one present in the syngas, and one produced from the electrolyzer. The surplus water is first pumped before being heated to the cell operating conditions.

The operating conditions of the electrolyzer were specified as 700°C and 20.1 bar. Moreover, the water-splitting reaction (3.5) was put under 'Reactions' tab with a fractional conversion of water of 0.8 (80%). The extent of reaction of 80% is in accordance with SOEC modeling work in literature [48]. The operating conditions and specifications of the SOEC stack were taken in accordance with the work of L. Wang et al. (2019), Anghilante et al. (2019) and S. Ali et al. (2020) [37, 48, 51].



To simplify the model, pressure losses and changes in kinetic and potential energies were neglected [51]. Considering the scope of this thesis, the SOEC is modeled to have a realistic situation of power consumption and cell efficiency, without further detailed analysis in terms of kinetics and electrochemistry.

To simulate the production of oxygen on the anode, a separator block is used to have the oxygen on a separate stream, which is then split into a recycle stream that is used as a gasifying agent and a stream of excess oxygen. The amount of O_2 that goes to the gasifier is controlled by a design-spec block, as previously explained in section 3.1. Before being split, the oxygen product stream is cooled to 55°C. Having the oxygen at low temperature is an advantage in terms of safety as well as for better heat integration in the system.

For the purpose of ensuring the reducing condition on the cathode, 20% of the exhaust of the cathode was recycled back to the cell after the separation of oxygen.

The reactions involved in the functioning of the solid oxide electrolysis cell are depicted in figure 3.7.

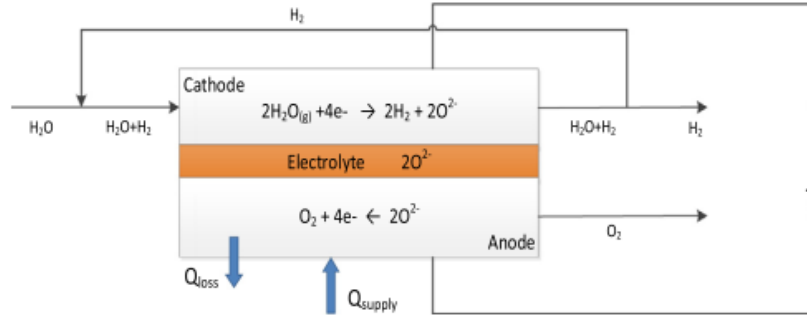


Figure 3.7: Schematic of Solid oxide electrolysis cell [51]

A flash drum, operating at 45°C and with a pressure drop of 0.1 bar, is used to separate the hydrogen gas from liquid water. The hydrogen is then heated to 140°C, which is the temperature of the cleaned syngas after being compressed to 20 bar. As the electrolysis cell is operating at 20 bar, there is no need for further compression of the produced hydrogen. For a total inlet steam flow of 11093.4 kg/h, 8210.09 kg/h of oxygen and 1071.68 kg/h of hydrogen are produced as final streams after separation. The amount of unreacted steam is 1811.72 kg/h and is at 45°C and 20 bar after the flash drum.

3.3.2. Electrochemical parameters

The important parameters to obtain the electricity consumed by the SOEC were calculated on Matlab. The reversible voltage of the cell or Nernst voltage (V_n) is computed as:

$$V_n = \frac{-\Delta G_f}{2 \cdot F} - \frac{R \cdot T}{2 \cdot F} \ln \left[\frac{y_{H_2O}}{y_{H_2} \cdot y_{O_2}^{0.5}} \left(\frac{P}{P_{std}} \right)^{-0.5} \right] \quad (3.6)$$

where

- F is Faraday's constant, equal to 96 485 C/mol,
- ΔG_f is the Gibbs free energy of formation of water, which is 237 000 J/mol,
- R is the universal gas constant (8.314 J/mol.K),
- y_i is the molar fraction of component i ,
- P_{std} is the atmospheric pressure (1.013 bar), and
- P, T are the pressure and temperature of the electrolyzer.

The area-specific resistance (ASR) is related to temperature and pressure through equation 3.7:

$$ASR(T, P) = 35.51 \cdot \exp(-0.0057 \cdot T) \cdot \exp(-0.021 \cdot P) \quad (3.7)$$

The relation between ASR and the cell pressure has some uncertainties at pressures higher than 10 bar. In order to account for this, the ASR is taken as the average of the ASR value calculated from equation 3.7 and the value from the same equation without the pressure term [9]. Accordingly, V_n and ASR are found to be equal to 1.33 V and $0.115 \Omega \cdot cm^2$.

For the SOEC performance to be at its peak value, the operating voltage (V_o) and the current density (j) were considered to be at thermo-neutral conditions (V_{tn} and j_{tn} respectively). j_{tn} is calculated as:

$$j_{tn} = \frac{(V_{tn} - V_n)}{ASR} \quad (3.8)$$

The thermo-neutral voltage of the SOEC was considered to be 1.45 V, resulting in a thermo-neutral current density of 1.05 A/cm^2 . Moreover, the electrical power consumed by the electrolyzer (P_{soec}) was calculated using the faradic current (I_f), which depends on the production rate of products:

$$P_{soec} = V_o \cdot I_f \quad (3.9)$$

and

$$I_f = n_R \cdot n_e \cdot F \quad (3.10)$$

where n_R is the fraction of the molar flow of the inlet reactant that undergoes electrochemical reactions (mol/s) and n_e is the number of electrons involved in reduction of steam. Faraday's law correlates the reactant consumption rate n_R to the Faradic current, as seen in equation 3.10.

n_R was calculated as:

$$n_R = n_{in} \cdot f \cdot x \quad (3.11)$$

where

- n_{in} is the inlet molar flow rate of the electrolyzer,
- f is the reactant fraction of n_{in} , which takes into consideration the recirculation of 20% of the cathode outlet, and
- x is the extent of reaction.

The extent of reaction (x) is referred to in literature ([9] and [39]) as the "reactant utilization" to account for the percentage of reactant that reacts in the cell. In the simulation of Aspen Plus of this study, n_{in} was 769.7 kmol/h or 213.8 mol/s . Considering an extent of reaction of 80% and a reactant fraction of 83.3%, n_R was found to be 142.5 mol/s . Hence, I_f was found to be $2.7498 \cdot 10^4 \text{ kA}$. Dividing the faradic current by the current density, the total active area (A) of the SOEC hardware is 2611.8 m^2 at thermo-neutral condition. The complete SOEC system was assumed to consist of 150 repeating units of 50-cell stacks, and each set of 150 units forms a module. Considering an active area of 87.7 cm^2 for each cell, similar to the design of Topsoe Fuel Cell [37], 40 SOEC modules are needed to have a total area of 2611.8 m^2 .

The theoretical power consumed by the electrolyzer is then equal to 39.87 MW. When calculating the actual electrical consumption, heat losses of 3% and losses from the inverter and other components of 2% are taken into consideration. This results in an actual power consumption (P_e) of 41.86 MW_{el} .

The main parameters and characteristics of the SOEC of this study are listed in table 3.7 and are compared to literature values.

Table 3.7: Main parameters of SOEC in this study and in two other studies

Parameter	This study	Pozzo et al. (2015) [39]	Giglio et al. (2015) [9]
V_{tn} (V)	1.45	1.44	1.29
j_{tn} (A/cm^2)	1.05	1.271	1.24
V_n (V)	1.33	-	1.03
ASR ($\Omega \cdot \text{cm}^2$)	0.115	0.340	0.212
n_{in} (mol/s)	142.5	8.20	64
I_f (kA)	$2.7498 \cdot 10^4$	557.8	7748
A (m^2)	2611.8	43.9	626
P_e (kW)	41866	810.2	10170
P_e/A (kW/m^2)	16.03	18.46	16.24

The main electrochemical parameters of the electrolyzer in this study are in accordance with values found in literature. As the faradic current is proportional to the amount of inlet

reactant to the SOEC, the values of I_f , the active area (A) and the input power (P_e) in this study are considerably larger than in the two other studies (table 3.7). Moreover, the ratio of P_e to A in this work is close to the one obtained by Giglio et al. (2015) [9], which process analysed is steam electrolysis.

3.3.3. Electrolysis energy demand

The total energy demand (enthalpy) ΔH for the electrolyzer includes the consumed electricity, represented by Gibbs free energy (ΔG), and the heat demand, represented by the entropy $T\Delta S$, as shown in equation 3.12.

$$\Delta H = \Delta G + T\Delta S \quad (3.12)$$

The change in electricity demand as well as heat demand with the increase in temperature have been studied by S. Ali et al. (2020) and is shown in figure 3.8.

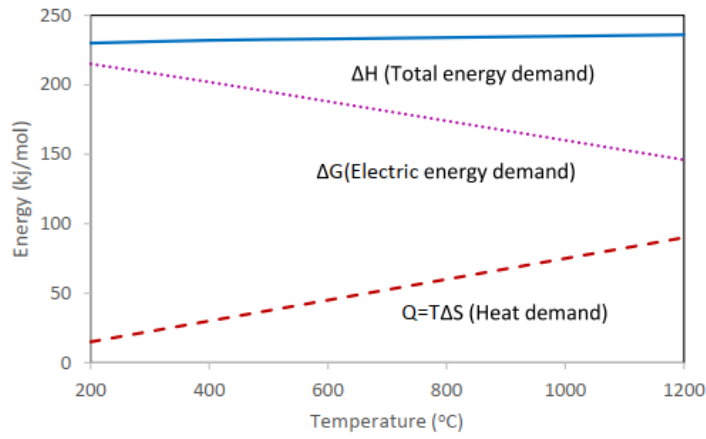


Figure 3.8: Electrolysis energy demand as a function of temperature [51]

In case of higher temperature electrolysis, lower amount of electricity is required in order to have the same production rate. Referring to figure 3.8, as the total energy demand is constant, the electrical energy is compensated by heat as temperature increases. Consequently, there would be less reliance on an external source of energy in case enough heat is generated in the system. The other advantage is that the SOEC will be less affected by the intermittency of the renewable electricity source. This is a critical point for solid-oxide electrolysis as it is vulnerable to degradation caused by excessive thermo-chemical cycling during shutdown and ramping periods [10].

The heat demand of the SOEC was calculated as the energy required to heat the inlet stream to the cell, using the following formula:

$$Q = \dot{m} \cdot C_p \cdot \Delta T \quad (3.13)$$

Considering a mass flow rate (\dot{m}) of 0.8 kg/s, a temperature difference (ΔT) of 655 and a heat capacity (C_p) of 7.30 kJ/kg.K, adding to 1888.65 kJ/kg as the heat of vaporisation of water, the heat demand for the electrolyzer was found to be 5336.12 kW or 5.34 MW. The total energy demand is then 47.2 MW, with the power requirement representing 88.7% of it.

3.4. Syngas catalytic upgrading

The last section of the process is bio-fuel synthesis, aimed to produce methane, more specifically compressed natural gas (bio-CNG) for transportation use. This part of the integrated system constitutes the last block in Aspen Plus simulation, which is presented in figure 3.9.

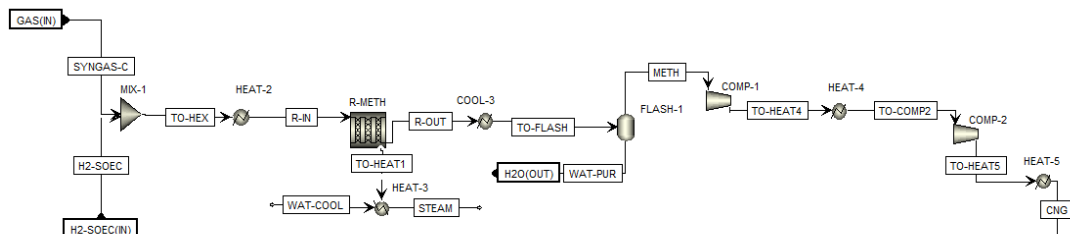


Figure 3.9: Screenshot of the methanation part of the simulation in Aspen Plus

3.4.1. Methane reactor modeling

Prior to undergoing methanation, the syngas stream needs to be adjusted in terms of amount of hydrogen and temperature. The initial feed ratio obtained from the clean syngas was:

$$\text{Feed ratio} = \frac{H_2 - CO_2}{CO_2 + CO} = \frac{111.2 - 83.6}{83.6 + 96.39} (\text{kmol}/h) = 0.15 \quad (3.14)$$

At this value, the inlet and outlet streams of the methanation reactor had the following molar compositions (dry basis):

Table 3.8: Molar composition (dry basis) of the inlet and outlet streams of the methanation reactor on Aspen Plus with a feed ratio of 0.15

	Inlet stream	Outlet Stream
CO	33.3%	32.2%
H ₂	38.0%	30.2%
CO ₂	28.7%	33.1%
CH ₄	0.0%	4.6%

The operating conditions of the reactor are T= 360°C and P= 20 bar. Further details about the reactor modeling will be discussed later. As it can be seen from table 3.8, when feeding the cleaned syngas without upgrading it with hydrogen, the concentrations of CO and H₂ decreased slightly and the one of CO₂ increased. The equilibrium of the water gas shift reaction would be towards the products when CO and water are at high concentrations. This could explain why more CO₂ was produced than consumed. When leaving the gasifier, the raw syngas had a water concentration of 42.5 mol% when having a steam-to-carbon ratio of 0.85 (molar based). As the syngas was cooled down to 60°C to enter the MDEA absorber unit, the water liquefied and was separated from the syngas in the absorber. This resulted in a concentration of water in the cleaned syngas of 0.6 mol%, being all water vapour. When feeding the cleaned syngas to the methane reactor, the amount of water increased to 4.9 mol%. Moreover, a small amount of methane was produced, resulting in a concentration of 4.6% (dry basis). This shows that the the feed ratio of the syngas needs to be adjusted to its optimum value of 3 (eq. 3.4) for methane production. For this, the hydrogen produced from SOEC was mixed with the syngas at similar conditions (at 140°C and 20 bar), as explained in section 3.3.

To simulate the methanation reactions, the thermodynamic model (called property method in Aspen Plus) needs to be able to calculate the binary interaction and other parameters for a mixture of non-polar and polar compounds, adding to light gases [13, 32]. Based on this, the chosen property method was Redlich-Kwong-Soave equation of state with Boston-Mathias modification (RKS-BM).

The methanation reactor was simulated using kinetic data. Kopyscinski's kinetic model was chosen due to the detailed experimental results of the model found in literature [30, 31], in addition to the presence of studies that include the simulation of methanation reactions on Aspen Plus using Kopyscinski's model [13, 32]. The kinetic studies were performed using a fluidized bed reactor and "a commercial Ni-alumina catalyst (50 wt% Ni/Al₂O₃, BET surface area ¼ 183 m²/g)" [30, 31]. The fluidized bed allows for isothermal operation and is thus a good option for highly exothermic conditions. As previously explained in section 2.4, nickel catalysts on metal support have high selectivity and activity, in addition to low price, which makes it a very suitable catalyst for methanation [54]. Considering that the reactions happen in a gaseous phase under high pressure and in a fluidized bed, the Aspen Plus reactor type that is best suited is a Plug Flow Reactor (PFR), in line with Liu et al. (2016) [32].

In accordance with the experimental kinetic study of Kopyscinski et al. (2010), the assumptions considered for modeling the reactor are [30]:

1. The PFR operates at steady-state conditions.
2. The gases behave according to ideal gas law.
3. The reactor is isothermal and is cooled, generating steam.
4. Pressure loss is neglected
5. Carbon deposition does not occur.
6. Intraphase transport resistance is ignored considering that the thickness of the catalyst is low.

Concerning assumption 3, the isothermal condition of the reactor has been confirmed by the experimental results of Kopyscinski et al. [30]. At isothermal conditions, the choice of the reactor temperature is critical. There are many factors that need to be considered for this. Firstly, experimental data of Kopyscinski et al. are best fitted by the kinetic model used, at temperatures between 280 and 360°C [30]. Secondly, the reactor temperature should allow for the catalyst to be activated, while still being below the equilibrium temperature of methanation [13]. Hence, in the simulation, the inlet stream (syngas with adjusted hydrogen concentration) is heated to 280°C prior entering the reactor. The cooling of the reactor to obtain isothermal conditions can be achieved in different ways. In Aspen Plus model, while keeping the temperature below 360°C, it is assumed that the heat from the methanation reactions is used to generate super-heated steam. Accordingly, using 8000 kg/h of demineralized water resulted in steam at 822°C. This superheated steam can be used to heat a cold stream in the process. Identifying which stream can be heated with it requires a heat integration study and heat exchanger network analysis, which will be tackled in the next chapter (ch. 4).

Regarding assumption 5, it is safe to assume that there is no carbon deposited due to coke formation for temperatures below 400°C and at high pressures (above 15 bar) [13]. For this reason, the operating pressure of the reactor is chosen to be 20 bar, being the same pressure value in the study performed by Liu et al. (2016) [32], which is used as a reference for model verification.

3.4.2. Methanation kinetics

In the kinetic study done by Kopyscinski et al. (2010), CO methanation and the water gas shift (WGS) reactions are considered. It has been found experimentally in multiple studies that the presence of CO, even in small amounts, inhibits the methanation of CO₂ [16, 30, 54]. One of the identified causes is that CO adsorption on the surface of metal catalyst is significantly faster than CO₂ adsorption. Moreover, CO₂ methanation mechanism includes the reduction of CO₂ to CO. This means that the carbon dioxide is first adsorbed and dissociated into CO, which will undergo hydrogenation to form methane. This implies that after the dissociation step, the route of CO₂ methanation is likely to be similar to the one of CO [16, 54, 60]. For these reasons, the kinetic model used to simulate methane production does not need to account for

CO₂ methanation.

In the experimental work of Kopyscinski et al. (2010), several kinetic models have been studied, each having a different assumption for the rate-determining step of CO methanation. The elementary steps of this process using nickel catalyst are not agreed upon in literature and two mechanisms have been suggested. The first one includes molecular adsorption and dissociation of CO with adsorbed carbon (C*) as an intermediate (reactions 3.15 and 3.16), which then undergoes a series of hydrogenation reactions to result in methane. The second mechanism proceeds via COH_x oxygenated compound as an intermediate.



The models have been discriminated using a simplified form of the Bayesian information criterion (BIC). It is based on the number of parameters (n_p) and data points (n_{dp}), and the sum of squares of the residuals:

$$\text{BIC} = n_{dp} \cdot \ln\left(\frac{\text{RSS}}{n_{dp}}\right) + n_p \cdot \ln(n_{dp}) \quad (3.17)$$

The most accurate models are those with the lowest BIC, which translates into those with the lowest RSS value, as all models have the same number of parameters and data-points [30]. Based on BIC discrimination, three models were found to have the lowest RSS (6b, 12b, and 14b), as well as the most fitted to the experimental data at the temperature range of 280-360°C. The RSS values of these three models were statistically similar, with a deviation lower than 2.5%. In these models, the formation of carbon surface species is fast, resulting in a negligible surface coverage of CO. Moreover, it was suggested that there was no considerable influence of hydrogen adsorption on the reaction rates. The reaction of the surface carbon species (C*, CH*, and COH*) is assumed to be the rate-determining step (RDS), along with a strong adsorption of hydrogen atoms (H*) and water adsorption as a hydroxyl species (OH*) [30].

Accordingly, the kinetic model used for the simulation of methanation of Aspen Plus was chosen to be model 12b in the study of Kopyscinski et al. (2010) [30]. In this model, it is assumed that the RDS is:



The rate equations of CO methanation and WGS reaction of the kinetic model 12b are respectively:

$$r_1 = k_1 \cdot \frac{K_C \cdot p_{\text{CO}}^{0.5} \cdot p_{\text{H}_2}^{0.5}}{(1 + K_C \cdot p_{\text{CO}} + K_{\text{OH}} \cdot p_{\text{H}_2\text{O}} \cdot p_{\text{H}_2}^{-0.5})^2} \quad (3.19)$$

$$r_2 = k_2 \cdot \frac{K_\alpha \cdot p_{\text{CO}} \cdot p_{\text{H}_2}^{-0.5} \cdot p_{\text{H}_2\text{O}} - \frac{p_{\text{CO}_2} \cdot p_{\text{H}_2}^{0.5}}{K_{\text{eq}}}}{(1 + K_C \cdot p_{\text{CO}} + K_{\text{OH}} \cdot p_{\text{H}_2\text{O}} \cdot p_{\text{H}_2}^{-0.5})^2} \quad (3.20)$$

The methanation kinetics are based on the Langmuir-Hinshelwood approach, having the following general reaction rate expression:

$$r = \frac{[\text{Kinetic term}] \cdot [\text{Driving force}]}{[\text{Adsorption term}]} \quad (3.21)$$

All of the kinetic term, driving force and adsorption term are expressed in terms of kinetic constants (rate constants), adsorption constants and the partial pressure of reactants and products. In the temperature range of 280-380°C, the equilibrium constant of methanation has a large value, which implies that the equilibrium of the CO methanation reaction is strongly towards the product side. Hence, the reverse reaction of methane reforming can be ignored. Considering that, the rate equation for methanation does not account for the reverse reaction [30]. Therefore, the partial pressures included in the kinetic rate equations are for components

CO, H₂, CO₂ and H₂O. Moreover, it is assumed that the methanation and WGS reactions occur on the same sites of the metal catalyst. Thus, the rate equations have the same denominator [30].

The kinetic constants and adsorption constants are formulated based on a finite reference temperature T_{ref} , with the following general expressions respectively:

$$k_i = k_i(T_{ref}) \cdot \exp\left[\left(\frac{\Delta E_a}{R \cdot T_{ref}} - \frac{\Delta E_a}{R} \cdot \frac{1}{T}\right)\right] \quad (3.22)$$

$$K_j = K_j(T_{ref}) \cdot \exp\left[\left(\frac{\Delta H}{R \cdot T_{ref}} - \frac{\Delta H}{R} \cdot \frac{1}{T}\right)\right] \quad (3.23)$$

where

- $k_i(T_{ref})$ is the pre-exponential factor of the rate constant,
- $K_j(T_{ref})$ is the pre-exponential factor of the adsorption constant,
- E_a is the activation energy (kJ/mol),
- H is the heat of adsorption (kJ/mol),
- R is the universal gas constant of value $8.314 J/mol.K$
- T is the reactor temperature (K), and
- T_{ref} is the reference temperature of value $325^\circ C$ ($598.15 K$)

The kinetic parameters along with their 95% highest posterior density (HPD) intervals are shown in table 3.9:

Table 3.9: Kinetic parameters for model 12b [30]

Parameter	Value
$\ln k_1(T_{ref})$	0.15 ± 0.02
$E_{a1}/(R \cdot T_{ref})$	14.9 ± 0.5
$\ln k_2(T_{ref})$	2.0 ± 0.07
$E_{a2}/(R \cdot T_{ref})$	32.5 ± 1.2
$\ln K_c(T_{ref})$	0.57 ± 0.06
$\Delta H_c/(R \cdot T_{ref})$	-12.3 ± 0.4
$\ln K_{OH}(T_{ref})$	-0.41 ± 0.05
$\Delta H_{OH}/(R \cdot T_{ref})$	-14.6 ± 1.0
$\ln K_\alpha(T_{ref})$	-1.07 ± 0.06
$\Delta H_\alpha/(R \cdot T_{ref})$	-1.3 ± 1.4

To simulate the production of methane on Aspen Plus, the reactions involved has been inputted along with the kinetic parameters. The reactions defined in the plug flow reactor (PFR) are:

CO methanation reaction:



The water gas shift reaction:



For the kinetic term ² of reactions 3.24 and 3.25, the pre-exponential factors are $1.16 mol \cdot s^{-1} \cdot kg_{cat}^{-1} \cdot bar^{-0.5}$ and $7.42 mol \cdot s^{-1} \cdot kg_{cat}^{-1} \cdot bar^{-1.5}$. The activation energies are $74.1 kJ/mol$ and

²kinetic factor on Aspen (fig. 3.10)

161.6 kJ/mol. The values of the kinetic parameters in table 3.9 have been cross-checked with another paper of Kopyscinski et al. [31], in which the values of the pre-exponential factor, the activation energy and the heat of adsorption are mentioned with their units. The pre-exponential factors of the adsorption constants have the unit of $\text{bar}^{-0.5}$ and the heat of adsorption has the unit of kJ/mol.

Figure 3.10: Kinetic specifications for methanation reaction on Aspen Plus

As for the driving force and adsorption term in the rate equations, the partial pressures and their exponents need to be specified for the reactants and products. The adsorption constants are expressed as:

$$\ln(K_i) = A + B/T = \ln(k_i(T_{ref})) \cdot \exp\left[\frac{\Delta H}{R \cdot T_{ref}} - \frac{\Delta H}{R} \cdot \frac{1}{T}\right] \quad (3.26)$$

Hence,

$$A = \ln(k_i(T_{ref})) + \frac{\Delta H}{R \cdot T_{ref}} \quad (3.27)$$

and

$$B = -\frac{\Delta H}{R} \quad (3.28)$$

Finally, it is important to specify on Aspen Plus that the reacting phase is vapour and the rate basis is the catalyst weight.

3.4.3. Model verification and results

Further reactor specifications are discussed in this part, as well as the model verification and the results.

The reactor configuration and the amount of catalyst loading have been specified based on the study performed by Liu et al. (2016). For the case of a fast fluidized bed, the authors proposed an equation that correlates the fluidized bed reactor diameter (D in m), the syngas volumetric flow rate (Q in Nm^3/h) and the reactor pressure (P in kPa) [32]:

$$\frac{\pi}{4} \cdot D^2 \cdot u = \frac{Q}{3600} \cdot \frac{101.325}{P} \cdot \frac{273.15 + T}{273.15} \quad (3.29)$$

For an inlet temperature (T) of 280°C, an operation gas velocity of 1.5 m/s, a pressure of 20 bar (2000 kPa) and a volumetric flow rate of 1875 Nm^3/h , the resulting reactor diameter is 0.7 m. Hence, considering a length of 4 m, the total reactor volume is 1.54 m^3 . The catalyst loading was taken as 750 kg, with a reactor bed voidage of 0.45. This gives a catalyst bed volume of

0.85 m³. At an average volumetric flow rate of 1523.8 m³/h (0.423 m³/s), the obtained residence time is 2 seconds.

The reactor temperature was limited to 360°C, which is the highest temperature at which Kopyscinski's kinetic model is more accurate and has a better fit to the experimental data. The gas composition (dry basis) at the inlet (after adjusting the feed ratio) and outlet of the methanation reactor are shown in table 3.10.

Table 3.10: Molar composition (dry basis) of the inlet and outlet streams of the methanation reactor on Aspen Plus with the syngas feed ratio of 3

	Inlet stream	Outlet Stream
CO	12.0%	0.0%
H ₂	77.6%	1.0%
CO ₂	10.4%	0.2%
CH ₄	0.0%	98.73%

The model of the reactor based on Kopyscinski's kinetics resulted in a product stream with 98.73 mol% (dry basis) of methane. This high concentration on dry basis was achieved as the conversions of CO, H₂ and CO₂ exceeded 99%. The outlet stream of the methane reactor consists of 59.56 mol% of water, which needs to be separated from methane. The separation step and further product upgrading will be discussed in the next sub-section. Moreover, as the outlet concentration of CO₂ is 0.2%, a downstream CO₂ removal unit is not required.

The simulation of the methanation reactor was verified with the results from Liu et al. (2016) [32]. For this, the reactor configuration and operating conditions mentioned in the study have been applied on Aspen Plus. The pressure was set to 20 bar and the outlet temperature was 500°C. The inlet syngas stream was composed of H₂, CO and N₂, with a ratio H₂:CO=3:1 and a volumetric flow rate of 20000 Nm³/h. Based on these inputs, the obtained concentrations of H₂, CO, CO₂ and CH₄ were in accordance with the results from Liu et al. (2016), shown in figure 3.11. The simulation resulted in very low final CO₂ and CO concentrations. These results were obtained experimentally in a laboratory fluidized bed by Kopyscinski et al. (2010) and Liu et al. (2016) [30, 32]. A potential explanation is that when the CO concentration becomes very small (below the equilibrium value of 1 vol% for the WGS reaction), the reverse water gas shift (RWGS) reaction occurs, leading to the reaction of CO₂ with hydrogen and hence consuming the previously formed carbon dioxide. Consequently, methane production can potentially be enhanced by the reaction of the carbon monoxide resulting from RWGS with the remaining hydrogen in the feed stream.

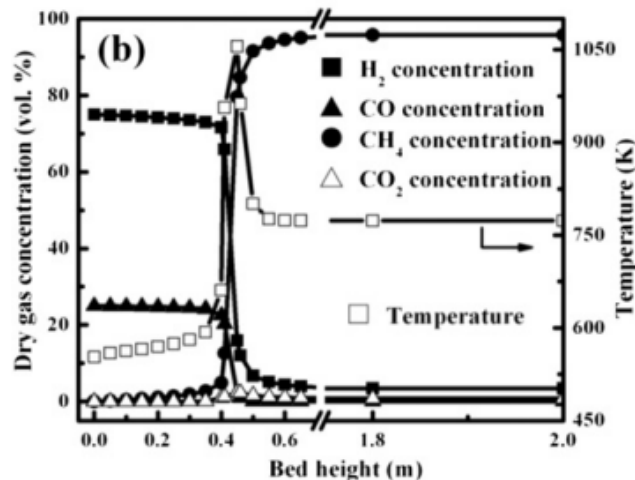


Figure 3.11: Axial profiles of the product dry gas composition and reactor temperature in a fast fluidized bed [32]

Furthermore, results obtained from the model on Aspen Plus showed that the absence of CO_2 in the feed stream to the methane reactor leads to a decrease in methane concentration (dry basis) by 81%. It was found that the conversion of hydrogen was 42.84% compared to CO conversion of 76.14%. Hence, there is a considerable amount of hydrogen that did not react to give methane. In case of having a feed stream with considerable amounts of CO_2 and CO , while maintaining a feed ratio of 3 or higher, the conversion process will be as follows:

Considering that the adsorption of CO on the surface of nickel catalyst is higher than the one of CO_2 , CO methanation occurs first, followed by RWGS reaction when the concentration of CO decreases significantly. This leads to higher concentrations of carbon monoxide which subsequently forms more methane.

Hence, it can be concluded that the presence of CO_2 as a reactant has beneficial consequences on methane production, considering that the feed ratio is at the optimum value (3 or higher). For this reason, it was mentioned in the 'Gas cleaning unit' section (section 3.2) that it is favourable to keep the concentration of CO_2 in the raw syngas as obtained at the outlet of the gasifier.

3.4.4. Final SNG upgrading

The final steps after methane production are cooling, separation from liquid water, and compression to get compressed natural gas (bio-CNG). The methanation reactor product stream is cooled to 20°C in order to separate the gas stream from liquid water in a flash separator, which operates with a pressure drop of 0.1 bar. At the outlet of the reactor, the methane and water molar concentrations are 40.0% and 59.6% respectively. After flash separation, the liquid water stream has a flow rate of 4824 kg/h with a purity higher than 99.99 (mol% and wt%). The final substitute natural gas stream obtained has a flow rate of 2906 kg/h and a purity of 98.63 mol% and 99.15 wt%.

The pressure of the substitute natural gas product needs to be raised to 250 bar. This increase in pressure requires a double stage compression: the first stage is from 20 to 79.5 bar; and the second is from 79.5 to 250 bar. The compressors are specified as isentropic, with an efficiency of 90% [55]. Raising the pressure from 20 to 250 bar leads to a large increase in the gas temperature, which makes inter-cooling necessary. The SNG is first cooled to 50°C and the final bio-CNG stream has a temperature of 15°C .

3.5. Sensitivity analysis

To study the effect of parameters on the performance of the gasifier and the methane reactor, sensitivity analyses have been performed using Model Analysis Tools on Aspen Plus.

3.5.1. Gasifier

There are many factors that affect the quality and composition of the obtained syngas. Nevertheless, the most relevant for this thesis are the oxygen equivalence ratio (λ) and the steam-to-carbon (S-C) ratio, which have been varied from 0.37 to 0.48 and from 0.1 to 1.2 respectively. When varying these two parameters, the carbon-to-gas ratio was kept as 0.96 kg/kg and the heat loss was taken as 5% of pyrolysis oil energy input. 3-D plots have been made on Matlab to better visualise the effect of both λ and S-C on the syngas composition (H_2 , CO and CO_2) and the gasifier outlet temperature, based on the sensitivity analysis on Aspen Plus. The plots of the molar fraction (dry basis) of H_2 , CO and CO_2 are shown on figures 3.12 to 3.14 respectively.

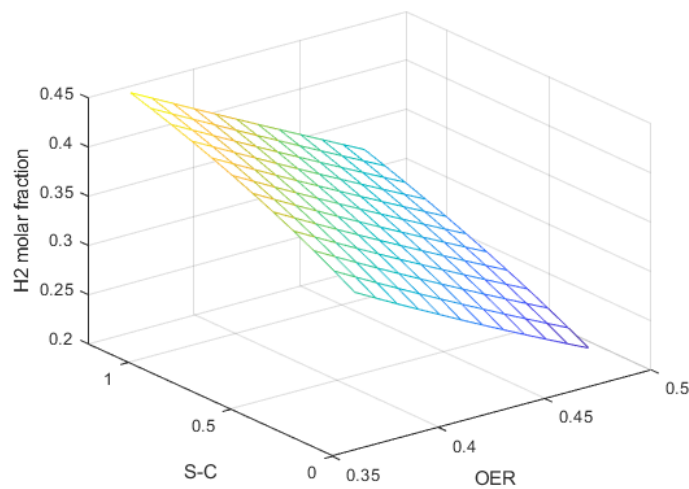


Figure 3.12: H_2 fraction at different oxygen equivalence ratio (OER) and steam-to-carbon (S-C) ratio values

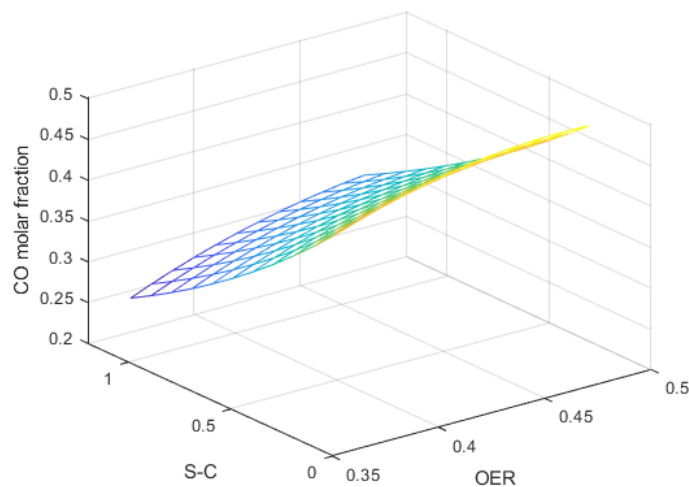


Figure 3.13: CO fraction at different oxygen equivalence ratio (OER) and steam-to-carbon (S-C) ratio values

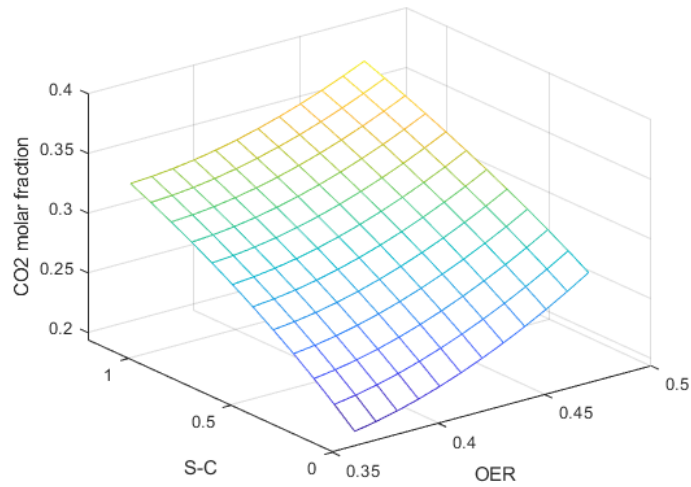


Figure 3.14: CO_2 fraction at different oxygen equivalence ratio (OER) and steam-to-carbon (S-C) ratio values

It can be seen from the graph 3.12 that higher amount of hydrogen is produced at low λ values and high steam-to-carbon ratios. While the molar fraction of CO_2 rises with both OER and S-C (figure 3.14), the fraction of CO increases at higher OER values and lower S-C ratios. More specifically, within the ranges of the sensitivity analyses, the molar fraction of H_2 gets doubled when having the favourable conditions (S-C=1.2 and OER=0.37) over the unfavourable conditions (S-C=0.1 and OER=0.48). A similar extent of change was observed for CO , with the conditions being opposite to H_2 . A possible explanation of these results is that the production of CO and CO_2 is favoured over H_2 in terms of chemical equilibrium at high OER values, as well as due to higher extent of combustion reactions (reactions R-1 to R-3 in table 3.2). Considering that an equilibrium RGibbs reactor was used to model the gasifier, it is difficult to say whether the prevailing reason is a lower consumption or a higher production of CO and CO_2 . As for the input steam to the gasifier, hydrogen is produced from it through reactions R-4, R-8 and R-9. Moreover, a higher amount of steam will cause the equilibrium of the water gas shift (WGS) reaction (reaction R-8) to move predominantly towards the product side. Consequently, water consumes carbon monoxide to produce hydrogen and carbon dioxide. It is safe to assume that the WGS reaction plays an important role in determining the output composition of the syngas as S-C ratio increases. The results from Aspen Plus obtained to observe the effect of these two parameters separately are shown in Appendix A.

Further, these results allow to optimize the quality of syngas by changing the amount of oxygen and steam inputted to the gasifier. However, due to the increase in CO_2 concentration along with H_2 , it is important to consider which parameter is used to assess the quality of syngas. In fact, having high S-C ratio at a fixed OER leads to a large H_2/CO ratio without significant change in the methanation feed ratio.

The changes in H_2/CO ratio and the feed ratio at different values of λ and S-C are depicted in figures 3.15 and 3.16.

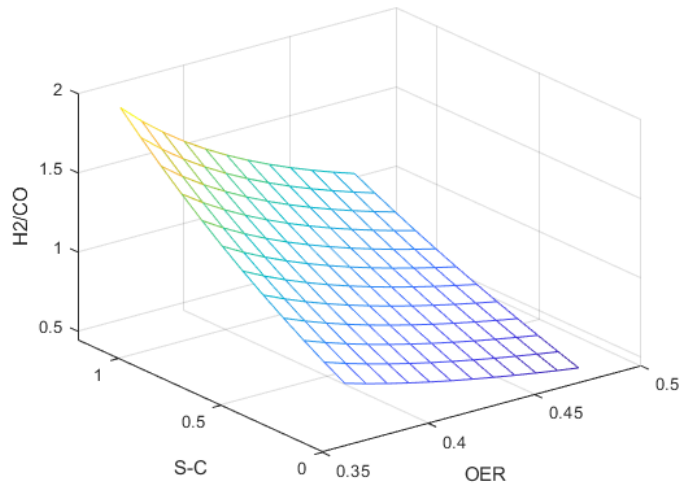


Figure 3.15: H_2/CO ratio at different oxygen equivalence ratio (OER) and steam-to-carbon (S-C) ratio values

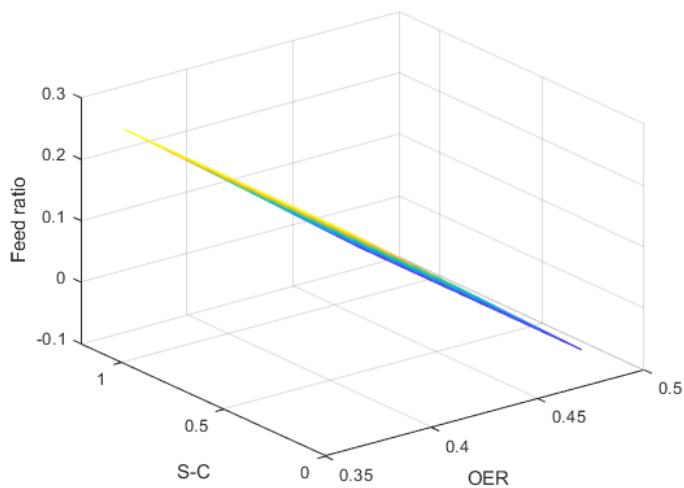


Figure 3.16: Feed ratio at different oxygen equivalence ratio (OER) and steam-to-carbon (S-C) ratio values

The results from Aspen Plus confirm that H_2/CO ratio is higher at high S-C and low OER. Moreover, figure 3.16 shows that the curve is horizontal along the y-axis (S-C). This means that the feed ratio only changes with OER and it is not affected by the amount of steam inputted. As the concentrations of CO and CO₂ get higher when increasing the OER, the feed ratio is reduced sharply, until getting negative starting from OER=0.46. Then, it can be concluded that in order to have a large feed ratio, the amount of inlet oxygen needs to be reduced. However, there are limits to the increase of the feed ratio by having lower OER. Deciding on the amount of oxygen to be inputted cannot be solely based on a specific criterion of the syngas quality. In fact, the OER affects the performance of the gasifier.

Referring to figure 3.17, the results from Aspen Plus sensitivity analysis show that the OER and S-C ratio have opposing effects on the outlet temperature of the gasifier. On one hand, steam, being at much lower temperature (110°C) than the reactor, will reduce the temperature of the syngas, which is assumed to be equal to the outlet temperature of the reactor. On the other hand, a higher amount of oxygen input translates into an increase in the degree

of combustion reactions. This consequently lead to a higher gasifier outlet temperature. The OER needs to allow for enough degree of combustion reactions and high temperatures, which gives as well a cleaner syngas as lower amount of tars is obtained in these conditions.

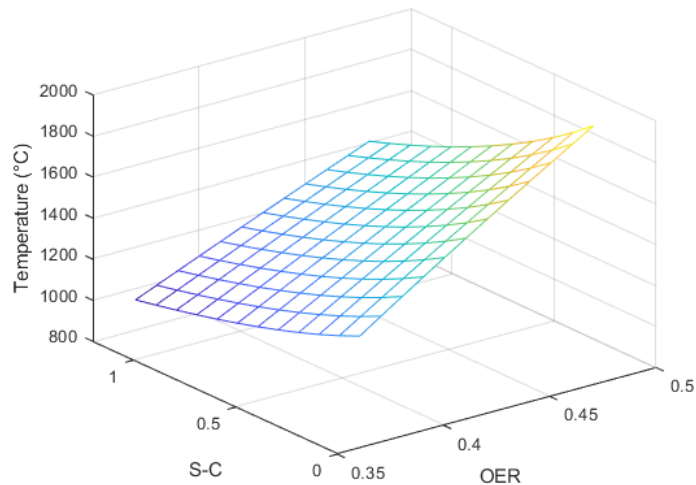


Figure 3.17: Gasifier outlet temperature at different oxygen equivalence ratio (OER) and steam-to-carbon (S-C) ratio values

It is crucial to note that one of the main goals of this thesis work is to model an integrated process in which the product of electrolysis, O_2 and H_2 , are efficiently used for the advantage of other units. In the case of the current system, hydrogen is used to upgrade the syngas to adjust the feed ratio to the optimum value for the methanation reactions. Hence, there is no incentive to favour a higher feed ratio for the syngas at the expense of the gasifier performance. For these reasons, the amount of steam and oxygen inputted were adjusted to result in a reactor temperature that is within the range of experimental setup values. Accordingly, Aspen Plus simulation was based on a steam-to-carbon ratio of 0.85 and an oxygen equivalence ratio of 0.4, in accordance with literature [11].

Furthermore, there are other parameters that have a considerable effect on the operating temperature of the gasifier. For the case of an entrained flow gasifier, the effect of the carbon-to-gas conversion (CtG ratio) and the amount of heat loss in the reactor were both analysed on Aspen Plus, which results are shown in figures 3.18 and 3.19 respectively.

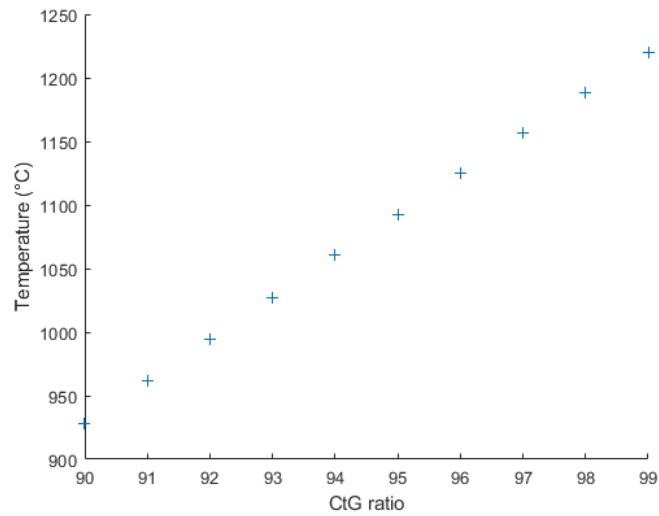


Figure 3.18: Gasifier outlet temperature vs. the carbon-to-gas ratio

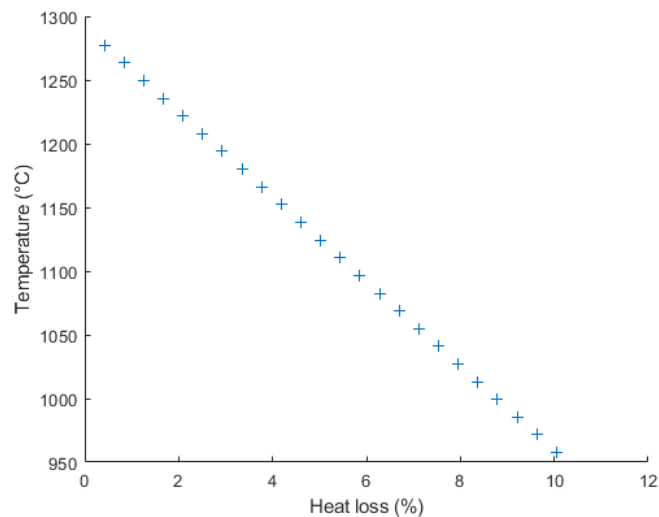


Figure 3.19: Gasifier outlet temperature vs. the percentage of heat loss

As higher amount of carbon is converted, the degree of combustion reactions is therefore higher, leading to an increase in the operating temperature of the gasifier, which was confirmed by Aspen Plus results (fig. 3.18). When the CtG ratio was changed from 92 to 98 kg/kg, the outlet temperature of the gasifier increased by around 20%. Moreover, it can be seen from figure 3.19 that when the heat loss increased from 2% to 10%, the temperature was reduced from 1221.8°C to 957.8°C, which is a reduction of around 22%. This implies that having a large-scale gasifier with lower heat loss would be advantageous in obtaining a higher reactor temperature with the same carbon-to-gas conversion, keeping other parameters constant.

3.5.2. Methane reactor

A sensitivity analysis was performed on the methane reactor to study the effect of the syngas composition on the methanation output. The syngas composition was varied by inputting different S-C and OER values. While the steam-to-carbon ratio was 0.75 and 1.25, four different OER were considered: 0.38, 0.40, 0.42 and 0.46. In all conditions, the feed ratio was changed to 3 by adding the necessary amount of hydrogen based on Excel calculations. This implies

that at different S-C and OER, the flow rates of the syngas constituents get altered but the feed ratio is maintained constant. In this case, the relevant parameter in terms of syngas composition is the molar ratio CO_2/CO , which values are shown in table 3.11 considering six different cases.

Table 3.11: Molar ratio CO_2/CO in the syngas obtained at six different cases of S-C and OER

Gasification conditions	CO_2/CO ratio
OER: 0.38 and S-C: 0.75	0.85
OER: 0.38 and S-C: 1.25	1.31
OER: 0.42 and S-C: 0.75	0.82
OER: 0.42 and S-C: 1.25	1.19
OER: 0.46 and S-C: 0.75	0.84
OER: 0.46 and S-C: 1.25	1.17

The molar flow rate and composition of the product stream of the methane reactor (R-OUT for short) are shown in table 3.12.

The results from the sensitivity analysis show that the syngas composition at different S-C and OER did not affect the amount of methane produced (around 181 kmol/h). This means that the methanation process cannot be optimized by varying the CO_2/CO ratio in the syngas. In all of the cases, CO was totally consumed and negligible amounts of CO_2 and H_2 remained. The major difference between the cases lies in the water output. These results were only observed when there is enough hydrogen fed to the methane reactor. A higher feed ratio would imply more hydrogen fed. However, as the CO and CO_2 are already consumed, higher amounts of hydrogen would not lead to an increase in methane production. Hence, it can be concluded that at the reactor conditions used, changes in the syngas composition have no considerable effect on methane production in case of very high conversion of reactants.

Table 3.12: Molar composition of the inlet and outlet streams of the methanation reactor on Aspen Plus at six cases of OER and S-C values

Syngas component	R-OUT flow rate (kmol/h)	R-OUT mol%
OER: 0.38 and S-C: 0.75		
CO	0.0	0.0%
H ₂	0.26	0.039%
CO ₂	0.06	0.010%
CH ₄	181.2	27.67%
H ₂ O	473.4	72.28%
OER: 0.38 and S-C: 1.25		
CO	0.0	0.0%
H ₂	0.29	0.038%
CO ₂	0.072	0.009%
CH ₄	181.2	24.18%
H ₂ O	567.8	75.77%
OER: 0.42 and S-C: 0.75		
CO	0.0	0.0%
H ₂	2.02	0.299%
CO ₂	0.002	0.0003%
CH ₄	181.2	26.80%
H ₂ O	493.0	72.89%
OER: 0.42 and S-C: 1.25		
CO	0.0	0.0%
H ₂	0.33	0.042%
CO ₂	0.081	0.01%
CH ₄	181.2	23.56%
H ₂ O	587.3	76.37%
OER: 0.46 and S-C: 0.75		
CO	0.0	0.0%
H ₂	0.089	0.013%
CO ₂	0.455	0.066%
CH ₄	180.8	26.09%
H ₂ O	511.6	73.82%
OER: 0.46 and S-C: 1.25		
CO	0.0	0.0%
H ₂	0.123	0.016%
CO ₂	0.464	0.059%
CH ₄	180.8	22.96%
H ₂ O	605.96	76.95%

4

Energy performance analysis

In this chapter, section 4.1 explains the methodology and results of the heat integration applied to the system, in addition to heat exchanger network in section 4.2. Then, the energy performance analysis of the complete process is presented in section 4.3. Knowing whether the integration of gasification, electrolysis and bio-fuel production results in an efficient system is one of the major outcomes of this thesis. The assessment of the energy efficiency, without and with heat integration is thus of high importance. Hence, this chapter aims to answer the questions:

*How efficient is the integrated process?
To what extent does heat integration improve the overall conversion efficiency?*

4.1. Heat integration

Based on Aspen Plus results and excel calculations, the heat integration of all cold and hot streams of the process was performed by Pinch analysis, using the numerical method. Pinch analysis allows to identify the potential pinch temperature (if available) and to know the quantity of cold and hot utilities required. In case no hot utility is needed, the heat generated by the system ('intra-process heat') is enough to get all the cold streams to the desired outlet temperatures. Otherwise, an additional source of energy is required to compensate the lack of intra-process heat. When there is surplus heat, a cold utility would be needed to cool the hot streams.

The additional heat available in the system can be used for diverse purposes, such as district heating, steam generation or as a heat source for another plant. In the case of this integrated system, the surplus heat is assumed, as a design choice, to be used to generate steam which is inputted to the electrolyzer for the production of oxygen and hydrogen. These can be considered as products that are useful for diverse applications and industries. The hydrogen is taken as an additional source of energy along with CNG.

A summary of the cold and hot streams is presented in table 4.1, with their respective inlet and outlet temperatures and heat capacity.

The pinch analysis using the numerical method was performed according to the following methodology:

1. The cold and hot streams were identified with their respective mass flow rate (\dot{m}), specific heat (C_p), and inlet and outlet temperatures (T_{in} and T_{out}).
2. The heat capacity (CP) was calculated for each stream by multiplying the specific heat by the mass flow rate.
3. Considering a minimum temperature approach (ΔT_{min}) of 10 °C, the lower and upper temperatures for each stream were found by adding ($\Delta T_{min}/2$) to the inlet and outlet temperatures of cold streams; and by subtracting ($\Delta T_{min}/2$) to the temperatures of hot streams.

These are referred to as 'shifted temperatures', and repeated temperatures (duplicates) are considered once.

4. All the temperatures (both cold and hot streams) were ranged in a decreasing order, in which each temperature difference ($\Delta T = T_i - T_{i+1}$) represents an interval.
5. The net heat capacity of each interval (CP_i) was calculated as the sum of the heat capacities of cold streams (ΣCP_{cold}) subtracted by the heat capacities of hot streams (ΣCP_{hot}).
6. Accordingly, the net enthalpy was obtained as:

$$\Delta H_i = \Delta T \cdot CP_i \quad (4.1)$$

When having water condensed or evaporated, the heat of condensation/vaporisation was taking into consideration in the calculation of the net enthalpy.

7. There is surplus heat in the process when the net enthalpy is negative and deficit heat in the opposite case.

Table 4.1: Summary of the cold and hot streams with their properties for heat integration'

Stream number	Stream name	Type	T_{in} (°C)	T_{out} (°C)	CP (kW/K)
1	steam to gasifier	cold	25	110	2.44
2	syngas	hot	1170	50	7.25
3	MDEA solvent	cold	50	100	5.79
4	MDEA solvent	hot	60	40	5.56
5	methanation reactor inlet	cold	140	280	4.59
6	steam from methanation	hot	745.15	220	4.71
7	methanation reactor outlet	hot	365	20	6.38
8	SNG	hot	151	50	1.97
9	CNG	hot	177	15	1.96
10	water feed to SOEC	cold	23	700	9.94
11	SOEC outlet	hot	700	45	5.84
12	H_2 (SOEC)	cold	45	140	4.30
13	O_2 (SOEC)	hot	700	55	2.28
14	pyrolysis oil	cold	25	80	3.33

The results of the pinch analysis are available in Appendix B (table B.2). Thus, by following this methodology, no pinch temperature was identified as there was no deficit in heat. The surplus heat was found to be equal to 14.29 MW. It is important to note that this amount is only a theoretical value as not all of it can be actually harvested using heat exchangers due to thermodynamic limitations as well as limitations in the matching between cold and hot streams. Hence, a heat exchanger network needs to be performed in order to know the actual amount of useful surplus heat generated by the integrated process. This is presented in the next section.

4.2. Heat exchanger network

The heat exchanger network analysis is necessary to identify which hot streams can heat the cold streams, as well as to know the amount of heat that cannot be directly used by having heat exchangers. In fact, there are specifications that determine whether one stream matches with another one or not. Amongst these requirements, CP_{hot} should be lower than CP_{cold} . As no pinch temperature was found, this is applicable for all the streams. This ensures that there is no temperature cross (violation of ΔT_{min}), and thus that the heating/cooling process is thermodynamically feasible.

By performing the heat exchanger network, it was found that seven heat exchangers are needed for the heat integration of the cold and hot streams of the integrated process. The heat exchangers, along with the heat involved (Q) are listed in table 4.2. Further parameters related

to the heat exchangers, such as the log mean temperature difference, the correction factor, and the heat exchanger area, can be found in appendix B (table B.3).

Table 4.2: Summary of the cold and hot streams with their properties for heat integration

HEX number	Hot stream	Cold stream	Q (kW)
1	syngas	water feed to SOEC	9384.4
2	SOEC outlet	water feed to SOEC	1165.9
3	O ₂ (SOEC)	methane reactor inlet	677.8
4	O ₂ (SOEC)	H ₂ (SOEC)	408.1
5	O ₂ (SOEC)	MDEA solvent	384.1
6	SOEC outlet*	steam to gasifier	2081.7
7	SNG	pyrolysis oil	183.3

* after heat integration (using the steam generated from excess heat)

Amongst the eight hot streams available in the process (table 4.1), four are used in heat exchangers; namely the raw syngas, the oxygen product of the electrolyzer, the methane product after the first compression stage (SNG) and the cathode exhaust of the electrolyzer (referred to as SOEC outlet in table 4.2). When inputting the steam generated from the surplus heat into the SOEC, additional heat is available when cooling the cathode exhaust as well as the oxygen stream. The hydrogen and unreacted steam need to be cooled from 700°C to 45°C before entering the flash separator and the oxygen to 40°C. These heat sources sum up to 4402.8 kW or 4.4 MW. The remaining four hot streams form the bulk of the surplus heat generated by the system, adding to the remaining heat from the SOEC outlet of the process, which was only partially used in the heat exchanger.

The network of the seven of heat exchangers can be visualised on the process flow diagram of the integrated process (figure 4.1), with the colour of the heat exchangers corresponding to the one of the HEX number in table 4.2.

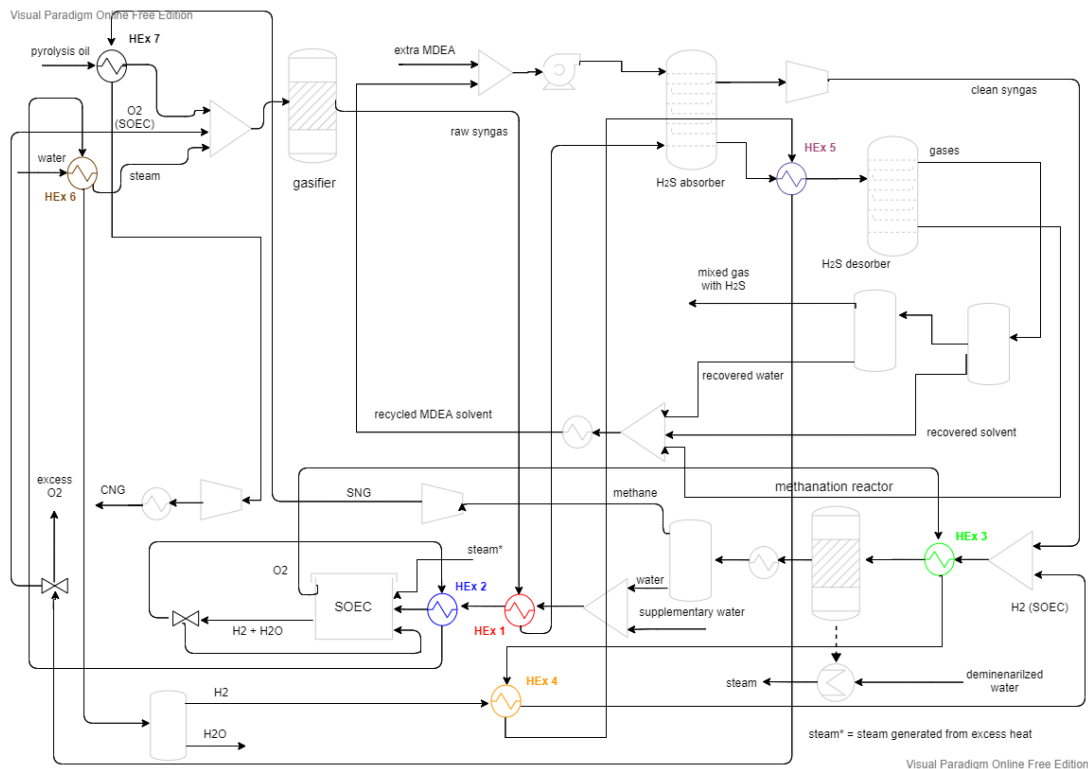


Figure 4.1: Process flow diagram with the heat exchanger network

Accordingly, after matching the cold and hot streams along the seven heat exchangers, the surplus heat generated by the process was found to be **10.71 MW**. This represents around 75% of the theoretical value obtained by pinch analysis. Hence, by performing heat integration for the integrated process, it was possible to know how much excess heat is generated by the system. Using this extra heat efficiently allows to have end products additionally to compressed natural gas (CNG). Considering that the water used for steam generation is first pumped to 20 bar, then heated to 600°C, 10.71 MW would be enough to generate 10 792 kg/h of steam. By simulating the electrolysis of this amount of steam on Aspen Plus, the model resulted in 7987 kg/h of oxygen and 1006 kg/h of hydrogen, along with 1771 kg/h of unreacted steam. Consequently, considering a heating value of 120 MJ/kg (LHV) and 141.7 MJ/kg (HHV), the additional amount of energy obtained from hydrogen is 33.54 MW (LHV) and 39.61 MW (HHV).

To allow for a good matching of the heat capacities between cold and hot streams, the outlet temperature (target heating/cooling temperature) attained by heat integration of some of the cold/hot streams was altered. Hence, in addition to the heat exchangers, heating and cooling utilities are required to get to the target temperatures. It was found that 285.7 kW of cooling is needed, and 1702.0 kW of heating. It is assumed that electrical heating is used for this purpose, and it is accounted for as an energy input to the process. As for the cooling utility, the amount of cooling water is considered in the economic analysis of the plant (chapter 5).

4.3. Process energy efficiency

The energy performance of the whole integrated process was assessed by accounting for the major energy inputs and outputs, which are summarized in tables 4.3 and 4.4. The total energy efficiency of the integrated process was initially calculated as:

$$\eta = \frac{\dot{m}_{CH_4} \cdot H_{CH_4}}{\dot{m}_{pyro} \cdot H_{pyro} + P_{el} + P_{comp} + P_{pump}} \quad (4.2)$$

where

- \dot{m}_i is the mass flow rate of component i (kg/h),
- H_i is the heating value of component i (MJ/kg),
- P_{el} is the electrical power input to the SOEC (MW),
- P_{comp} and P_{pump} the power consumed by compressors and pumps (MW), and
- P_{heat} is the power needed for electrical heating (MW).

For unit consistency with the electrical power terms, the energy content of the components is converted to *MW*. Compared to compressors, the power consumed by pumps is negligible. Nevertheless, it has been accounted for to include the different units of the process in the energy performance assessment.

After the use of the excess heat by inputting the steam in the SOEC, the hydrogen stream is considered as an additional product of the process. Hence, it is accounted for in the process energy outlets. Moreover, the power consumed by the pump and electrolyzer when using steam generated from surplus heat need to be considered amongst the energy inputs, in addition to the electrical heating. Accordingly, the energy efficiency post heat integration becomes:

$$\eta = \frac{\dot{m}_{CH_4} \cdot H_{CH_4} + \dot{m}_{H_2} \cdot H_{H_2}}{\dot{m}_{pyro} \cdot H_{pyro} + P_{el} + P_{comp} + P_{pump} + P_{heat}} \quad (4.3)$$

where

- P_{heat} is the power needed for electrical heating.

In this case, P_{el} and P_{pump} include both the values after heat integration.

The heating value (LHV) of the pine wood derived pyrolysis oil, taken from literature [11], is 17.2 MJ/kg. As the difference between the values of LHV and HHV is approximately equal to the amount of latent heat of vaporization of water ¹, the HHV of pyrolysis oil was considered to be 4.48 MJ/kg higher than the LHV value. The energy content of the power consumption for the compressors and pumps have been taken from Aspen Plus simulation.

Table 4.3: Energy inputs to the process

Main feedstock	Energy flow (MW)
Pyrolysis oil (5000 kg/h)	23.89 (LHV) ; 30.11 (HHV)
Power consumption	Power (MW)
Syngas compressor	0.276
SNG compressor 1	0.246
SNG compressor 2	0.220
Pumps	0.006
SOEC ¹	41.87
Total in	66.50 (LHV) ; 72.73 (HHV)
With heat integration	Power (MW)
Power for SOEC ¹	40.72
Power for pump	0.009
Electrical heating	1.8
Total in with heat integration	109.0 (LHV) ; 115.2 (HHV)

¹ Including 5% losses.

Table 4.4: Energy outputs of the process

Major products	Mass flow (kg/h)	Energy content (MW)
CNG	2906.8	42.48 (LHV) ; 46.10 (HHV)
With heat integration		
H_2 ¹	1006.3	33.54 (LHV) ; 39.61 (HHV)
Q_{rem}	- -	4.51
Total out with heat integration		80.43 (LHV) ; 90.11 (HHV)

¹ Obtained from electrolysis of steam generated by excess heat.

As described in section 3.3 of the previous chapter, the power consumption of the electrolyzer has been obtained from Matlab calculations. Moreover, the LHV of the synthetic natural gas has been calculated from the higher bound value of the Wobbe index of high calorific gas (H-gas) ², in accordance with RVO (Rijksdienst voor Ondernemend) ³. The Wobbe index is defined as [9]:

$$WI = \frac{HHV}{\sqrt{GG}} \quad (4.4)$$

where HHV is the higher heating value, and GG is the gas gravity, being the ratio of the density of SNG to the one of air at standard conditions (288.15 K and 101,325 kPa):

$$WI = \frac{\rho_{SNG}}{\rho_{air}} \quad (4.5)$$

The density of air is 1.22 kg/m^3 and the one of SNG is 0.77 kg/m^3 . With the higher bound of the H-gas Wobbe index equal to 55.7 MJ/m^3 , the HHV of SNG is 44.36 MJ/m^3 , which is equivalent

¹Taken from <https://www.clarke-energy.com/heating-value/> [26/07/2021].

²Taken from <https://wetten.overheid.nl/BWBR0035367/2019-01-01> [20/05/2021].

³Taken from <https://www.rvo.nl/onderwerpen/duurzaam-ondernemen/energie-en-milieu-innovaties/gassamenstelling> [20/05/2021].

to 57.09 MJ/kg. As the lower heating value (LHV) does not take into account the latent heat of vaporisation of water (water vapour is not recovered amongst the reaction products), the LHV can be derived from the HHV by subtracting from it the latent heat of vaporisation of water of 4.48 MJ/kg. This gives LHV of SNG of 52.61 MJ/kg.

Accordingly, the obtained energy efficiency of the integrated process was found to be **63.9% (LHV)** and **63.4% (HHV)**, calculated as the energy output from CNG divided by the total energy input. When including heat integration in the system, extra hydrogen is produced, that is not used within the system, and hence is considered as a product. Without considering the energy consumed in compressing, cooling and storing the hydrogen as a final product stream, the amount of chemical power obtained from the hydrogen stream after heat integration is 33.54 MW (LHV) and 39.61 MW (HHV). The process efficiency post heat integration then becomes **73.8% (LHV)** and **78.2% (HHV)**. Thus, the efficient use of the heat generated within the system allowed for an increase in the process efficiency by roughly 15% on LHV basis and 23% on HHV basis.

To assess other efficiencies within the process, the heating value of the syngas was obtained by multiplying the heating values of individual components multiplied by their flow rates. This resulted in a value of 15.15 MW (LHV). Taking into consideration the heat loss (5% of thermal heat), the unconverted carbon and the steam input, the cold gas efficiency (CGE) was found to be 56% (LHV). Moreover, the obtained energy efficiency from electricity to hydrogen was 82% (LHV) and 97.2% (HHV). When operating below the thermoneutral cell voltage, the efficiency of electricity to hydrogen of the solid oxide electrolysis cell can be higher than 100% (LHV) in case of high temperature heat input to the SOEC [4].

In order to compare the energy performance of the system modeled in this thesis with literature, several studies on the integrated process of gasification, steam electrolysis and methanation have been considered. Monaco et al. (2018) analysed the production of synthetic fuels through catalytic upgrading and SOEC co-electrolysis with different feed streams (recovered CO₂ or residual biomass). The syngas composition was taken from another study (Pozzo et al., 2015 [39]) as the gasification process was not considered. Their analysis resulted in an efficiency of 74% for SNG production.

Furthermore, Anghilante et al. (2019) have modeled different power-to-gas plant concepts aiming at converting bio-syngas to methane through steam electrolysis and catalytic methanation [48]. Both studies have used a definition of the energy conversion efficiency similar to equations 4.2 and 4.3. The authors studied the energy performance of each process plant and they performed pinch analyses using Matlab algorithm to obtain the thermal requirements and the maximal plant efficiency (assuming heat is all generated by the system). Moreover, the gasifier has been modeled on Aspen Plus. One of the plant concept includes the gasification of wood, along with SOEC electrolysis and the production of CNG at 250 bar. By using Simulink plant models, they evaluated the efficiencies in static regime. Accordingly, they obtained a plant efficiency of 75.1% (LHV) and 81.0% (HHV) after heat integration, which was found to be the same as the maximal theoretical efficiency [48]. These values are 1.73% (LHV basis) and 3.58% (HHV basis) higher than the ones obtained in this thesis.

In conclusion of the energy performance analysis of the integrated process, the obtained energy efficiencies after heat integration in this work are close to values found in literature. With an overall efficiency of 73.8% (LHV) and 78.2% (HHV), the process can be considered to be efficient. Hence, the integration of pyrolysis oil gasification with high-temperature electrolysis and methane production has been found to be advantageous.

5

Economic analysis

This chapter tackles the economic analysis of the complete integrated process. The performance of the analysis includes: the capital cost (also known as capital expenditure or CAPEX), the operating cost (OPEX), adding to the revenues, as well as other financial expenses. Within the part of operating cost, the main factors affecting the price of CNG and the sources of electricity are tackled. The capital cost estimations and major economic assumptions were based on the economic analysis performed by Giglio et al. (2015), studying the production of synthetic natural gas through the integration high-temperature electrolysis and methanation [8]. Their analysis used the methodology adopted by the National Energy Technology Laboratory (NETL). While the cost estimations are presented in sections 5.1 and 5.2, the profitability analysis is discussed in section 5.3. The conclusion of this chapter answers the following question:

Is the implementation of the process in a plant economically feasible while maintaining a reasonable CNG product price?

5.1. Capital cost estimation

The capital expenditure (CAPEX) includes the money invested in fixed assets, mainly equipment, buildings, vehicles and land. The capital cost is estimated by calculating a set of parameters. The bare erected cost (BEC) includes direct expenses from purchased equipment cost (PEC), installation materials, labour to install equipment, and material. Indirect expenses include all equipment and material transportation costs, construction overhead and engineering expenses. The engineering, procurement and construction cost (EPCC) includes "the cost of services provided by contractors" [8]. The total plant cost (TPC) considers the BEC and EPCC items as well as uncertain costs called contingencies. The latter include two types: process contingency, that are related to uncertainties due to the performance changes of the technologies, as well as project contingencies. The contingencies associated to the project as a whole were assumed to be 20% of the sum of process contingency and EPCC, in accordance with [8].

The total overnight capital (TOC) includes all of the following costs [8]:

- Pre-production costs and inventory capital; (2.5% of TPC).
- Cost for securing financing; (2.7% of TPC).
- Other owner's costs, such as legal fees, preliminary feasibility studies, and improvement of infrastructures; (15% of TPC).

The escalation of capital cost is considered because capital expenditure must be escalated at a defined nominal annual rate (r_{cap}) to produce a consistent economic analysis framework. Given a distribution of TOC over the capital expenditure period, the overall escalated TOC (ETOC) is

computed as:

$$ETOC = \sum_{i=1}^Y TOC_i \cdot (1 + r_{cap})^{-1} \quad (5.1)$$

where Y is the number of years the plant is under construction; and TOC_i is the total overnight cost of the i-th year.

The interest during construction (IDC) is depended on the debt interest rate (r_d), the total debt disbursement (TDD), and the debt share (ζ_D) through the following equations:

$$IDC = \sum_{j=1}^M [TDD \cdot r_d] \quad (5.2)$$

where M is the construction duration expressed in months;
and

$$TDD = \sum_{j=1}^m \cdot ETOC_k \cdot \zeta_D \quad (5.3)$$

where the subscript k is a generic year.
The debt share is assumed to be 50%.

The total as-spent cost (TASC) is expressed as:

$$TASC = ETOC + IDC \quad (5.4)$$

Considering an equity share (ζ_E) of 50%, the cash flow in a year k during capital expenditure period can be calculated as:

$$CF_k = -TASC_k \cdot \zeta_E \quad (5.5)$$

The equations used for the calculations of the bare erected costs of the process equipment were taken from the academic book 'Analysis, Synthesis, and Design of Chemical Processes' (3rd ed.) by R. Turton, R. Bailie, W. Whiting and J. Shaeiwitz [49]. The costs presented in this book edition were in 2001 U.S. dollars. Accordingly, in order to convert the cost values to 2020 dollars, the Chemical Engineering Plant Cost Index (CEPCI) was used. Considering that the CEPCI of 2001 was 397 [49] and the one of 2020 was 596.2¹, the correcting factor for having 2020 dollars is 1.5.

In order to obtain the total bare erected cost (BEC), the purchased cost at bare conditions (C_{p0}) has been calculated for each equipment using equation 5.6.

$$\log(C_{p0}) = k_1 + k_2 \cdot \log(A) + k_3 \cdot \log(A)^2 \quad (5.6)$$

where k1, k2 and k3 are constants and A is the capacity of the equipment, which depends on the type of equipment in question. These parameters are listed in table 5.1 for each type of equipment.

Table 5.1: Parameters for the purchased cost at bare conditions C_{p0}

Equipment	k1	k2	k3	Capacity A
Heat exchanger (U-tube)	4.188	-0.250	0.197	Area (m^2)
Compressors (centrifugal, axial)	2.290	1.360	-0.103	Fluid power (kW)
Mixers (impeller)	3.851	-0.291	-0.0003	Power (kW)
Process vessels (horizontal)	3.557	0.378	0.091	Volume (m^3)
Process vessels (vertical & towers)	3.497	0.449	0.107	Volume (m^3)
Pumps (reciprocating)	3.869	0.316	0.122	Shaft power (kW)
Pumps (positive displacement)	3.477	0.135	0.144	Shaft power (kW)

¹Taken from <https://www.chemengonline.com/2020-annual-cepci-average-value/> [31/05/2021].

For vessels (horizontal and vertical), heat exchangers and pumps, the bare erected cost (C_{bm}) was derived from Cp_0 considering material and pressure factors (F_m and F_p), and correlation constants (B1 and B2) that are specific to the equipment, as in equation 5.7.

$$C_{bm} = Cp_0 \cdot (B1 + B2 \cdot F_m \cdot F_p) \quad (5.7)$$

For vessels, the formula for the pressure factor (F_p) is:

$$F_p = \frac{(P + 1) \cdot \frac{D}{2} \cdot (850 - 0.6 \cdot (P + 1) + 0.00315)}{0.0063} \quad (5.8)$$

For heat exchangers (U-tube) and pumps, F_p was calculated as:

$$\log(F_p) = C1 + C2 \cdot \log(P) + C3 \cdot [\log(P)]^2 \quad (5.9)$$

The material factors were taken from curves in [49] that correlate the factor to the type of material used for different equipment. The suitable material that is recommended to be used depends on the operating temperature (T) of the equipment, considering the following cases [8]:

- T < 350°C: carbon steel (CS)
- 350 < T < 550°C: stainless steel (SS)
- T > 550°C: Ni-alloy

The material factor of each equipment can be found in Appendix B.

For mixers, C_{bm} has been obtained by multiplying Cp_0 by a bare module factor (F_{bm}). For compressors, the Cp_0 was multiplied by the material factor F_m to get C_{bm} .

After calculating all the equipment costs along with the other cost parameters included in CAPEX, the total capital expenditure or the total capital investment (TCI) was found to be 28 466 500 US dollars, which is equivalent to 23 747 900 euros. The exchange rate from US dollars to euros, taken for September 2020, is 1.1987, according to the representative rates of the International Monetary Fund ². With an initial biomass input of 23.89 MW, the TCI is 889.5 Euros/kW, which is 31.35% lower than the one estimated in a study made by the Energy research Centre of the Netherlands (ECN) for a 1 GW bioSNG plant. Moreover, technology learning is expected to decrease the TCI of bioSNG production by 30% within a decade (2030) [17].

5.2. Operational cost estimation and revenues

The operational cost is calculated from the plant startup to its final shut-down.

The operational cash flow is:

$$CF_k = Rev_k - Exp_k - Tx_k - An_k \quad (5.10)$$

where Rev are the revenues, Exp the expenses, Tx the taxes and An the annuity to debt repayment.

The incomes got from selling the products of the whole process are considered as revenues. The expenses of each year are divided into fixed and variable costs. The fixed part mainly include maintenance, labour and insurance costs. The maintenance and insurance costs are taken as 2% and 1% of TPC respectively. The labour expenses are calculated by assuming an average wage of 36000 \$/person/yr and 100 employees considering a small sized enterprise, according to the European Commission's definition of small and medium-sized enterprises (SMEs) [5].

The variable expenses are dependent on plant utilisation and include energy use, feedstock and chemicals input, and replacement of degraded parts of the process units, as well as other

Table 5.2: Parameters for variable operating costs

Methanation catalyst cost	16296 \$/m ³
MDEA solvent cost	2600 \$/ton
Demineralized water	1 \$/ton
Pyrolysis oil price	250 €/ton
Electricity cost	8 cents/kWh
SOEC cell degradation rate	0.5%/1000 h
Annual operating hours	8000 h

costs. These costs are summarized in table 5.2 and are partially based on values reported by Giglio et al. (2015) [8].

Considering a voidage of 0.55, the catalyst in the methane reactor constitutes 0.847 m³. It is assumed that it is refilled every 4 years [8], which results in a cost of 3450\$. The cost of pyrolysis oil was taken based on information given by the Biomass Technology Group (BTG) company ³, which is a local supplier of pyrolysis oil in the Netherlands. The value is taken as an average between the cost of pyrolysis oil based on clean wood (300 euros/ton) and the one based on wood residues (200 euros/ton), considering that the feed stream is a mix of both clean wood and residues. The flow rate of pyrolysis oil was taken as 5 ton/h in Aspen Plus model.

The cell degradation rate was considered to be 0.5%/1000h, as proposed by Giglio et al. (2015) and Wang et al. (2019) for commercial electrolyzers of Topsoe and SOLIDpower [8, 37]. The SOEC needs to have a spare capacity to allow for a stable functioning and productivity. When the SOEC cell degrades, the area specific resistance (ASR) increases linearly with time [8]:

$$ASR(t) = ASR_0 \cdot (1 + d \cdot t) \quad (5.11)$$

where

- ASR_0 is the initial ASR ($\Omega \cdot cm^2$),
- d is the degradation rate (0.5%/1000h), and
- t is time (h).

The current density can then be computed as:

$$j(t) = \frac{V_o - V_n}{ASR(t)} = j_0 \cdot (1 + d \cdot t) \quad (5.12)$$

where V_o is the operating voltage (V), V_n is the reversible Nernst voltage (V), and j_0 is the operating current density.

By having a higher area specific resistance, the current density decreases. At a fixed active area, a lower current density would reduce the faradic current (I_f), leading to a lower production of oxygen and hydrogen. Thus, in order to maintain the production rate and stack performance, a higher active area is required. It is assumed that when the degradation attains a threshold value of 20% ASR with respect to its initial value (ASR_0), the modules are replaced by new ones [8]. In terms of operating cost, more electricity input is needed for the additional active area. In addition, the transport and placement costs are also considered.

While the taxes are considered to be 26% of the net income, the debt payments along the operational period are called annuities and are expressed as [8]:

$$An = \frac{r_d \cdot (1 + r_d)^n}{(1 + r_d)^n - 1} \cdot TASC \cdot \xi_D \quad (5.13)$$

²Taken from https://www.imf.org/external/np/fin/data/param_rms_mth.aspx [15/07/2021]

³Further details in <https://www.btgworld.com/en>

where n is the total repayment period, taken as 15 years, and r_d is the debt interest rate, which is considered to be 4.5%.

Accordingly, the annuities are found to be 2 135 900\$.

In order to estimate the revenues generated from the process, the price of pure oxygen was assumed to be 25\$/t based on the production cost of oxygen in cryogenic high-capacity plants [8]. The price of bio-CNG is highly dependent on the price of electricity that is mainly used to power the electrolyzer. Based on statistics of prices for industry in the Netherlands ⁴, the electricity price of energy was assumed to be 8 cents/kWh, taken as an average value of the prices of the past ten years while giving more weight to the decreasing prices in the year 2020. The price of bio-CNG at which the integrated process is economically feasible is referred to as the cost of product (COP). The obtained COP is **22.4 Euros/GJ** (2020 value). The plant is considered to be profitable when the net present value (explained in section 5.3) is positive. A study performed in 2014 by the Energy research Centre of the Netherlands (ECN) on the 'Economy of large scale biomass to substitute natural gas plants' found that the cost price of bioSNG is 24.8 \$₂₀₁₃/GJ [17], which is equivalent to 21 Euros/GJ (2020 value). This value is taken as a reference for assessing the economic feasibility. Hence, the obtained COP for an electricity price of 8 cents/kWh is 7% higher than the one estimated by ECN. With the application of incentives and policies to facilitate the introduction of sustainable biofuels in the market, the price of bioSNG can be reduced for it to be competitive with SNG produced from coal but not natural gas [17].

Considering all the variable and fixed costs, the total operating expenses were found to be 19 897 100 euros, with the costs converted to euros at the exchange rate of 1.1987. Moreover, the revenues from oxygen and CNG sum up to 29 638 400 euros.

⁴Taken from <https://www.statista.com/statistics/596254/electricity-industry-price-netherlands/> [26/07/2021]

5.2.1. Factors affecting the price of CNG

The cost of pyrolysis oil and the price of electricity are two factors that are important to consider to have a reasonable price of CNG, allowing it to be introduced in the market. In fact, the thermal energy of pyrolysis oil and the power consumption of the electrolyzer constitute respectively around 22% and 75% of the total energy input to the process. Hence, changes in their costs has a significant effect on the cost of product. To study this effect, the price of industrial electricity was varied from 4 to 16 cents/kWh, and the cost of pyrolysis oil from 100 to 450 Euros/ton. The plots obtained from Matlab are shown in figures 5.1 and 5.2.

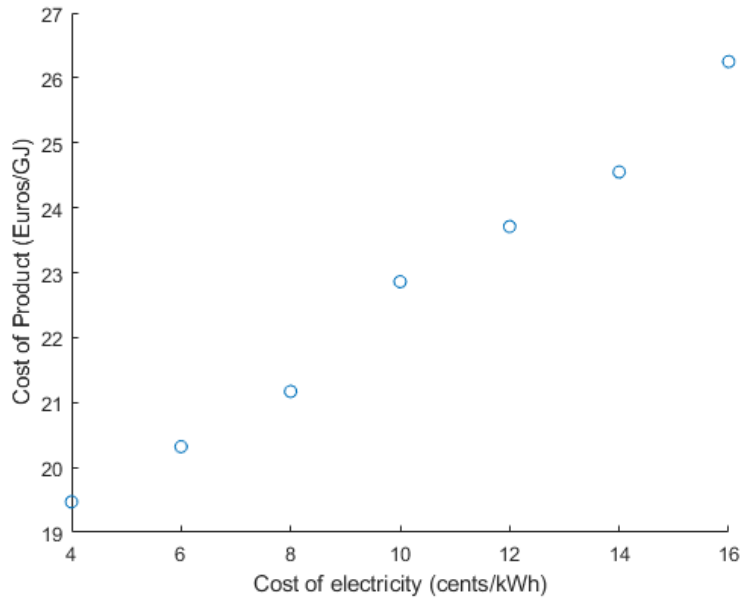


Figure 5.1: Cost of Product (COP) vs. price of electricity

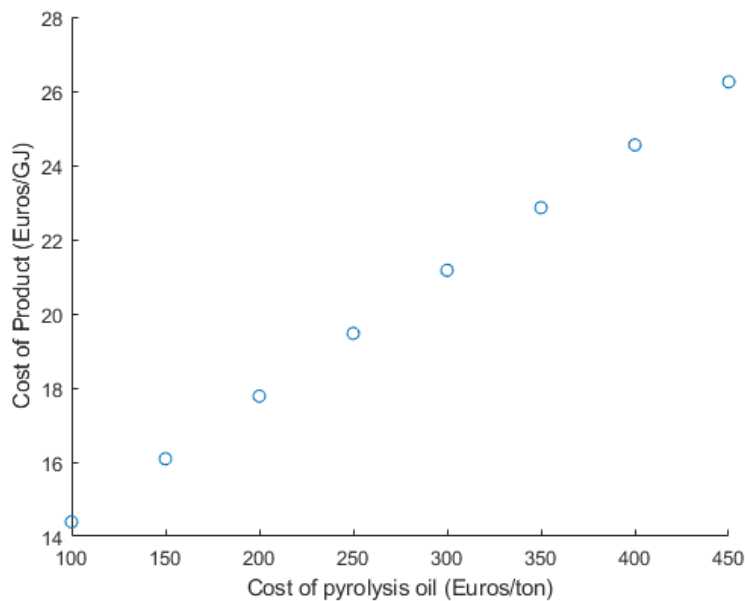


Figure 5.2: Cost of Product (COP) vs. cost of pyrolysis oil

It can be derived from the graphs that for an electricity price higher than 15 cents/kWh and

at a cost of pyrolysis oil above 400 euros/ton, the price of CNG becomes approximately 20% higher than the one estimated by ECN study. This means that, at these conditions, CNG becomes less competitive, which can undermine the economic feasibility of the plant.

5.2.2. The source of electricity

An important factor to consider is the source of electricity in the context of the Netherlands, affecting both its price and its environmental impact. This boils down to the following question:

Taking into consideration the technological limitations of having a fully renewable electricity source to power the SOEC, to what extent can the electricity be fossil-based?

On one hand, the intermittency of a 100% renewable electricity from solar and wind energies form many constraints to the operation of the electrolysis. Firstly, without sufficient storage capacity, the electrolyzer cannot operate when both sources of renewable energies are not available. Secondly, the cycling due to excessive shutdown and ramping will lead to faster degradation of the cells. On the other hand, the electricity can only be based on fossil-fuel to a certain threshold, beyond which the production of bio-CNG will have higher GHG emissions than conventional fuels.

The overall carbon footprint of the biofuel production is largely dependent on the one of the electrolyzer as the footprint of the other units only varies to a limited extent through potential improvement of their technological performance. A think tank called 'Carbon 4' performed a 'well-to-wheel' study to assess the carbon footprint of different types of vehicles depending on the fuel used. The study considered the complete lifetime of a vehicle, starting from manufacture to use and end of life [52]. Figures 5.3 and 5.4 show the average carbon footprint of segment D passenger cars⁵ and buses respectively, when having battery electric vehicle (BEV) and fuel cell electric vehicle (FCEV) with two different hydrogen production routes.

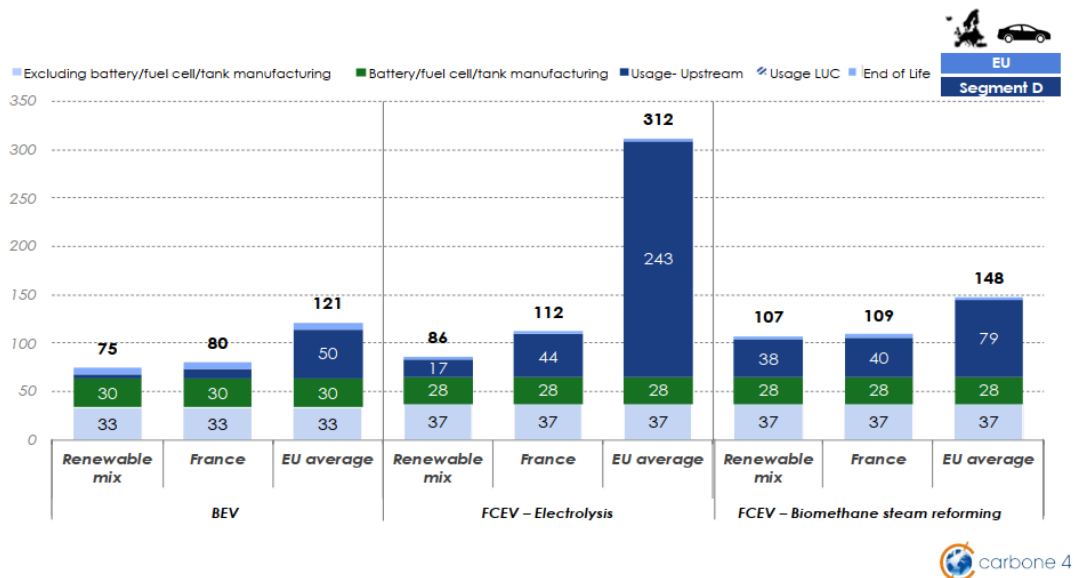


Figure 5.3: Average carbon footprint over the lifetime of passenger cars (segment D) sold in 2020 ($GtCO_2eq/km$) - France and Europe [52]

⁵large/family cars according to European categorisation.

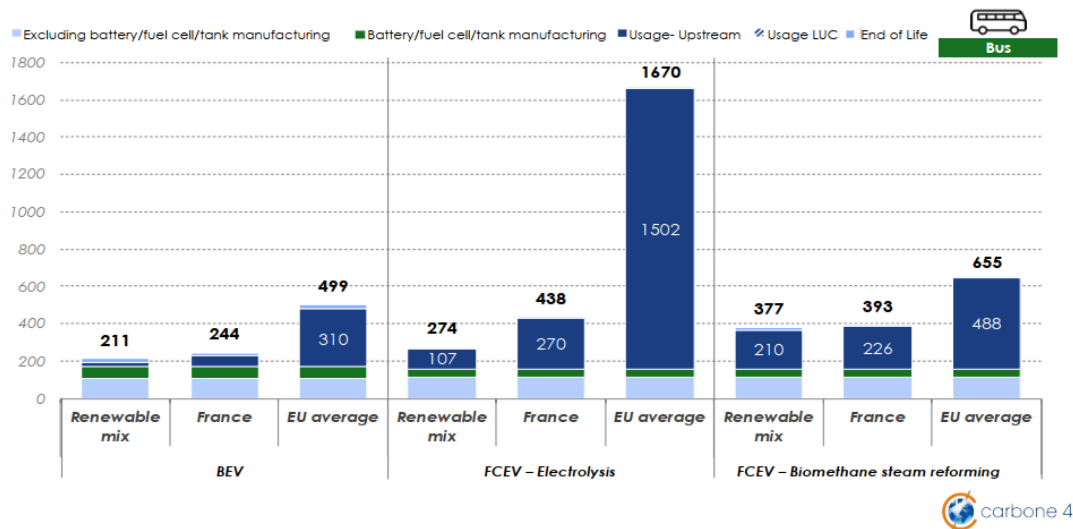


Figure 5.4: Average carbon footprint over the lifetime of buses sold in 2020 ($GtCO_2eq/km$) - France and Europe [52]

It can be seen from these figures that for a fuel cell electric vehicle running on hydrogen produced from electrolysis, the source of electricity has a significant impact on the carbon footprint originating from upstream usage. Considering segment D passenger cars sold in 2020, the average carbon footprint of a FCEV was found to be $86 gCO_2eq/km$ in case of hydrogen produced from electrolysis powered by a fully renewable electricity mix (100% RE), which is close to the footprint of a battery electric vehicle (BEV) when having a highly decarbonised electricity source (as in the case of France). In contrast, the footprint of internal combustion engine vehicle (ICEV) running on diesel and CNG (not shown in the figures) was calculated to be 271 and $210 gCO_2eq/km$ respectively. When the average European electricity mix is used for hydrogen production, the FCEV will lead to emissions that are higher than in the ones of conventional ICEV. The environmental impact is significantly higher in case of large vehicles (such as buses) than for light duty vehicles. It is crucial to note that the major incentive behind producing biofuels is to decarbonise the transport sector by lowering the emissions related to the upstream usage, i.e. to the production of the fuel itself. Hence, with regards to the integrated process of this thesis, the electricity powering the SOEC needs to be sufficiently decarbonised to have a biofuel that represents a suitable alternative for conventional fuels. The authors of the Carbon 4 study emphasize that it is necessary to have hydrogen produced from fully renewable electrolysis or steam-reforming of biogas in order for FCEV to have lower GHG emissions than ICEV.

Hence, to make sure that the use of the bio-CNG for transportation will lead to lower GHG emissions, the source of electricity needs to be sustainable and low-carbon. One possibility, in the context of the Netherlands, is to have an electricity mix made of different sources, including wind, nuclear and ultra-deep geothermal (UDG) energies. For UDG energy, drilling depth needs to be higher than 3-4 km to get heat of temperature higher than $130^{\circ}C$, required for generating electricity through turbines. Using geothermal energy with lower heat temperatures is more technologically feasible but at the expense of efficiency. Nuclear power and ultra-deep geothermal energy can both form a baseline for minimal supply to the SOEC. Offshore wind power in the Netherlands has a current total installed capacity of 2.5 GW and it is aimed to be increased to 11 GW by 2030 [45]. In addition, the 2020 onshore wind energy capacity was 4 GW⁶. With an average capacity factor for the European wind energy generation of 26%, the electricity supply from wind energy based on 2020 data sums up to 1.69 GW [23]. In 2019, geothermal energy output amounted to 1.11 TWh as heat [50]. There are increasing interest in investigating the potentials of UDG but more experience is to be acquired in drilling at depth

⁶Taken from <https://www.statista.com/statistics/868488/onshore-wind-energy-capacity-in-the-netherlands/> [01/08/2021]

higher than 3 km. Therefore, it is expected that a few percentage of geothermal energy is used for electricity generation. As for nuclear energy, it constitutes 10% of the electricity used in the Netherlands, with around 4 TWh, according to governmental data [44]. No current plans exist for increasing the share of nuclear power in the electricity mix of the Netherlands. Hence, the use of nuclear energy for powering the SOEC depends on the share of industrial consumption in electricity from nuclear. The availability of additional power will necessitate around 10 years, being the time of building and commissioning a nuclear plant.

The values presented provide a rough idea of the quantity of sustainable energy mix that can possibly be used for powering the integrated process. Solar energy was not considered as it constitutes a very small fraction of the electricity supply in the Netherlands. Considering this, the electricity consumption of the plant of 84.6 MW⁷ represents approximately 0.017% of the total electricity generation from wind, nuclear and ultra-deep geothermal. In addition, a storage system can be used to store the surplus wind energy. Depending on the situation, electricity from the grid could be used as a back-up system in case of supply shortage from low-carbon sources and/or insufficient stored energy. Nevertheless, the power system should be designed such that these cases are limited to very short periods of time.

To conclude, this section aimed at giving a brief and mainly qualitative discussion on the possible sources of electricity used to power the SOEC, within the actual context of the Netherlands. Further quantitative details are beyond the scope of this thesis.

⁷Considering all of the SOEC, compressors, pumps and electrical heating.

5.3. Profitability analysis

After calculating the net cash flows of the biofuel plant implementing the integrated process, it is possible to assess the economic feasibility of the project using several tools. The main one considered is the net present value (NPV), which is a tool to measure the discounted cumulative cash position over the plant lifetime. It is defined as:

$$NPV = \frac{\sum CF_k}{(1+i)^k} \quad (5.14)$$

The plant lifetime t_{plant} was considered to be 20 years, based on consultation of a technical expert in BTG company. The discount rate was taken as 15%, which is an average of two values proposed in [49] and [8]. Accordingly, the NPV was found to be equal to 6.0342 million Euros. The discounted payback period is used to identify the time after the plant start-up required to recover (payback) the initial capital cost invested [49], considering the discount rate. It was found to be 12 years, which represents 60% of the whole plant lifetime.

Moreover, the rate of return on investment (ROI) is a criterion used to represent the rate at which profit is generated given the fixed capital investment [49]:

$$ROI = \frac{\text{Average annual net profit}}{\text{Fixed capital investment}} \quad (5.15)$$

Based on equation 5.15, the ROI is 30.02%.

Thus, based on these profitability criteria, it can be concluded that the integrated process is economically feasible, with the constraint of having a bio-CNG price higher than the one needed for market competition against conventional natural gas. Nevertheless, technological improvements and policies can allow bio-CNG to be introduced in the market, especially in the context of the Netherlands (and Europe in general), where there are incentives to develop a bio-SNG market for the transport sector.

6

Conclusion and Recommendations

Science is a way of thinking much more than it is a body of knowledge.

Carl Sagan

This chapter lays down the conclusion of the thesis by answering the research questions in section 6.1 and provides recommendations for future work in section 6.2.

6.1. Answers to the research questions

The motivation behind performing this work (in line with BTG project) is the assessment of the technical and economic performance of the production of biofuel for the transport sector, in an efficient manner. For this, the purpose of this thesis was to model and analyse a process which integrates pyrolysis oil gasification, steam electrolysis and syngas catalytic upgrading. These three technologies are aimed to be complementary by using the products of electrolysis as feed streams for the other two units. The study was based on a literature review of the different technologies used, along with the theoretical background related to each. After then, the basis of design of the process was presented with the model building explained. The process was simulated on Aspen Plus software with complementary calculations on Fortran and Matlab. The simulation included different sections (blocks) of the integrated process for easier handling and visualisation of the model.

sq1: *What are the important parameters for the gasification process in order to optimize the quality of the syngas?*

The entrained flow gasifier was modeled on Aspen Plus as an equilibrium (RGibbs) reactor and in quasi-adiabatic conditions. Hence, the simulation of the gasification process relies on the specifications and the inputs of the reactor. Concerning the former, the calculation option and the possible products were specified. Adding to the pyrolysis oil, the inputs constituted steam, oxygen and a heat stream that models the internal heat generation by the combustion reactions, taking into account 5% of heat loss. By performing sensitivity analyses on Aspen, it was found that the main parameters that are critical for the performance of the reactor and the quality of the syngas are the oxygen equivalence ratio, and the steam-to-carbon ratio. The increase in steam-to-carbon ratio led to the enhancement of hydrogen and CO_2 concentrations in syngas. This affected the H_2/CO molar ratio but not the feed ratio which takes into account the concentration of CO_2 .

The oxygen equivalence ratio (OER) was found to have a significant effect on the feed ratio for methanation, through the increase in CO and CO_2 production and the decrease in H_2 concentration in syngas. In addition, the OER alters the extent of combustion reactions, which changes the outlet temperature of the reactor. Consequently, there is a trade off between the

syngas quality and the reactor performance when choosing the OER at which the gasifier operates. As hydrogen from electrolysis is used to adjust the feed ratio of the syngas, the parameters were chosen such that the gasifier temperature lies within the range reported experimentally in literature. Considering this, the gasifier was designed with a steam-to-carbon ratio of 0.85 and an OER of 0.4. This resulted in a H_2/CO ratio of 1.14 and a methanation feed ratio of 0.15.

SG2: *Which type of electrolysis results in a more efficient integrated process?*

Based on studies in literature that compared the performance of biofuel production process using low-temperature and high-temperature electrolysis, solid oxide electrolysis cell (SOEC) was chosen for the design of the process. The use of high-temperature electrolysis allows for better heat integration, which reduces the amount of external heat required. Moreover, the cell stack can operate at lower power-operating range, hence consuming less electricity. These advantages lead to higher energy efficiency, which was the major criterion used for choosing the type of electrolysis. Hence, even though it is still under development, steam SOEC was favoured over other types of electrolysis (alkaline electrolysis and proton-exchange membrane electrolysis).

SG3: *What is the most suitable product of catalytic syngas upgrading in terms of overall process efficiency?*

Amongst the different biofuels produced out of syngas, substitute natural gas (SNG) was found to give the highest process energy efficiency, based on the literature review performed. It also has the advantage of having high energy content (LHV MJ/kg) and low CO_2 emission factor. Hence, considering as well better integration in the existing transport fuel infrastructure, it was decided to consider compressed natural gas (bio-CNG) as the final product of the system.

SG4: *How does the use of the heat generated by the system affect the overall process efficiency?*

The complete integrated process includes two exothermic units and two endothermic ones. Using the heat generated within the system to meet the heat requirements of the cold streams leads to an increase in the efficiency of the process. Part of the feedstock (pyrolysis oil) to the entrained flow gasifier is used for heat generation to initiate the combustion reactions with the presence of partial oxygen intake. The induced and additional heat from the combustion reactions results in syngas with high temperature. Adding to gasification, methanation is a highly exothermic process that needs cooling. On the other hand, the desorption of H_2S in MDEA and the high-temperature electrolysis are both endothermic processes. The numerical method of Pinch analysis coupled with heat exchanger network was performed to know which hot streams can be used in heat exchangers with the cold streams. It was found that the integrated process needs seven heat exchangers, adding to 1.8 MW of electrical heating and 0.286 MW of cooling requirement (using cooling water) due to thermodynamic limitations. The heat integration study resulted in 10.71 MW of useful excess heat, that was assumed to be used for steam generation. The steam is then inputted to the electrolyzer to get additional hydrogen, that is considered as a product and hence can be included as an energy output in addition to CNG. Thus, the advantage of heat integration is double:

1. The substitution of external heating and cooling requirements by the use of heat generated within the system, through the matching of cold and hot streams, within thermodynamic boundaries.
2. The harvesting of the excess heat from the hot streams not used in the heat exchangers to have hydrogen as a product using the SOEC.

As a result, the overall efficiency of the process increased from 63.8% to 73.8% on LHV basis and from 63.4% to 78.2% on HHV basis. Hence, it can be concluded that heat integration leads to a significant increase in energy efficiency of 15% (LHV basis) and 23% (HHV basis).

SQ5: *Is the integrated process economically feasible?*

The economic analysis of the process was done by considering the different cost parameters to calculate the total capital expenditure (CAPEX), as well as the variable and fixed operating costs (OPEX) and the annuities. The revenues consist of the income coming from selling the compressed natural gas and oxygen as products. The profitability of the plant was assessed using the net present value (NPV) and the the rate of return on investment (ROI). NPV was obtained as 6.0342 million euros and the ROI was 30.02%. The process was found to be economically feasible when the price of the compressed natural gas (bio-CNG) is required to be 22.4 Euros/GJ (2020 value), which is a value close to the value found in literature. The economic feasibility of the process depends on the price of the bio-CNG, which is mainly affected by the price of the electricity mix and the cost of pyrolysis oil.

Main question: *How can the use of electrolysis derived oxygen as a bio-oil gasifying agent and hydrogen as feedstock for downstream biofuel production result in an efficient integrated process?*

The main research question emphasizes on the two principal reasons behind the incorporation of electrolysis with gasification and biofuel production. Firstly, the entrained flow gasifier uses oxygen as a gasifying agent. Secondly, the gasification of pyrolysis oil resulted in a syngas with a methanation feed ratio of 0.15, which should be equal to 3 or higher for an optimum methane production. The syngas needs then to be upgraded by adding hydrogen at the inlet of the methane reactor.

The integration of the solid-oxide electrolysis cell in the 'pyrolysis oil to CNG' process has many advantages:

- The electrolysis cell provides two products simultaneously. This eliminates the energy requirement of producing these products or the costs of buying them as chemical input streams.
- Lower electricity consumption and better heat integration can be achieved through high-temperature electrolysis.
- Additional amount of hydrogen can be produced as an end-product when using the heat generated in excess to produce steam.

These benefits enhance the energy performance of the process and increases its efficiency. The use of the SOEC for the production of CNG was thus found to result in an efficient process that is economically feasible and profitable within the constraints of the bio-CNG price. In fact, a high overall energy efficiency of 73.8% (LHV) and 78.2% was obtained.

The answer to the main research question can hence be summarized as:

The integration of pyrolysis oil gasification with steam electrolysis and methane production provides an efficient way of producing a bio-fuel for transportation uses, while having the advantages of harnessing surplus renewable electricity and using processed biomass (bio-oil) as an initial feedstock.

6.2. Recommendations

The boundaries of the scope of this thesis are drawn by technical and time constraints. For this, multiple areas of further research can be suggested. The recommendations are divided into two parts. While the first is related to variables and parameters of the integrated process, the second focuses on potential analyses that can enhance the understanding of the process.

6.2.1. Process variables

The initial feedstock to the process is the first relevant variable to look at. The elemental composition of the bio-oil affects the syngas quality as well as the cleaning requirements downstream the gasifier. As the pyrolysis oil (PO) considered in this study is derived from pine wood, it contains a very small fraction of ash and char, and negligible amounts of minerals and contaminants. The amounts of sulfur and phosphorus are 4.6% and 0.11% respectively on dry weight basis. If the pyrolysis oil contains higher amounts of contaminants, ash and char, then the model of the process will need to be modified to include a cyclone and possibly other cleaning units. For example, oil resulting from pyrolysis of straw has a concentration of sulfur around 13 times higher than the one in pine-wood PO. The concentration of nitrogen is also significantly higher in straw PO, which can lead to the formation of nitrogen oxides (NO_x) in the syngas [11]. Moreover, the elemental composition of the pyrolysis oil in terms of carbon, hydrogen and oxygen changes the amount of oxygen required for complete combustion, and hence affects the flow rate of oxygen fed to the gasifier for a fixed oxygen equivalence ratio. Based on the results obtained from Aspen Plus model, the additional cleaning units and processes required in case of a more contaminated syngas have more impact on the amount of energy consumed and the capital and operating costs than changes in inlet oxygen. This is due to the fact that excess amount of oxygen is produced by electrolysis to have enough hydrogen to meet the target methanation feed ratio. Modeling the process with different types of pyrolysis oil can be useful for assessing the effect on the energy efficiency and economic performance.

Another variable worthy of consideration is the biofuel produced from syngas. This thesis was limited to compressed natural gas, as mentioned in the introductory section on research framework (section 1.2). As the Aspen Plus simulation is divided into sections (represented by blocks), it can be used as a basis to model the integrated process for producing other biofuels. These further modeling work and analysis of several product routes are in line with BTG project.

6.2.2. Further analyses

For the aim of using this thesis as a basis for future research and expanding on it, it is important to complement the theoretical work with an experimental one. In this way, it is possible to analyse the actual performance of the technologies used and derive empirical correlations and parametric relations.

One of the parameters that can be further investigated is the carbon-to-gas conversion (CtG ratio), which was inputted manually in Aspen Plus simulation. Experiments on pyrolysis oil gasification allow to study the effect of operating conditions on the CtG ratio. The obtained correlations from the experimental data can then be incorporated into the model to predict the amount of carbon in the pyrolysis oil that is actually converted into syngas at different operating conditions. This gives the possibility of having the CtG ratio as an output parameter to the gasifier rather than a manual input in the model.

Another parameter that has an important effect on the gasification process is the droplet size of the pyrolysis oil. As previously discussed in section 2.1 of the chapter on literature review, the diameter of the bio-oil droplet has an effect on the heating rate and on char formation. This will consequently alter the CtG ratio. Thus, the simulation of the gasification can be modified according to the experimental data to have a more accuracy modeling of the conversion of carbon in pyrolysis oil. The model can then be optimized to maximize the carbon-to-gas conversion.

Further improvements can be done by using kinetic data for modeling the gasification of pyrolysis oil if the kinetic parameters are well defined in literature for this type of process, considering

the differences with the gasification of solid biomass.

Additionally, the analysis of the process has been focused on the techno-economic aspects, within the scope of a master thesis project. This can be complemented by an exergy analysis, to study the weight of the different technologies and process units on the final result [19].

Furthermore, in order to have a better assessment of the potentials and challenges of implementing the technologies together for producing transportation biofuels, the study of the environmental impact of the production process is highly valuable. This can be realized by a carbon footprint analysis or a life cycle assessment (LCA). In fact, the underlying purpose of BTG national project is to provide alternatives to fossil fuels for the decarbonisation of the transportation sector. Within this vision, it is necessary that the production of the biofuel is performed in a sustainable way, by having low GHG emissions and low environmental impact. The assessment of this impact includes several factors. Land use change is important to consider as the initial feedstock is pyrolysis oil, which is obtained from biomass. The type of biomass used affects significantly the amount of land use emissions. Other relevant factors include water consumption and material resources and minerals. Notably, the materials used for the cathode and anode of the electrolyzer can have negative consequences on the ecological and social levels due to mining operations and in case rare metals are involved.

As the topic of the thesis is the integration of gasification with electrolysis for biofuel production, the main focus was not on the electrolyzer. Amongst these technologies, the SOEC has the lowest technological maturity. Hence, the durability and long-term performance of the solid oxide electrolysis cells are important to consider for future work. To give better insight on the applicability of the process on the long-term, more research can be done to study the electro-chemical performance of the SOEC stacks. Major improvements need to be made to increase their reliability and robustness, especially with the use of intermittent renewable energy, which brings about the next point.

In chapter 5, the sources of electricity for powering the SOEC have been discussed briefly and qualitatively. The discussion was centred around the possible mix of sustainable sources of power, as well as the degree at which electricity can have a grey component (that is fossil-fuel based), as a back-up for the intermittent renewable electricity. More quantitative details and practical information can be given on the mix of electricity sources that can actually be applied in the context of the Netherlands.

Bibliography

- [1] P. Antonucci A. Malara, P. Frontera and A. Macario. Smart recycling of carbon oxides: Current status of methanation reaction. *Green and Sustainable Chemistry*, 2020. doi: <https://doi.org/10.1016/j.cogsc.2020.100376>.
- [2] C-C Cormos A. Padurean and P-S Agachi. Pre-combustion carbon dioxide capture by gas-liquid absorption for integrated gasification combined cycle power plants. *International Journal of Greenhouse Gas Control*, (7):1–11, 2012. doi: [doi:10.1016/j.ijggc.2011.12.007](https://doi.org/10.1016/j.ijggc.2011.12.007).
- [3] National Minerals Information Center. Iron ore. Technical report, 2020.
- [4] L.R. Clausen. Energy efficient thermochemical conversion of very wet biomass to biofuels by integration of steam drying, steam electrolysis and gasification. *Energy*, (125):327–336, 2017. doi: [http://dx.doi.org/10.1016/j.energy.2017.02.132](https://dx.doi.org/10.1016/j.energy.2017.02.132).
- [5] European Commission. Internal market, industry, entrepreneurship and smes - sme definition. https://ec.europa.eu/growth/smes/sme-definition_en, 2021. Online; accessed 03/06/2021.
- [6] W. de Jong and R. van Ommenn. *Biomass as a Sustainable Energy Source for the Future*. John Wiley Sons, Inc., 2015.
- [7] J. Dymont and S. Watanasiri. Acid gas cleaning using depg physical solvents: Validation with experimental and plant data. Technical report, 2013.
- [8] M. Santarelli E. Giglio, A. Lanzini and P. Leone. Synthetic natural gas via integrated high-temperature electrolysis and methanation: Part ii—economic performance. *Journal of Energy Storage*, (2):64–79, 2015. doi: [http://dx.doi.org/10.1016/j.est.2015.06.004](https://dx.doi.org/10.1016/j.est.2015.06.004).
- [9] M. Santarelli E. Giglio, A. Lanzini and P. Leone. Synthetic natural gas via integrated high-temperature electrolysis and methanation: Part i—energy performance. *Journal of Energy Storage*, (1):22–37, 2015. doi: [http://dx.doi.org/10.1016/j.est.2015.04.002](https://dx.doi.org/10.1016/j.est.2015.04.002).
- [10] R. Miranda E. Taibi, H. Blanco and M. Carmo. Green hydrogen cost reduction. Technical report, 2020.
- [11] L. van de Beld F. Weiland H. Wiinikka P. Carlsson E.J. Leijenhurst, D. Assink and O.G.W. Ohrman. Entrained flow gasification of straw- and wood-derived pyrolysis oil in a pressurized oxygen blown gasifier. *Biomass and bioenergy*, (79):166–176, 2015. doi: [http://dx.doi.org/10.1016/j.biombioe.2014.11.020](https://dx.doi.org/10.1016/j.biombioe.2014.11.020).
- [12] Enapter. Aem water electrolysis: how it works. <https://www.enapter.com/aem-water-electrolysis-how-it-works>, 2020. Online; accessed 27/01/2020.
- [13] Hanaa Er-rbib and C. Bouallou. Modeling and simulation of co methanation process for renewable electricity storage. *Energy*, (75):81–88, 2014. doi: [http://dx.doi.org/10.1016/j.energy.2014.05.115](https://dx.doi.org/10.1016/j.energy.2014.05.115).
- [14] A. Lanzini F. Monaco and M. Santarelli. Making synthetic fuels for the road transportation sector via solid oxide electrolysis and catalytic upgrade using recovered carbon dioxide and residual biomass. *Journal of Cleaner Production*, (170):160–173, 2018. doi: [http://dx.doi.org/10.1016/j.jclepro.2017.09.141](https://dx.doi.org/10.1016/j.jclepro.2017.09.141).

- [15] M. Marklund H. Wiinikka O. Ohrman F. Weiland, H. Hedman and R. Gebart. Pressurized oxygen blown entrained-flow gasification of wood powder. *Energy Fuels*, (27):932941, 2013. doi: dx.doi.org/10.1021/ef301803s.
- [16] J. Falconer and A. Zagli. Adsorption and methanation of carbon dioxide on a nickel/silica catalyst. *Journal of Catalysis*, (62):280–285, 1980.
- [17] A. van der Drift G. Aranda and R. Smit. The economy of large scale biomass to substitute natural gas (biosng) plants. Technical report, 2014.
- [18] S. H. Jensen G. Butera and L. R. Clausen. A novel system for large-scale storage of electricity as synthetic natural gas using reversible pressurized solid oxide cells. *Energy*, (166):738–754, 2019. doi: https://doi.org/10.1016/j.energy.2018.10.079.
- [19] M. Santarelli G. Lorenzi, A. Lanzini and A. Martin. Exergo-economic analysis of a direct biogas upgrading process to synthetic natural gas via integrated high-temperature electrolysis and methanation. *Energy*, (141):1524–1537, 2017. doi: https://doi.org/10.1016/j.energy.2017.11.080.
- [20] S. Wu G. Lyu and H. Zhang. Estimation and comparison of bio-oil components from different pyrolysis conditions. *Front. Energy Res*, (3:28), 2015. doi: https://doi.org/10.3389/fenrg.2015.00028.
- [21] S. R. A. Kersten G. van Rossum and W. P. M. van Swaaij. Catalytic and noncatalytic gasification of pyrolysis oil. *Ind. Eng. Chem. Res.* 2007, (46):3959–3967, 2007. doi: http://dx.doi.org/10.1021/ie061337y.
- [22] Biomass Technology Group. Tar definitions. <https://www.btgworld.com/en/rtd/analysis/btg-tar-definitions.pdf>, 2020. Online; accessed 13/01/2020.
- [23] G. Brindley I. Komusanac and D. Fraile. Geothermal energy in the netherlands. Technical report, 2020.
- [24] IEA. Total final energy consumption in the transport sector in the nze2050. <https://www.iea.org/data-and-statistics/charts/total-final-energy-consumption-in-the-transport-sector-in-the-nze2050-2010-2030>, 2020. Online; accessed 25/06/2021.
- [25] IEA. World energy model. <https://www.iea.org/reports/world-energy-model>, 2020.
- [26] IEA. Global supply of low-carbon fuel by scenario, 2019-2040. <https://www.iea.org/data-and-statistics/charts/global-supply-of-low-carbon-fuel-by-scenario-2019-2040>, 2020.
- [27] Nickel Institute. Nickel availability. <https://nickelinstitute.org/about-nickel/#02-nickel-availability>, 2020. Online; accessed 22/01/2020.
- [28] IPCC. Technical report.
- [29] P. Massoli J. D'Alessio, M. Lazzarro and V. Moccia. Thermo-optical investigation of burning biomass pyrolysis oil droplets. *Twenty-Seventh Symposium (International) on Combustion*, (79):1915–1922, 1998.
- [30] F. Vogel S. Biollaz J. Kopyscinski, T. Schildhauer and A. Wokaun. Applying spatially resolved concentration and temperature measurements in a catalytic plate reactor for the kinetic study of co methanation. *Journal of Catalysis*, (271):262–279, 2010. doi: doi:10.1016/j.jcat.2010.02.008.
- [31] T. Schildhauer J. Kopyscinski and S. Biollaz. Fluidized-bed methanation: Interaction between kinetics and mass transfer. *Ind. Eng. Chem. Res.*, (50):2781–2790, 2011. doi: dx.doi.org/10.1021/ie100629k.

- [32] C. Yao J. Yu F. Su J. Liu, D. Cui and G. Xu. Syngas methanation in fluidized bed for an advanced two-stage process of sng production. *Fuel Processing Technology*, (141):130–137, 2016.
- [33] X-Y Zhao J-P Cao J. Ren, Y-L Liu. Methanation of syngas from biomass gasification: An overview. *Hydrogen energy*, (45):4223–4243, 2020. doi: <https://doi.org/10.1016/j.ijhydene.2019.12.023>.
- [34] I. Hannula K. Onarheim and Y. Solantausta. Hydrogen enhanced biofuels for transport via fast pyrolysis of biomass: A conceptual assessment. *Energy*, (199), 2017. doi: <https://doi.org/10.1016/j.energy.2020.117337>.
- [35] J. Kopyscinski. *Production of synthetic natural gas in a fluidized bed reactor*. PhD thesis, 2010.
- [36] S. Shiva Kumar and V. Himabindu. Hydrogen production by pem water electrolysis – a review. *Materials Science for Energy Technologies*, (2):442–454, 2019. doi: <https://doi.org/10.1016/j.mset.2019.03.002>.
- [37] R. Kungas-T-E Lin-S. Diethelm F. Maréchal L. Wang, M. Chen and J. Van herle. Power-to-fuels via solid-oxide electrolyzer: Operating window and techno-economics. *Renewable and Sustainable Energy Reviews*, (110):174–187, 2019. doi: <https://doi.org/10.1016/j.rser.2019.04.071>.
- [38] E. Leijenhorst. *Biomass Gasification via Fast Pyrolysis (doctoral dissertation)*. PhD thesis, 2016.
- [39] A. Lanzini M. Pozzo and M. Santarelli. Enhanced biomass-to-liquid (btl) conversion process through high temperature co-electrolysis in a solid oxide electrolysis cell (soec). *Fuel*, (145):39–49, 2015. doi: <http://dx.doi.org/10.1016/j.fuel.2014.12.066>.
- [40] L. De Prada-M. Padella M. Prussi, M. Yugo and R. Edwards. Jec well-to-wheels report vs. well-to-wheels analysis of future automotive fuels and powertrains in the european context. Technical report, 2020.
- [41] V. Nemanova M. Samavati, A. Martin and M. Santarelli. Integration of solid oxide electrolyser, entrained gasification, and fischer-tropsch process for synthetic diesel production: Thermodynamic analysis. *Hydrogen energy*, (43):4785–4803, 2018. doi: <https://doi.org/10.1016/j.ijhydene.2018.01.138>.
- [42] A. Kulkarni N. Abdoulmoumine, S. Adhikari and S. Chattanathan. A review on biomass gasification syngas cleanup. *Applied Energy*, (155):294–307, 2015.
- [43] E. Pettersson A. Johansson H. Hedman O. Ohrman, F. Weiland and M. Pedersen. Pressurized oxygen blown entrained flow gasification of a biorefinery lignin residue. *Fuel Processing Technology*, (115):130–138, 2013. doi: <http://dx.doi.org/10.1016/j.fuproc.2013.04.009>.
- [44] Government of the Netherlands. Nuclear energy. <https://www.government.nl/topics/renewable-energy/nuclear-energy>, 2021.
- [45] Government of the Netherlands. Renewable energy. <https://www.government.nl/topics/renewable-energy>, 2021.
- [46] S. Rodat Q. Bellouard, S. Abanades and N. Dupassieux. Solar thermochemical gasification of wood biomass for syngas production in a high-temperature continuously-fed tubular reactor. *Hydrogen energy*, (42):13486–13497, 2017. doi: <http://dx.doi.org/10.1016/j.ijhydene.2016.08.196>.
- [47] Z. A. Putra M. R. Bilad Y. Kim C. H. Yun R. Andika, A. B. D. Nandiyanto and M. Lee. Co-electrolysis for power-to-methanol applications. *Renewable and Sustainable Energy Reviews*, (95):227–241, 2018. doi: <https://doi.org/10.1016/j.rser.2018.07.030>.

- [48] M. Schmid D. Colomara F. Ortloff R. Spörl A. Brissea R. Anghilante, c. Müller and F. Graf. Innovative power-to-gas plant concepts for upgrading of gasification bio-syngas through steam electrolysis and catalytic methanation. *Energy Conversion and Management*, (183):462–473, 2019. doi: <https://doi.org/10.1016/j.enconman.2018.12.101>.
- [49] W. Whiting R. Turton, R. Bailie and J. Shaeiwitz. *Analysis, Synthesis, and Design of Chemical Processes - 3rd ed.* Prentice Hall, 2009.
- [50] P. Ramsak. Geothermal energy in the netherlands. Technical report, 2020.
- [51] K. Sørensen S. Ali and M. Nielsen. Modeling a novel combined solid oxide electrolysis cell (soec) - biomass gasification renewable methanol production system. *Renewable Energy*, (3):684–698, 2015. doi: <https://doi.org/10.3390/pr3030684>.
- [52] N. Meunier S. Amant and C. de Cossé Brissac. Road transportation: what alternative motorisations are suitable for the climate? Technical report, 2020.
- [53] P. U. Foscolo S. Heidenreich, M. Muller and. *Advanced biomass gasification : new concepts for efficiency increase and product flexibility.* Academic Press, 2016.
- [54] S. Matthischke M. Schlüter M. Götz J. Lefebvre P. Prabhakaran S. Bajohr S. Rönsch, J. Schneider. Review on methanation – from fundamentals to current projects. *Fuel*, (166):276–296, 2016. doi: [dx.doi.org/10.1016/j.fuel.2015.10.111](https://doi.org/10.1016/j.fuel.2015.10.111).
- [55] H. Sigurjonsson and L.R. Clausen. Solution for the future smart energy system: A polygeneration plant based on reversible solid oxide cells and biomass gasification producing either electrofuel or power. *Applied Energy*, (216):323–337, 2018. doi: <https://doi.org/10.1016/j.apenergy.2018.02.124>.
- [56] Y. K. Salkuyeh T. A. Adams and J. Nease. *Processes and simulations for solvent-based CO2 capture and syngas cleanup.* 2014. doi: <http://dx.doi.org/10.1016/B978-0-444-59566-9.00006-5>.
- [57] Aspen Technology. Aspen plus - getting started modeling processes with solids. Technical report, 2013.
- [58] M.C. Tucker. Progress in metal-supported solid oxide electrolysis cells: A review. *International journal of hydrogen energy*, (45):24203–24218, 2020. doi: <https://doi.org/10.1016/j.ijhydene.2020.06.300>.
- [59] H. Prajitno J. Yoo J. Patel Y. Yang W. J. Lee, C. Li and S. Lim. Recent trend in thermal catalytic low temperature co2 methanation: A critical review. *Catalysis today*, 2020. doi: <https://doi.org/10.1016/j.cattod.2020.02.017>.
- [60] G. Weatherbee and C. Bartholomew. Hydrogenation of co2 on group viii metals. *Journal of Catalysis*, (77):460–472, 1982.
- [61] O. Rezzazgui Z. Zhang, B. Delcroix and P. Mangin. Methanol production from pyrolysis oil gasification—model development and impacts of operating conditions. *Applied Sciences*, (10):7371, 2020. doi: [doi:10.3390/app10207371](https://doi.org/10.3390/app10207371).
- [62] S. Larose Z. Zhang, P. Mangin and B. Delcroix. Simulation of syngas production via pyrolysis oil gasification - impacts of operating conditions on syngas properties. *BioResources*, (15):729–745, 2020.

A

Aspen Plus plots

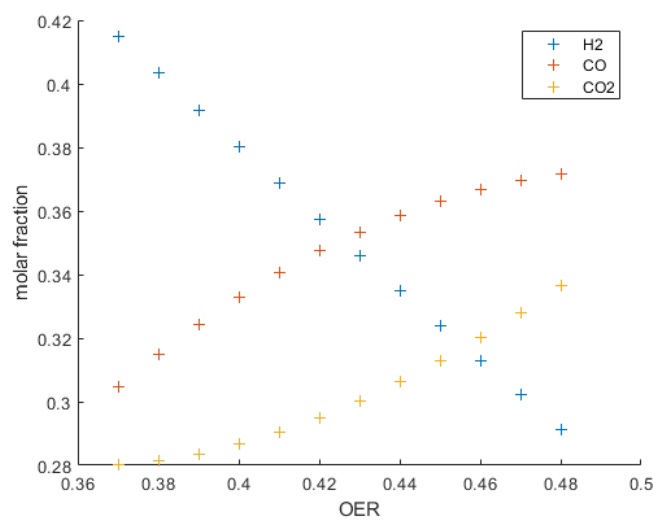


Figure A.1: Syngas composition (dry basis) vs. the oxygen equivalence ratio (OER) on Aspen Plus

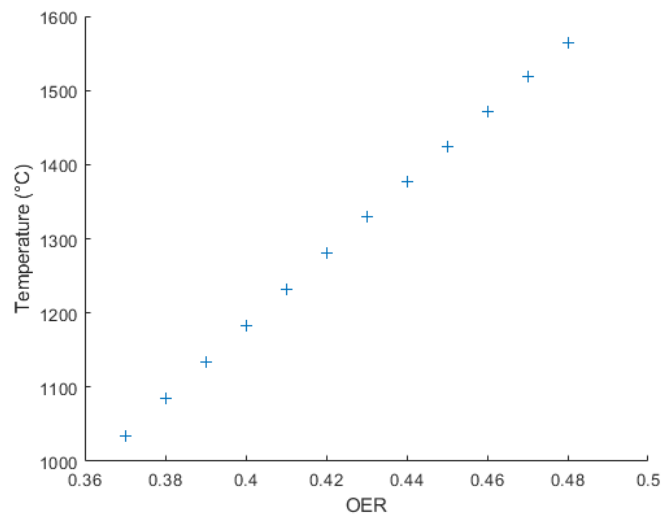


Figure A.2: Gasifier outlet temperature vs. the oxygen equivalence ratio (OER) on Aspen Plus

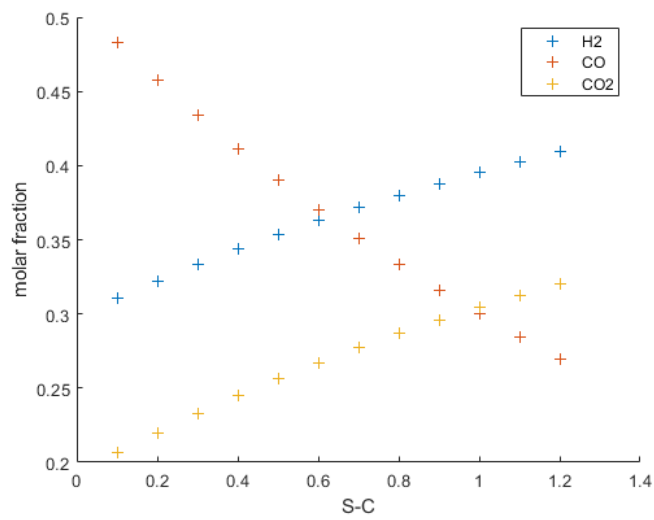


Figure A.3: Syngas composition (dry basis) vs. the steam-to-carbon ratio on Aspen Plus

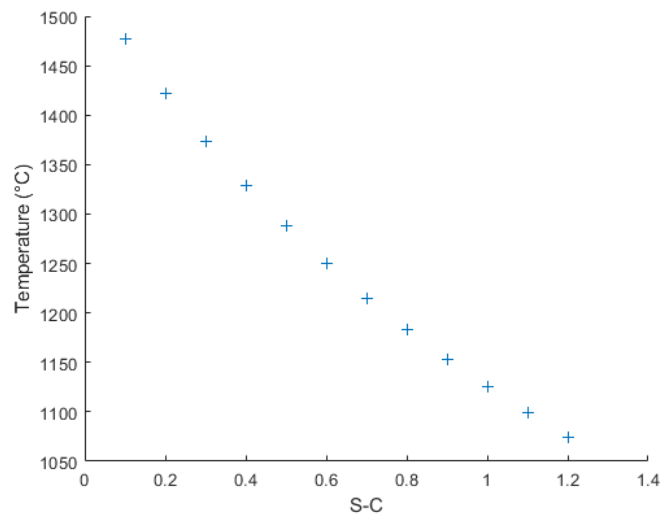


Figure A.4: Gasifier outlet temperature vs. the steam-to-carbon ratio on Aspen Plus

B

Heat integration and heat exchanger network calculations

Table B.1: Summary of the cold and hot streams with their properties for heat integration

Stream number	Stream name	Type	T_{in} (°C)	T_{out} (°C)	CP (kW/K)
1	steam to gasifier	cold	25	110	2.44
2	syngas	hot	1170	50	7.25
3	MDEA solvent	cold	50	100	5.79
4	MDEA solvent	hot	60	40	5.56
5	methanation reactor inlet	cold	140	280	4.59
6	steam from methanation	hot	745.15	220	4.71
7	methanation reactor outlet	hot	365	20	6.38
8	SNG	hot	151	50	1.97
9	CNG	hot	177	15	1.96
10	water feed to SOEC	cold	23	700	9.94
11	SOEC outlet	hot	700	45	5.84
12	H_2 (SOEC)	cold	45	140	4.30
13	O_2 (SOEC)	hot	700	55	2.28
14	pyrolysis oil	cold	25	80	3.33

The temperature differences $\Delta T1$ and $\Delta T2$ were calculated as:

$$\delta T1 = Thot_{in} - Tcold_{out} \quad (B.1)$$

and

$$\delta T2 = Thot_{out} - Tcold_{in} \quad (B.2)$$

The log mean temperature difference δT_{lm} is expressed as:

$$\frac{\delta T1 - \delta T2}{\ln\left(\frac{\delta T1}{\delta T2}\right)} \quad (B.3)$$

F is the correction factor, R and S are constants used to calculate F:

$$F = \frac{\sqrt{R^2 + 1} \cdot \ln(1 - S) / (1 - R \cdot S)}{(R - 1) \cdot \ln\left(\frac{2 - S(R + 1 - \sqrt{R^2 + 1})}{2 - S(R + 1 + \sqrt{R^2 + 1})}\right)} \quad (B.4)$$

R and S are respectively defined as:

$$R = \frac{(Thot_{in} - Thot_{out})}{(Tcold_{out} - Tcold_{in})} \quad (B.5)$$

$$S = \frac{(T_{cold_{out}} - T_{cold_{in}})}{(T_{hot_{in}} - T_{cold_{in}})} \quad (\text{B.6})$$

Table B.2: Summary of the intervals and process streams for the pinch analysis

Interval	T_i to T_{i-1}	ΔT	[Streams involved]	sum CP	ΔH	ΔH_{i-1} to ΔH_i
0	1165 to 740.15	424.85	[2]	-7.25	-3080.2	3080.2
1	740.15 to 705	35.15	[2;6]	-11.96	-420.4	3500.7
2	705 to 695	10	[2;6;10]	-2.03	-20.25	3520.9
3	695 to 360	335	[2;6;10;11;13]	-16.52	-5535.1	9056.0
4	360 to 285	75	[2;6;7;10;11;13]	-16.52	-1239.2	10295.2
5	285 to 215	70	[2;5;6;7;10;11;13]	-11.93	-1119.9	11415.0
6	215 to 172	43	[2;5;7;10;11;13]	-7.22	-310.5	11725.6
7	172 to 146	26	[2;5;7;9;10;11;13]	-9.18	-238.7	11964.3
8	146 to 145	1	[2;5;7;8;9;10;11;13]	-11.15	-11.15	11975.4
9	145 to 115	30	[2;7;8;9;10;11;12;13]	-11.44	-343.3	12318.8
10	115 to 105	10	[1;2;7;8;9;10;11;12;13]	-9.00	-90.0	12408.8
11	105 to 85	20	[1;2;3;7;8;9;10;11;12;13]	4.03	-1732.9	14141.6
12	85 to 55	30	[1;2;3;7;8;9;10;11;12;13;14]	0.12	3.52	14138.1
13	55 to 50	5	[1;2;4;7;8;9;10;11;12;13;14]	-3.98	-19.9	14158.0
14	50 to 45	5	[1;2;3;7;8;9;10;11;14]	-8.28	-41.4	14199.4
15	45 to 40	5	[1;4;7;9;10;11;14]	-4.03	-20.13	14219.5
16	40 to 35	5	[1;4;7;9;10;14]	1.82	9.08	14210.4
17	35 to 30	5	[1;7;9;10;14]	7.38	36.9	14173.6
18	30 to 28	2	[7;9;10]	1.60	3.20	14170.4
19	28 to 15	13	[7;9]	-8.34	-108.4	14278.7
20	15 to 10	5	[9]	-1.96	-9.80	14288.5

Table B.3: Summary of the cold and hot streams with their properties for heat exchanger network

HEx number	Q (kW)	U (kW/m ² · K)	ΔT_1	ΔT_2	ΔT_{lm}	R	S	F	A (m ²)
1	9384.4	3.123	799.85	27.0	228.1	3.2	0.3	0.75	17.57
2	1165.9	0.325	150.0	109.0	128.4	1.48	0.48	0.85	32.86
3	677.8	0.325	420	262.6	335.2	2.12	0.25	0.93	6.66
4	408.1	0.325	262.2	178.5	217.9	1.88	0.27	0.94	6.15
5	384.1	0.75	123.5	5.00	36.96	3.37	0.29	0.8	17.32
6	2081.7	3.123	590.0	269.9	409.3	4.77	0.126	0.96	1.69
7	183.3	0.75	71	32.95	49.6	1.69	2.29	0.8	6.17

C

Economic analysis - Parameters

Equipment type	Material	Material factor, F_m
Heat exchangers	CS shell/tube	1
	CS shell and SS tube	1.8
	SS shell/tube	2.75
	CS shell and Ni-alloy tube	2.7
	Ni-alloy shell/tube	3.75
	Reactor vessels	Ni-alloy
SS		0.7
Compressors		CS
	Pumps	cast iron
carbon steel		1.5

Table C.1: Material factors for different materials per equipment

The abbreviates of the material used are: carbon steel (CS), and stainless steel (SS). Only the values used for the economic analysis are listed in the table.